

# Gravitational Lensing by Black Holes in General Relativity and $\mathcal{R}^2$ Gravity



by

Shafia Maryam

(Registration No: 00000402924)

Supervised by

Dr. Mubasher Jamil

*A thesis submitted in the partial fulfillment of the requirements  
for a Master's Degree in Mathematics*

School of Natural Sciences

National University of Sciences and Technology (NUST)

Islamabad, Pakistan

(2024)

## THESIS ACCEPTANCE CERTIFICATE

Certified that final copy of MS thesis written by Shafia Maryam (Registration No 00000402924), of School of Natural Sciences has been vetted by undersigned, found complete in all respects as per NUST statutes/regulations, is free of plagiarism, errors, and mistakes and is accepted as partial fulfillment for award of MS/M.Phil degree. It is further certified that necessary amendments as pointed out by GEC members and external examiner of the scholar have also been incorporated in the said thesis.

Signature: \_\_\_\_\_

Name of Supervisor: Prof. Mubasher Jamil

Date: 11-10-2024

Signature (HoD): \_\_\_\_\_

Date: 11/10/2024



Signature (Dean/Principal): \_\_\_\_\_

Date: 17.11.2024

ET

**National University of Sciences & Technology****MS THESIS WORK**

We hereby recommend that the dissertation prepared under our supervision by: Shafia Maryam, Regn No. 00000402924, Titled Gravitational Lensing by Blackholes in General Relativity and R<sup>2</sup> Gravity be Accepted in partial fulfillment of the requirements for the award of MS degree.


**Examination Committee Members**1. Name: PROF. TOOBA FEROZESignature: 2. Name: DR. SAADI ISHAQSignature: Supervisor's Name PROF. MUBASHER JAMILSignature: 

  
Head-of Department

17/10/2024  
Date

**COUNTERSIGNED**

Dean/Principal 17/10/2024

  
Dean/Principal

*Dedicated to the inspiring memory of my father, Tauqeer Ahmed Aneel, and  
to my mother, Musarrat Nazir, for her unwavering support.*

# Acknowledgement

First and foremost; I would like to thank Almighty Allah, the most Gracious and the most Merciful, for blessing me with strength to complete this task. I would like to take this opportunity to express my gratitude to Dr. Mubasher Jamil for his encouragement and direction throughout the last year. I could not have asked for more knowledgeable and patient supervisor; it was a privilege to learn from him.

I sincerely appreciate my GEC members, Prof. Tooba Feroze and Dr. Saadi Ishaq, for their valuable comments.

I am grateful to my colleague, Ms. Nagina Rehman, for her assistance in my research. I acknowledge the insightful comments and suggestions by Dr. Khadije Jafarzade. Their remarks helped me to refine my work.

Lastly, I would like to extend my gratitude to my mother and both of my brothers for their unconditional support.

# Abstract

The phenomenon of gravitational lensing in both strong and weak deflection limits is discussed in this thesis. Solutions of Buchdahl's ODE in  $\mathcal{R}^2$  gravity are considered as spacetimes in this work. Weak deflection angle by the application of Gauss Bonnet theorem for asymptotically flat *special* Buchdahl-inspired metric was found and the magnification and image distortions are observed modeling M87\* black hole as a lens. Also, analytic expression for strong deflection angle is determined followed by modeling black holes Sgr A\* and M87\* as lens. On the basis of which image positions and separations are investigated. For the stationary axi-symmetric SBI solution in  $\mathcal{R}^2$  gravity, weak deflection angle is computed. Magnifications for primary and secondary images are explored by considering M87\* as a lens.

# Contents

<b>1</b>	<b>Introduction</b>	<b>1</b>
1.1	General relativistic dynamics . . . . .	7
1.1.1	Spacetime . . . . .	7
1.1.2	Black holes . . . . .	8
1.1.3	Geodesics . . . . .	10
1.1.4	Deflection of light . . . . .	12
1.1.5	Gravitational lensing . . . . .	12
1.1.6	Gauss Bonnet theorem . . . . .	13
1.1.7	The lens equation . . . . .	14
<b>2</b>	<b>Kerr Black Hole - Weak and Strong Gravitational Lensing</b>	<b>17</b>
2.1	Gravitational lensing in WDL . . . . .	17
2.1.1	Optical metric . . . . .	18
2.1.2	Deflection angle computation . . . . .	19
2.2	Gravitational lensing in SDL . . . . .	23
2.2.1	Equations for null geodesics . . . . .	24
2.2.2	Impact parameter . . . . .	25
2.2.3	Radius of photon sphere . . . . .	26
2.2.4	Deflection angle in SDL . . . . .	27

<b>3</b>	<b>Gravitational Lensing by <i>Special</i> Buchdahl-Inspired Metric</b>	<b>35</b>
3.1	Metric overview . . . . .	37
3.1.1	Asymptotic flatness of SBI metric . . . . .	38
3.2	Weak gravitational lensing in SBI spacetime . . . . .	39
3.2.1	The optical metric . . . . .	39
3.2.2	Deflection angle computation . . . . .	40
3.2.3	Image magnification and distortion . . . . .	42
3.3	Gravitational lensing in SDL . . . . .	50
3.3.1	Equations for null Geodesic . . . . .	50
3.3.2	Impact parameter . . . . .	51
3.3.3	Photon sphere . . . . .	52
3.3.4	Deflection angle in the strong field limits . . . . .	53
3.3.5	Observables . . . . .	56
<b>4</b>	<b>Gravitational Lensing by axi-symmetric SBI Metric in Pure <math>\mathcal{R}^2</math> Gravity</b>	<b>65</b>
4.1	Metric overview . . . . .	67
4.2	Event horizon and ergosphere . . . . .	68
4.3	Deflection angle in the weak field limit . . . . .	71
4.3.1	The optical metric . . . . .	71
4.3.2	OIA approach of Gauss Bonnet theorem . . . . .	72
4.3.3	Image magnification and distortion . . . . .	77
<b>5</b>	<b>Results and Discussions</b>	<b>84</b>



# List of Figures

1.1	First ever image of black hole M87* [1]. . . . .	2
1.2	First image of Sagittarius A* [2]. . . . .	3
1.3	The Canarias Einstein ring [3]. . . . .	6
1.4	Schematic diagram of Gauss Bonnet theorem [4]. A polygon $T$ with $n$ vertices is bounded by $n$ curves namely, $C_1, C_2, \dots, C_n$ . The jump angles (external angles) are represented by $\theta_n$ . . . . .	14
1.5	The lens diagram [5] for static and spherically symmetric spacetimes. The letters O, S and L represents the observer, light source and lens respectively. The impact parameter is given by $b$ and $\alpha$ is the deflection angle. . . . .	15
1.6	The lens diagram [6] for axi-symmetric spacetime. The prograde and retrograde motion of photons is depicted respectively by red and blue color. . . . .	16
2.1	The critical impact parameter $b_{sc}$ is plotted against spin parameter $a$ . The plot convention reads: Schwarzschild black hole (black), Kerr prograde (dashed red) and Kerr retrograde (dotted blue). . . . .	27

2.2	The spin parameter $a$ is plotted against coefficient $\bar{a}$ of deflection angle. The plot convention reads: Schwarzschild black hole (black) for $a = 0$ , Kerr prograde (dashed red) and Kerr retrograde (dotted blue). . . . .	31
2.3	The spin parameter $a$ is plotted against coefficient $\bar{b}$ of deflection angle, the plot convention reads: Schwarzschild black hole (black) for $a = 0$ , Kerr prograde (dashed red) and Kerr retrograde (dotted blue). . . . .	34
3.1	The weak deflection angle $\hat{\alpha}$ of SBI metric is plotted vs impact parameter $b$ for different values of Buchdahl parameter $\tilde{k}$ , corresponding to three different cases. The black curve shows the angle in WDL for Schwarzschild black hole. . . . .	42
3.2	Magnification of images for SBI spacetime is plotted against parameter $\mathcal{D}$ in WDL. For primary images, the tangential magnification $\mu_{pt}$ , radial magnification $\mu_{pr}$ and total magnification $\mu_p$ are graphed respectively in (a), (c) and (e) - against the dimensionless parameter $\mathcal{D}$ . For secondary images; the absolute tangential magnification $ \mu_{st} $ , the absolute radial magnification $ \mu_{sr} $ and the absolute total magnification $ \mu_s $ is plotted against the parameter $\mathcal{D}$ in (b), (d) and (f), each in order. Plot convention: The black, green and red curves are respectively representing the plots for parameter values $\tilde{k} = 0$ , $-0.5$ and $0.5$ . . . . .	47

3.3	Magnification of images for SBI spacetime is plotted against ratio $M/D_{OL}$ in WDL. For primary images, the tangential magnification $\mu_{pt}$ , radial magnification $\mu_{pr}$ and total magnification $\mu_p$ are graphed respectively in (a), (c) and (e) - against ratio $M/D_{OL}$ . For secondary images; the absolute tangential magnification $ \mu_{st} $ , the absolute radial magnification $ \mu_{sr} $ and the absolute total magnification $ \mu_s $ is plotted against $M/D_{OL}$ in (b), (d) and (f), each in order. Plot convention: The black, green and red curves are respectively representing the plots for parameter values $\tilde{k} = 0, -0.5$ and $0.5$ . . . . .	48
3.4	Logarithmic distortion is plotted for SBI spacetime in WDL. The logarithmic distortion of the primary images ( $\delta_p$ ) and the secondary images ( $\delta_s$ ) is plotted against angular position of source $\beta$ , distance parameter $\mathcal{D}$ and $M/D_{OL}$ in (a), (b) and (c), respectively. . . . .	49
3.5	The deflection angle $\hat{\alpha}$ of SBI metric is plotted vs impact parameter $b$ for two different values of Buchdahl parameter $\tilde{k}$ in SDL. The black curve represents the case of Schwarzschild black hole in SDL. . . . .	56
3.6	Einstein Rings of outermost relativistic images of SBI spacetime for $\tilde{k} = 0$ (orange), $\tilde{k} = 0.03$ (purple) and $\tilde{k} = -0.04$ (dashed) is depicted modelling supermassive black hole Sgr A* as a SBI lens. . . . .	60
3.7	Magnification of the outermost image for SBI spacetime for $\tilde{k} = 0$ (black), $\tilde{k} = 0.03$ (green) and $\tilde{k} = -0.04$ (red) has been plotted versus angular source position modelling Sgr A* as a SBI lens. . . . .	60

3.8	Formation of Einstein Rings of outermost relativistic images of SBI spacetime for $\tilde{k} = 0$ (orange), $\tilde{k} = 0.03$ (purple) and $\tilde{k} = -0.04$ (dashed) is demonstrated modelling massive black hole M87* as a SBI lens. . . . .	61
3.9	Magnification of the outermost image for SBI spacetime for $\tilde{k} = 0$ (black), $\tilde{k} = 0.03$ (green) and $\tilde{k} = -0.04$ (red) has been plotted versus angular source position modelling M87* as SBI spacetime lens. . . . .	62
4.1	Ergosphere is plotted for axi-symmetric spacetime in $\mathcal{R}^2$ gravity in WDL for $\tilde{k} = 0$ . Shaded pink region depicts ergoregion.	69
4.2	Ergosphere is plotted for axi-symmetric spacetime in $\mathcal{R}^2$ gravity in WDL for $\tilde{k} = 0.7$ . Shaded pink region depicts ergoregion.	70
4.3	Ergosphere is plotted for axi-symmetric spacetime in $\mathcal{R}^2$ gravity in WDL for $\tilde{k} = -0.4$ . Shaded pink region depicts ergoregion.	70
4.4	The weak deflection angle $\hat{\alpha}_{prog}$ for prograde light ray is plotted for different values of Buchdahl parameter $\tilde{k}$ against impact parameter $b$ for axi-symmetric spacetime. The spin is taken as $a = 0.3$ . . . . .	77

- 4.5 Magnification is plotted for axi-symmetric spacetime in  $\mathcal{R}^2$  gravity in WDL. Plots for tangential, radial and total magnifications versus the dimensionless parameter  $\mathcal{D}$  is given in (a), (b) and (c); each in order. In graphs (c), (d) and (f) respectively; tangential, radial and total magnifications are plotted against the ratio  $M/D_{OL}$ . Plot convention: Primary magnifications for  $\tilde{k} = -0.5, \tilde{k} = 0$  and  $\tilde{k} = 0.5$  are respectively represented by dashed blue, orange and green curves. Secondary magnifications for  $\tilde{k} = -0.5, \tilde{k} = 0$  and  $\tilde{k} = 0.5$  are respectively represented by solid black, red and green curves. . . . . 81
- 4.6 Logarithmic distortion is plotted for axi-symmetric metric in  $\mathcal{R}^2$  gravity. The primary logarithmic distortion ( $\delta_p$ ) and the secondary logarithmic distortion ( $\delta_s$ ) is plotted against angular position of source  $\beta$  in (a) and (b). The primary logarithmic distortion ( $\delta_p$ ) and secondary logarithmic distortion ( $\delta_s$ ) is plotted against the dimensionless parameter  $\mathcal{D}$  in (c) and (d). The primary( $\delta_p$ ) and secondary( $\delta_s$ ) logarithmic distortion is plotted against  $M/D_{OL}$  in (e) and (f). Plot convention: Primary logarithmic distortion for  $\tilde{k} = -0.5, \tilde{k} = 0$  and  $\tilde{k} = 0.5$  are respectively represented by dashed blue, orange and green curves. Secondary logarithmic distortion for  $\tilde{k} = -0.5, \tilde{k} = 0$  and  $\tilde{k} = 0.5$  are respectively represented by solid black, red and green curves. . . . . 82

# List of Tables

1.1	Types of gravitational lensing . . . . .	13
3.1	Some relativistic images observables estimates for SBI space-time in strong lensing using Sgr A* as a lens. Also, the lensing coefficients $\bar{a}$ and $\bar{b}$ for different values of Buchdahl parameter $\tilde{k}$ has been approximated. . . . .	59
3.2	Approximates for observables and strong lensing coefficients of SBIM in SDL, considering M87* black hole as a lens, for different values of Buchdahl parameter $\tilde{k}$ . . . . .	61

# List of Abbreviations

EHT	Event Horizon Telescope
GBT	Gauss Bonnet theorem
GR	General Relativity
KBH	Kerr Black Hole
ODE	Ordinary Differential Equation
OIA	Ono, Ishihara and Asada
SBH	Schwarzschild Black Hole
SBI	<i>Special</i> Buchdahl-Inspired
SDL	Strong Deflection Limit
WDL	Weak Deflection Limit
VLBI	Very-Long-Baseline Interferometry

# Chapter 1

## Introduction

I worked horribly strenuously,  
strange that one can endure  
that.

---

*A. Einstein*[7]

A global array of synchronized radio telescope known as Event Horizon Telescope (EHT) employing very-long-baseline interferometry (VLBI), in the year 2017, started to observe the massive black holes at the center of Milky Way and Messier 87 galaxies [8, 9]. Mission of the EHT and VLBI collaboration was to get images of the black holes and observe the lensing phenomenon such as shadows and Einstein rings. On 10<sup>th</sup> April, 2019 EHT collaboration captured the image of one of the black hole candidate M87\* in the center of galaxy M87 based on VLBI observations [10, 11]. A prominent aspect of the images produced is the ring surrounding a dark region in center- a black hole *shadow*.

In fact, the observations by EHT are indicating the phenomenon of *gravitational lensing*. According to theory of General Relativity (GR), the curvature of spacetime leads to deviation in straight line trajectory of photons.



This bending of light is based on the gravitational effect of the massive black holes. This in turn, makes the photons to orbit around black holes appearing as a bright ring around dark black hole.

First image of black hole M87\* at the center of massive galaxy Messier 87 shows a very bright region-*accretion disk* around black hole, can be seen in Figure 1.1. One side of ring appears brighter than other because of the Doppler effect. The dust/material orbiting around M87\*, when moving towards the observer, creates a bright ring. On the other side of ring, the material is moving away from the observer and consequently the light from the material appears dimmer. This orbiting of matter in disc like structure suggests that it (matter) is influenced by the spin of black hole. Thus, the asymmetry in the brightness also strongly indicates rotation of black hole M87\*. Overall, the image is consistent with the theoretical expectations of a rotating KBH.



Figure 1.1: First ever image of black hole M87\* [1].

The EHT collaboration provides crucial information featuring geometry of the spacetime of M87\*. The mass of central black hole of galaxy M87 is deduced to be  $(6.5 \pm 0.7) \times 10^9 M_{\odot}$ .

After this first successful scientific feat of EHT, the pursuit for the imaging of the other candidate black hole in the heart of Milky Way galaxy remained un-achieved until 2022. Direct visual evidence of the Sagittarius A\* black hole of our galaxy for the first time was revealed on 12<sup>th</sup> May, 2022 [12, 13, 14, 15]. Despite being small in mass relative to the black hole of galaxy Messier 87, Sgr A\* has a very similar picture for *shadow* as can be seen in Figure 1.2. The mass of Sgr A\* is inferred as  $4.1 \times 10^6 M_{\odot}$ .

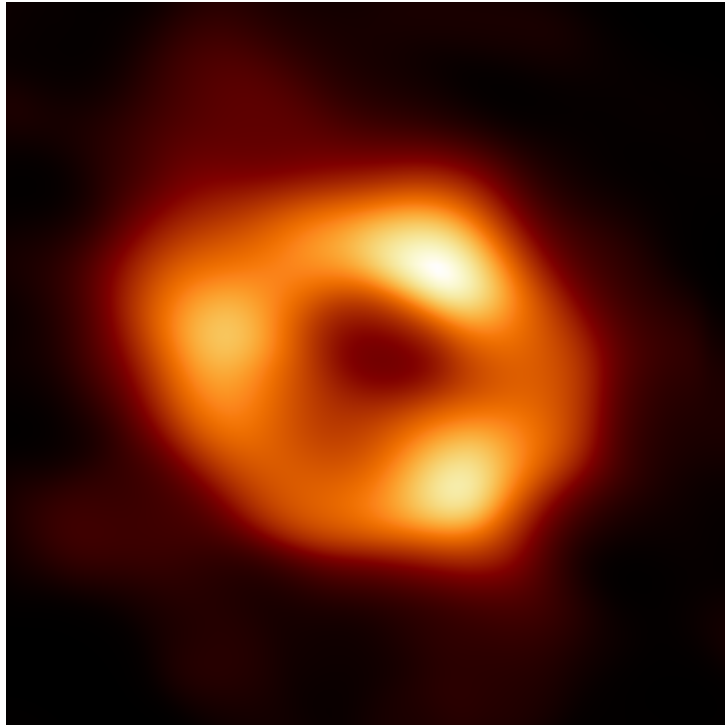


Figure 1.2: First image of Sagittarius A\* [2].

The detection of supermassive black holes M87\* and Sgr A\* located at the center of Messier 87 and Milky Way galaxies, respectively; have reignited interest of researchers in black hole astrophysics and Einstein's theory of GR. The ground-breaking discoveries by Event Horizon Telescope lead to fascinating start of era of gravitational lensing together with experimental tests of gravity.

Whilst the firsthand observations of astrophysical black holes have recently been established, they have been extensively theoretically researched for decades.

Einstein's GR theory was published in the year 1915 which describes gravity as a consequence of spacetime curvature- due to energy and mass [16]. Two of the major predictions of Einstein was existence of black hole phenomenon and bending of light caused by gravity. Einstein gave a set of differential equations, known as Einstein Field Equations (EFEs). A year past this development, Karl Schwarzschild produced first solution to the vacuum EFEs which described a black hole geometry of a static, spherically symmetric spacetime [17]. Then came the generalization of Schwarzschild black hole by Reissner and Nordström, in which electric charge was involved [18, 19]. Studies of the gravitational sources continued by many researchers. In the year 1963, marking the beginning of the golden age of black holes physics, Kerr found an exact solution to EFEs describing a rotating black hole [20].

Along with the development in solution of EFEs, the detection of black holes by experiment and theory establishment was carried out. In 1919, the experiment in solar eclipse was carried out to observe light deflection in the gravitational field of Sun [21]. Results revealed that in the neighbourhood of Sun, deflection of light can take place and the angle of deflection can be similar as demanded by Einstein. Following this detection, phenomenon of gravitational lensing was further developed by researchers including Liebes [22] (in 1964) and Refsdal [23] (in 1994) based on the work of Einstein [24].

Gravitational lensing in the vicinity of massive black holes provide avenue to test GR. Leveraging gravitational lensing; stars, black holes have been used as lenses to view/observe distant astronomical entities. This was

made possible by revolutionary work of Virbhadra and Ellis in the year 2000. They developed gravitational lens equation which was used to approximate Schwarzschild lensing numerically [25]. They demonstrated that strong deflection angle, in static spherically symmetric spacetimes, approaches infinity and multiple images are formulated. Bozza corroborated and further told that in the deflection angle, the divergence is logarithmic [26]. Bozza extended his works in lensing to compute analytical expression of spherically symmetric black holes [27]. Later Tsukamoto [28] also studied strong lensing of a static, asymptotically flat and spherically symmetric spacetime analytically. These works produced general expression of deflection angle in strong limits with two analytical lensing coefficients. Strong lensing for KBH with spin  $a$  and Kerr-Newman black hole with spin  $a$  and electric charge  $Q$  was studied in [6].

In 2008, weak deflection angle using the Gauss Bonnet theorem was discussed by Gibbons and Werner for an asymptotically flat spacetime [29]. Few years later, Werner independently extended this concept to stationary spacetimes [30]. He calculated deflection angle of rotating black holes, particularly Kerr-Randers optical geometry. These works presumed infinite distance of lens from the source and receiver. Ishihara et al. continued to apply GBT to the finite distance approach [31].

Einstein ring is a magnificent consequence of gravitational lensing in astrophysics. If a luminous source, distant observer and a gravitational lens are perfectly aligned then the photons bend due to gravitational field of the massive lens constructing an Einstein ring. It is very rare that an isolated gravitational lens forms a complete Einstein ring. An almost complete “Canarias Einstein ring” was observed in the year 2016 by M. Bettinelli and others [3]. The detected image is illustrated in Fig. (1.3). It is approximately

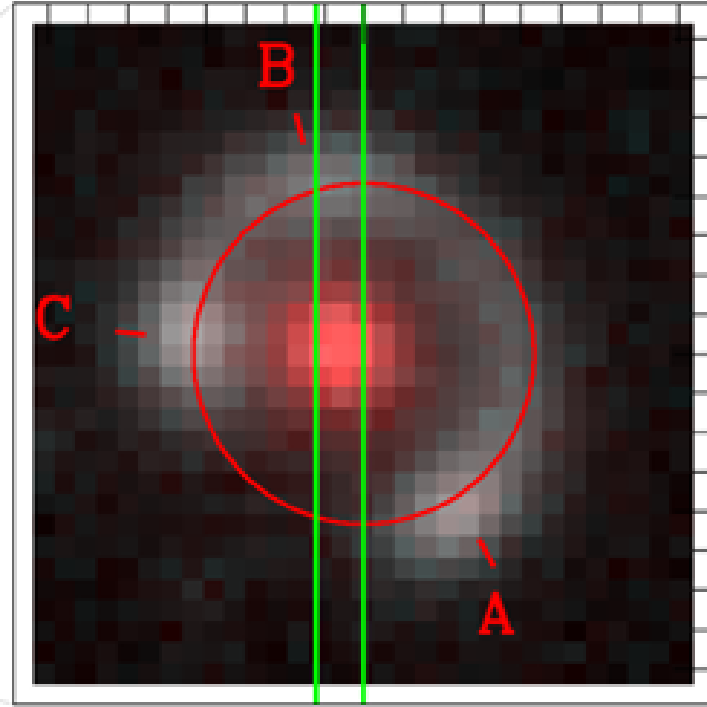


Figure 1.3: The Canarias Einstein ring [3].

300° circular ring.

The scientific feat of Event Horizon Telescope capturing images of black hole M87\* and Sgr A\* in the center of massive galaxies Messier 87 and Milky Way, respectively; provides overwhelming evidence of Einstein's general theory of relativity. Ceaseless development in the theoretical aspects of gravitational lensing, together with experimental image formulation and Einstein rings establishment is the true motivation behind this research.

***The structure of this thesis is as follows:*** This chapter focuses on some definitions and concepts in GR that are related to our work. Chapter 2 contains a comprehensive review of strong and weak deflection angles for a KBH. Remaining chapters are our new work. In Chapter 3, the analytic expression of deflection angle for *special* Buchdahl-inspired metric in strong and weak field limits is determined. Lensing phenomena such as Einstein

rings, angular separation of images and magnification is investigated. In Chapter 4, expressions for weak deflection angle for a axi-symmetric SBI metric in pure  $\mathcal{R}^2$  gravity are found. Magnification of primary and secondary images modeling M87\* as a lens has been investigated. Finally, Chapter 5 concludes the thesis with discussion and future work direction.

## 1.1 General relativistic dynamics

This section reviews some mathematical tools and techniques that are helpful to understand the concepts before readers delve into the rest of thesis.

### 1.1.1 Spacetime

In GR, three dimensional space and one dimensional time are both fused into a four dimensional entity called *spacetime*. The mathematical apparatus needed to describe this spacetime is known as *Manifold*. To learn about manifolds, readers can consult the book [32]. An important concern for any space is to find the distance between two points in it. To do so for a spacetime, *Metric tensor* is defined as a type  $(0, 2)$  tensor  $g$  as

$$g = g_{\mu\nu} dx^\mu \otimes dx^\nu. \quad (1.1)$$

The *line element*, which describes invariant distance between points  $x^\mu$  and  $x^\mu + dx^\mu$  on a smooth manifold, is often represented by the notation  $ds^2$

$$ds^2 = g_{\mu\nu} dx^\mu dx^\nu, \quad (1.2)$$

where  $g_{\mu\nu}$  denotes the covariant components of a metric tensor,  $dx^\mu$  and  $dx^\nu$  are the basis one-forms. In this thesis, spacetime as a Lorentzian manifold  $\mathcal{M}$  is considered for which the signature of the metric is  $(-, +, +, +)$ .

**Minkowski spacetime:** Einstein's field equation has simplest vacuum solution known as Minkowski spacetime. In the cartesian coordinates, its line element can mathematically be represented as

$$ds^2 = \eta_{\mu\nu} dx^\mu dx^\nu \equiv -dt^2 + dx^2 + dy^2 + dz^2. \quad (1.3)$$

For the manifold to be locally flat means that the line element  $g_{\mu\nu}$  metric reduces to Minkowski spacetime for which metric components attain the form

$$\eta_{\mu\nu} = \begin{pmatrix} -1 & 0 & 0 & 0 \\ 0 & 1 & 0 & 0 \\ 0 & 0 & 1 & 0 \\ 0 & 0 & 0 & 1 \end{pmatrix}. \quad (1.4)$$

### 1.1.2 Black holes

In the year 1783, John Michell proposed the concept of a dark star and its strong gravitational pull [33]. Later in the year 1796, Pierre-Simon Laplace also introduced the similar concept of compact dark objects with strong gravitational field [34]. Einstein revolutionized the concept of gravity through GR, leading to the theoretical existence of black hole.

The region of space where a compact mass (enormous mass tightly packed in a tiny volume with gravitational radius  $r = 2M$ ) deforms spacetime into a dark dense object called black hole. This region has the gravitational pull so strong that not even electromagnetic radiations, including light, are capable to escape.

#### a. Event horizon and the information loss paradox

Event horizon surrounds the black hole; it is the boundary which does not allow any matter once went inside its premises, to escape beyond into outside

world [35]. Often it is called as *a point of no return* with its escape velocity being equivalent to the speed of light.

The black hole information paradox is a conflict revolving around the question that what happens to all that matter or objects fallen inside a black hole. Classical physics suggests that when anything crosses the event horizon, there is no way out and all the information has then been lost for forever. The discovery of Stephen Hawking adds complexity with the concept that black holes emit Hawking radiations [36]. This means black holes gradually lose mass and thus will possibly evaporate ultimately. It leads to concerns that the information trapped inside the black hole will be destroyed or retained since principles of quantum mechanics are strongly in favour of preservation of physical information.

## b. Black hole spacetimes

Some examples of black hole spacetimes in GR are:

***Schwarzschild Spacetime:*** A year after the Einstein's remarkable theory of GR, in 1916, Karl Schwarzschild gave an exact vacuum solution of Einstein's field equations. It described an uncharged and non-rotating black hole. The line element of a SBH is described in [17] as

$$ds^2 = -f(r)dt^2 + \frac{1}{f(r)}dr^2 + r^2d\Omega^2, \quad (1.5)$$

where  $f(r) = 1 - \frac{2M}{r}$  and  $d\Omega^2 = d\theta^2 + \sin^2\theta d\phi^2$ . Also  $M$  is the black hole mass. The event horizon is defined by the radius  $r_{EH} = 2M$ . At  $r = 0$ , the Schwarzschild spacetime has point singularity.

***Kerr Spacetime:*** In 1963, Roy Kerr gave the solution to Einstein's field equation which described a rotating Kerr black hole [20]. In Boyer-Lindquist coordinates, the line element describing the geometry of uncharged, axi-



symmetric KBH as [37]

$$\begin{aligned}
ds^2 = & -\frac{\Delta - a^2 \sin^2 \theta}{\Sigma(r, \theta)} dt^2 - 2 \left( \frac{a \sin^2 \theta (2Mr)}{\Sigma(r, \theta)} \right) dt d\phi + \frac{\Sigma(r, \theta)}{\Delta} dr^2 + \Sigma(r, \theta) d\theta^2 \\
& + \left( (a^2 + r^2)^2 - \Delta a^2 \sin^2 \theta \right) \frac{\sin^2(\theta)}{\Sigma(r, \theta)} d\phi^2,
\end{aligned} \tag{1.6}$$

where  $\Delta = r^2 + a^2 - 2Mr$ , and  $\Sigma(r, \theta) = r^2 + a^2 \cos^2 \theta$ . Also, mass of the black hole is represented here by  $M$  and the spin parameter  $a$  is defined by angular momentum  $J = aM$ . For solving  $\Delta(r) = 0$ , there are two event horizons, inner ( $r_-$ ) and outer ( $r_+$ ). Expressions of which are as under

$$r_{\pm} = M \pm \sqrt{M^2 - a^2}. \tag{1.7}$$

Moreover, ring-shaped singularity for a KBH occurs when  $\Sigma(r, \theta) = 0$ .

### 1.1.3 Geodesics

Geodesics are described as shortest and straightest paths between two point in a curved Manifold. In spacetime, a geodesic is a curve  $\gamma$  whose tangent vector  $u^\mu$  moves in a parallel direction along the curve. This is mathematically expressed as:

$$u^\rho \nabla_\rho u^\mu = 0. \tag{1.8}$$

For a curve on a manifold to qualify as a geodesic, it is necessary that the direction of tangent vector remain constant but its magnitude may vary as it travels around the curve.

An affinely parameterized geodesic, denoted by  $\gamma(\lambda)$ , can be described in a particular coordinate system as a curve  $x^\mu(\lambda)$ , where  $\lambda$  is the affine parameter. The tangent vector to this geodesic is  $u^\mu = \dot{x}^\mu$ , where the over-dot denotes differentiation with respect to  $\lambda$ .

Mathematically, the geodesic equation obtained from Einstein field equations is used to describe geodesics. It can be expressed as follows:

$$\ddot{x}^\mu + \Gamma_{\nu\rho}^\mu \dot{x}^\nu \dot{x}^\rho = 0, \quad (1.9)$$

here  $x^\mu$  depicts the coordinates of particle,  $\Gamma_{\nu\rho}^\mu$  represents Christoffel symbol and the over dots here represents derivative of spacetime coordinates with respect to proper time.

### Types of geodesics

A geodesic  $\gamma$  with tangent vector  $u^\mu$  is classified based on the sign of  $g_{\mu\nu}u^\mu u^\nu$  along  $\gamma$ . It is timelike if  $g_{\mu\nu}u^\mu u^\nu < 0$  everywhere along  $\gamma$ , null if  $g_{\mu\nu}u^\mu u^\nu = 0$  everywhere along  $\gamma$ , and spacelike if  $g_{\mu\nu}u^\mu u^\nu > 0$  everywhere along  $\gamma$ . Timelike and null geodesics are collectively known as *causal geodesics* [38]. For a timelike geodesic, the proper time  $\tau$  measured along the curve is defined as

$$\tau = \int_\gamma \sqrt{-g_{\mu\nu}u^\mu u^\nu} d\tau. \quad (1.10)$$

The sign under the square root is negative because  $ds^2 < 0$  for timelike geodesics and the proper time is required to be real and positive. For a spacelike geodesic, the proper length  $\ell$  is defined as

$$\ell = \int_\gamma \sqrt{g_{\mu\nu}u^\mu u^\nu} d\lambda \quad (1.11)$$

For null geodesics, there is no meaningful definition of proper time or proper length, and they are considered to have zero proper time and proper length.

In the case of null geodesics, the norm  $u^\mu u_\mu$  is 0. The norm  $u^\mu u_\mu$  is +1 for spacelike geodesics (parameterised by proper length) and -1 for timelike geodesics (parameterised by proper time). A massless particle, like a photon,

follows a null geodesic in general relativity, whereas a freely falling hefty particle follows a timelike geodesic. Lightlike geodesic, light ray, and null geodesic are all interchangeable concepts.

#### 1.1.4 Deflection of light

Before the theory of GR was proposed, Einstein in 1911 claimed that propagation of light is influenced by gravity [39].

Light deflection occurs when massive objects, like stars or black holes, produce a gravitational field that causes the curvature of spacetime. As light rays approach such a massive body, the curvature of spacetime bends the path of photons leading to the deflection of light.

This effect has been observed with varying degrees of precision across distance scales ranging from  $10^{11}$  to  $10^{23}$  meters and mass scales from  $10^{-3}$  to  $10^{13}$  solar masses [40]. Gravitational lensing, a phenomenon in which massive objects such as black holes bend light due to curvature of spacetime from distant sources, is based on this deflection of light.

#### 1.1.5 Gravitational lensing

Gravitational lensing has developed into a powerful tool to analyse dark universe including black holes. It is a phenomenon that was predicted by theory of GR. A massive body causes the spacetime curvature due to gravity, which in turn bends the light around it. The corresponding body is called *gravitational lens* and the phenomenon is known as gravitational lensing. In general, it involves consequences of gravitational field influencing the electromagnetic radiation, described by light rays, propagation [41].

Gravitational lensing is characterized by three types:

***Weak gravitational lensing:*** The weak gravitational field of the dark

body produces distortion in the source galaxy. A single, highly deformed image is produced in weak lensing which has a magnification factor close to 1. It is often due to combination of foreground sources.

***Strong gravitational lensing:*** Strong lensing happens in presence of highly massive objects. The gravitational field of the dark object is very strong that multiple images of distant source of light is produced [42].

***Microlensing:*** Smaller compact objects, such as stars, lead to microlensing. It is a phenomenon when the stars or planets passes by any distant star and as a consequence, temporary brightness of the latter is observed. Multiple resolvable images are formed in this type of lensing [43].

Type of GL	Main Features	Astronomical purposes
Weak GL	Slight distortions in galaxy shapes	Map dark matter and large-scale structure
Strong GL	Einstein rings and multiple images	Investigate quasars and distant galaxies
Microlensing	Brighten distant stars	Detection of dark matter and exoplanets

Table 1.1: Types of gravitational lensing

### 1.1.6 Gauss Bonnet theorem

The Gauss Bonnet theorem that connects the topology and geometry of a surface is defined for a light source S and receiver R. Assume  $T$  (be a polygon) is a two dimensional orientable surface bounded by differentiable curves represented by  $\partial C_a$  with the jump angles  $\theta_a$  where  $a = (1, 2, \dots, n)$

[44]. Mathematically the GBT is expressed as

$$\int \int_T \mathcal{K} dS + \sum_{a=1}^n \int_{\partial C_a} \kappa_g d\ell + \sum_{a=1}^n \theta_a = 2\pi, \quad (1.12)$$

here  $\mathcal{K}$  is the Gaussian curvature of  $T$  with surface element  $dS$ , and  $\kappa_g$  denotes the geodesic curvature of  $\partial C_a$  with line element  $\ell$  along the boundary.

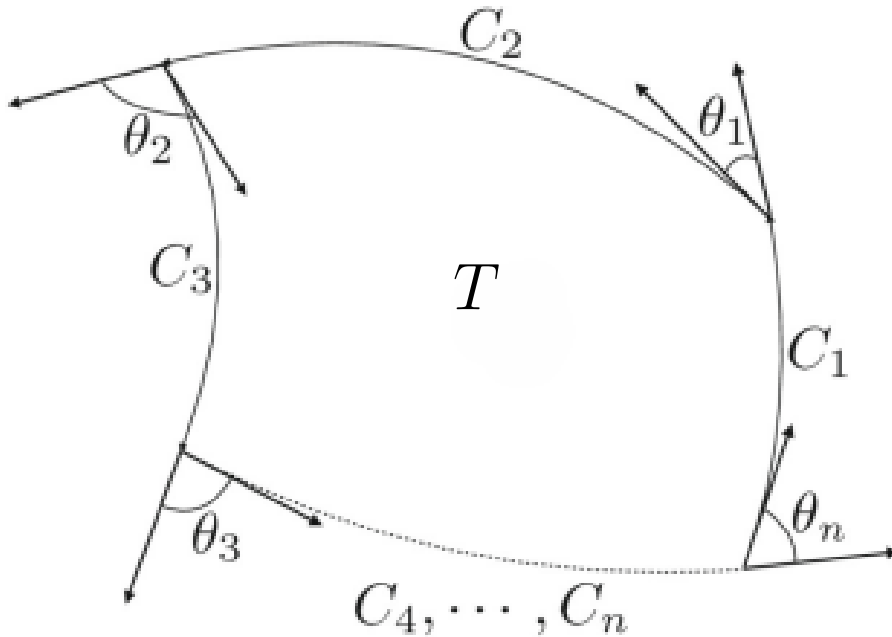


Figure 1.4: Schematic diagram of Gauss Bonnet theorem [4]. A polygon  $T$  with  $n$  vertices is bounded by  $n$  curves namely,  $C_1, C_2, \dots, C_n$ . The jump angles (external angles) are represented by  $\theta_n$ .

### 1.1.7 The lens equation

Ellis and Virbhadra introduced the lens equation for the sake of studying strong gravitational lensing phenomenon [25]. They applied it to investigate the Schwarzschild black hole lensing and obtained numerical observations. Later, without the choice of spacetime, exact form of lens equation was proposed by Frittelli et al. [45].

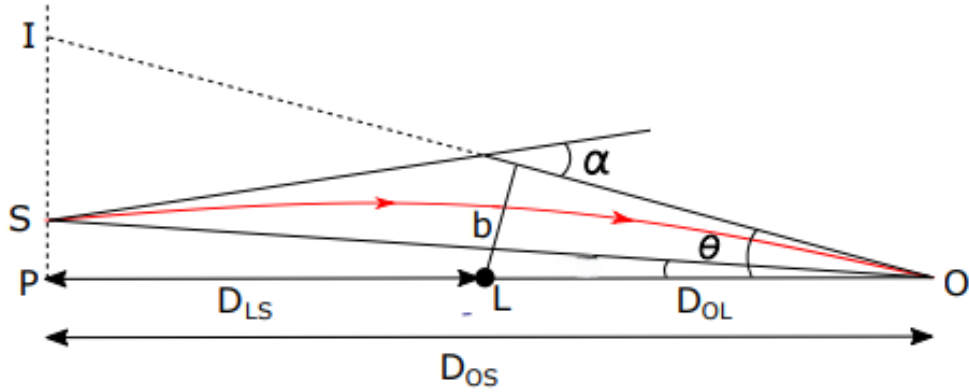


Figure 1.5: The lens diagram [5] for static and spherically symmetric spacetimes. The letters O, S and L represents the observer, light source and lens respectively. The impact parameter is given by  $b$  and  $\alpha$  is the deflection angle.

Consider the planar light rays case depicted in Fig. (1.6). Assume  $D_S$  and  $D_L$ , respectively, are the distance of light source and the deflector (lens) to the observer. The lens equation for both static spacetime (depicted in Fig. 1.5) and axi-symmetric spacetime (illustrated in Fig. 1.6) is expressed in the form [5, 6]:

$$\tan \beta = \tan \theta - \alpha, \quad (1.13)$$

where

$$\alpha = \frac{D_{LS}}{D_{OS}} \tan(\hat{\alpha} - \theta), \quad (1.14)$$

here  $\hat{\alpha}$  denotes the deflection angle. The Greek letters  $\theta$  and  $\beta$  represents angular image position and angular source position, respectively.  $D_{LS}$  symbolizes the distance between source and lens. Also, the distance between source and observer is denoted by  $D_{OS}$ .

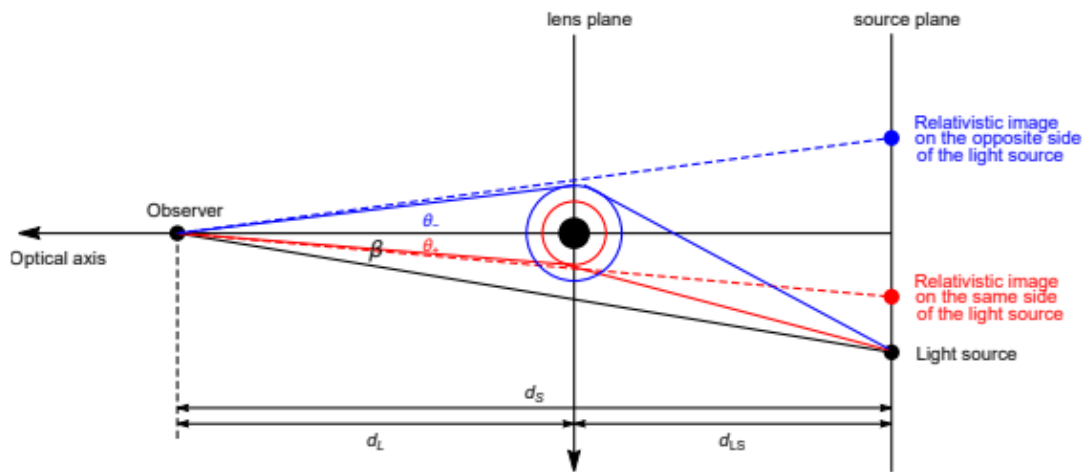


Figure 1.6: The lens diagram [6] for axi-symmetric spacetime. The prograde and retrograde motion of photons is depicted respectively by red and blue color.

# Chapter 2

## Kerr Black Hole - Weak and Strong Gravitational Lensing

This chapter is dedicated to the review of gravitational lensing, in the weak and strong field limits, of Kerr black hole. The analytic expressions of deflection angles for strong deflection and weak deflection are reanalyzed. Section 2.1 focuses on the review of weak gravitational lensing employing Gauss Bonnet theorem (GBT). Section 2.2 is devoted to the evaluation of strong gravitational lensing by axi-symmetric KBH. Nearly half a century past the establishment of Einstein's field equations, Roy P. Kerr gave the solution to equations in vacuum [20]. The line element of a Kerr black hole in Boyer-Lindquist coordinates  $\{t, r, \theta, \phi\}$  is expressed in (1.6).

### 2.1 Gravitational lensing in WDL

This section is centered on the OIA method to find deflection angle of a KBH in weak field limit using Gauss Bonnet theorem, readers may refer to the original reading of OIA [46]. Since Kerr metric is in polar coordinates,



the general form of line element of stationary axi-symmetric spacetime is given by [46]

$$ds^2 = -\mathcal{A}(r, \theta)dt^2 - 2\mathcal{H}(r, \theta)dtd\phi + \mathcal{B}(r, \theta)dr^2 + \mathcal{C}(r, \theta)d\theta^2 + \mathcal{D}(r, \theta)d\phi^2, \quad (2.1)$$

where metric coefficients are functions of  $r$  and  $\theta$  only.

### 2.1.1 Optical metric

The generalized form of optical metric represented by  $\gamma_{ij}$ , where  $i$  and  $j$  runs from 1 to 3, can be obtained using null condition  $ds^2 = 0$ . Solving this for the slice of time  $dt$ , according to OIA method [46, 47] leads optical metric as follows

$$dt = \sqrt{\gamma_{ij}dx^i dx^j} + \beta_i dx^i, \quad (2.2)$$

here  $\gamma_{ij}$  is defined as

$$\gamma_{ij}dx^i dx^j = \frac{\mathcal{B}(r, \theta)}{\mathcal{A}(r, \theta)}dr^2 + \frac{\mathcal{C}(r, \theta)}{\mathcal{A}(r, \theta)}d\theta^2 + \frac{\mathcal{A}(r, \theta)\mathcal{D}(r, \theta) + \mathcal{H}^2(r, \theta)}{\mathcal{A}^2(r, \theta)}d\phi^2, \quad (2.3)$$

and the component  $\beta_i$  is given as

$$\beta_i dx^i = -\frac{\mathcal{H}(r, \theta)}{\mathcal{A}(r, \theta)}d\phi. \quad (2.4)$$

For Kerr spacetime, using (1.6) and (2.1) leads to

$$\begin{aligned} \mathcal{A}(r, \theta) &= \frac{\Delta - a^2 \sin^2 \theta}{\Sigma(r, \theta)}, & \mathcal{B}(r, \theta) &= \frac{\Sigma(r, \theta)}{\Delta}, & \mathcal{C}(r, \theta) &= \Sigma(r, \theta), \\ \mathcal{D}(r, \theta) &= \left( (a^2 + r^2)^2 - \Delta a^2 \sin^2 \theta \right) \frac{\sin^2 \theta}{\Sigma(r, \theta)}, & \mathcal{H}(r, \theta) &= \left( \frac{a \sin^2 \theta (2Mr)}{\Sigma(r, \theta)} \right). \end{aligned} \quad (2.5)$$

Using (2.5) in (2.3), we get

$$\begin{aligned} \gamma_{ij}dx^i dx^j &= \frac{\Sigma^2}{\Delta(\Sigma - 2Mr)}dr^2 + \frac{\Sigma^2}{\Sigma - 2Mr}d\theta^2 \\ &+ \frac{(\Sigma - 2Mr)(a^2 + r^2) + 2a^2 Mr \sin^2 \theta}{(\Sigma - 2Mr)^2} \Sigma \sin^2 \theta d\phi^2. \end{aligned} \quad (2.6)$$

Also substituting expressions of  $\mathcal{A}(r, \theta)$  and  $\mathcal{H}(r, \theta)$  from (2.5) into (2.4), the component  $\beta_i$  has the form

$$\beta_i dx^i = -\frac{2Mar \sin^2 \theta}{\Sigma - 2Mr} d\phi. \quad (2.7)$$

### 2.1.2 Deflection angle computation

According to OIA method, general expression of deflection angle  $\hat{\alpha}$  for a source  $S$  and receiver  $R$  using Gauss Bonnet theorem in axi-symmetric space-time reads [46, 47]

$$\hat{\alpha} = - \int \int_{R^\infty S^\infty} \mathcal{K} dS + \int_S^R \kappa_g dl, \quad (2.8)$$

here  $\mathcal{K}$  represents Gaussian curvature and the geodesic curvature of light rays is denoted by  $\kappa_g$ . Further  $dl$  and  $dS$  represents the arc length and surface element, respectively. For  $dl > 0$  and  $dl < 0$ , the photons orbit around the black hole respectively in prograde and retrograde direction.

#### Surface integral of Gaussian curvature

The Gaussian curvature is defined in relation to Riemann tensor as [30]

$$\mathcal{K} = \frac{R_{r\phi r\phi}}{\gamma} = \frac{1}{\sqrt{\gamma}} \left[ \frac{\partial}{\partial \phi} \left( \frac{\sqrt{\gamma}}{\gamma_{rr}} \Gamma_{rr}^\phi \right) - \frac{\partial}{\partial r} \left( \frac{\sqrt{\gamma}}{\gamma_{rr}} \Gamma_{r\phi}^\phi \right) \right]. \quad (2.9)$$

For equatorial lensing, we take  $\theta = \frac{\pi}{2}$  and  $\dot{\theta} = 0$ . For a Kerr spacetime

$$\gamma = \det \gamma_{ij} = \frac{r^5}{(r - 2M)^3}. \quad (2.10)$$

Use of (2.10) and the optical metric (2.6) with  $\theta = \frac{\pi}{2}$  in (2.9) gives Gaussian curvature for a KBH as below

$$\mathcal{K} = \frac{M [r(6M^2 - 7Mr + 2r^2) - 6a^2(M - r)]}{(2M - r)r^5}. \quad (2.11)$$

Expanding the above into series results in

$$\mathcal{K} = -\frac{2M}{r^3} + \mathcal{O}\left(\frac{M^2}{r^4}, \frac{a^2 M}{r^5}\right). \quad (2.12)$$

In the expression of Gaussian curvature, we truncate the higher order terms because of weak gravitational field and slow rotation. Next task is to find the expression of surface element for a KBH which is

$$dS = \sqrt{\det \gamma_{ij}} dr d\phi = \sqrt{\frac{r^5}{(r-2M)^3}} dr d\phi. \quad (2.13)$$

Since the Gaussian curvature  $\mathcal{K}$  for a KBH begins with  $\mathcal{O}(M)$ , therefore linear order of surface element is enough in our computation of deflection angle. Therefore, we expand the series of (2.13) as follows

$$dS = \left[3M + r + \mathcal{O}\left(\frac{M^2}{r}\right)\right] dr d\phi. \quad (2.14)$$

With the use of Gaussian curvature (2.12) and the surface element (2.14), the surface integral in the weak deflection limits can be found as

$$\begin{aligned} - \int \int_{R^\infty S^\infty} \mathcal{K} dS &= - \int_{r_{OE}}^{\infty} dr \int_{\phi_S}^{\phi_R} d\phi \left(-\frac{2M}{r^3}\right) (r + 3M) + \mathcal{O}\left(\frac{M^2}{r^3}\right), \\ &= - \int_{r_{OE}}^{\infty} dr \int_{\phi_S}^{\phi_R} d\phi \left(-\frac{2M}{r^2}\right) + \mathcal{O}\left(\frac{M^2}{r^3}\right), \\ &= 2M \int_{\infty}^{r_{OE}} dr \int_{\phi_S}^{\phi_R} d\phi \left(-\frac{1}{r^2}\right) + \mathcal{O}\left(\frac{M^2}{r^3}\right). \end{aligned} \quad (2.15)$$

Now that the straight line approximation in *zeroth* order gives  $r = \frac{b}{\sin \phi}$ , making the substitution  $u = r^{-1}$  implies that  $u = \frac{\sin \phi}{b}$ . Surface integral (2.15) attains the form

$$\begin{aligned} - \int \int_{R^\infty S^\infty} \mathcal{K} dS &= 2M \int_0^{\frac{\sin \phi}{b}} du \int_{\phi_S}^{\phi_R} d\phi + \mathcal{O}(M^2 u^3), \\ &= \frac{2M}{b} \int_{\phi_S}^{\phi_R} \sin \phi d\phi + \mathcal{O}(M^2 u^3), \\ &= \frac{2M}{b} [\cos \phi_S - \cos \phi_R] + \mathcal{O}(M^2 u^3), \end{aligned}$$

$$= \frac{2M}{b} \left[ \sqrt{1 - b^2 u_S^2} + \sqrt{1 - b^2 u_R^2} \right] + \mathcal{O}(M^2 u^3). \quad (2.16)$$

The last line is obtained by making use of the substitution  $\sin \phi_S = bu_S$  and  $\sin \phi_R = bu_R$ .

### Path integral of geodesic curvature

Geodesic curvature  $\kappa_g$  for axi-symmetric spacetime, as given by OIA [46]

$$\kappa_g = -\frac{1}{\sqrt{\gamma\gamma^{\theta\theta}}} \beta_{\phi,r}. \quad (2.17)$$

The component  $\gamma^{\theta\theta}$  is the reciprocal of  $\gamma_{\theta\theta}$  since the metric  $\gamma_{ij}$  is purely diagonal (2.6). Using (2.6), (2.7) and (2.17);  $\kappa_g$  for Kerr spacetime has the expression

$$\begin{aligned} \kappa_g &= -\frac{1}{\sqrt{\left(\frac{r^8}{(2M-r)^4}\right) \left(-\frac{2M-r}{r^3}\right)}} \frac{2aM}{(2M-r)^2}, \\ &= -\frac{2aM}{r^{5/2} \sqrt{r-2M}}. \end{aligned}$$

Series expansion of the above leads to further simplified form

$$\kappa_g = -\frac{2aM}{r^3} + \mathcal{O}\left(\frac{aM^2}{r^4}\right). \quad (2.18)$$

In order to evaluate the path integral, the arc length element  $dl$  is required. The photon orbit has a linear approximation  $r = \frac{b}{\cos \phi}$  and  $l = b \tan \phi$ , which yields

$$dl = \frac{b}{\cos^2 \phi} d\phi. \quad (2.19)$$

Using (2.18) and (2.19), path integral of geodesic curvature can be determined as follows

$$\begin{aligned}
\int_S^R \kappa_g dl &= \int_S^R -\frac{2aM}{r^3} dl + \mathcal{O}\left(\frac{aM^2}{r^4}\right), \\
&= -\frac{2aM}{b^2} \int_{\phi_S}^{\phi_R} \cos \phi d\phi + \mathcal{O}\left(\frac{aM^2}{b^3}\right), \\
&= \frac{2aM}{b^2} [\sin \phi_S - \sin \phi_R] + \mathcal{O}\left(\frac{aM^2}{b^3}\right),
\end{aligned}$$

with the use of  $\sin \phi_S = \sqrt{1 - b^2 u_S^2}$  and  $\sin \phi_R = -\sqrt{1 - b^2 u_R^2}$  as mentioned in Appendix A of [46]

$$\int_S^R \kappa_g dl = \pm \frac{2aM}{b^2} \left[ \sqrt{1 - b^2 u_S^2} + \sqrt{1 - b^2 u_R^2} \right] + \mathcal{O}\left(\frac{aM^2}{b^3}\right). \quad (2.20)$$

Note that  $\pm$  comes from  $dl$  since it has positive sign for prograde motion of light ray and negative sign for retrograde motion of light ray.

### Weak deflection angle

Now that the surface integral and path integral of Gaussian curvature and geodesic curvature, respectively; have been obtained, it is straightforward to assess the deflection angle expression in WDL. Through the use of (2.16), (2.20) in (2.8), the deflection angle in finite distance is determined as follows

$$\hat{\alpha} = - \int \int_{R^\infty S^\infty} \mathcal{K} dS - \int_R^S \kappa_g dl. \quad (2.21)$$

In prograde and retrograde photon orbits, the deflection angles respectively are:

$$\hat{\alpha}_{prog} = \frac{2M}{b} \left[ \sqrt{1 - b^2 u_S^2} + \sqrt{1 - b^2 u_R^2} \right] - \frac{2aM}{b^2} \left[ \sqrt{1 - b^2 u_S^2} + \sqrt{1 - b^2 u_R^2} \right], \quad (2.22)$$

$$\hat{\alpha}_{retro} = \frac{2M}{b} \left[ \sqrt{1 - b^2 u_S^2} + \sqrt{1 - b^2 u_R^2} \right] + \frac{2aM}{b^2} \left[ \sqrt{1 - b^2 u_S^2} + \sqrt{1 - b^2 u_R^2} \right]. \quad (2.23)$$

This is for the finite distance of source  $S$  and observer  $R$ . For far distance limit, there is  $u_R \rightarrow 0$  and  $u_S \rightarrow 0$ . Therefore, for infinite distance limit (2.22) and (2.23) are respectively expressed in the form

$$\hat{\alpha}_{prog} = \frac{4M}{b} - \frac{4aM}{b^2}. \quad (2.24)$$

$$\hat{\alpha}_{retro} = \frac{4M}{b} + \frac{4aM}{b^2}. \quad (2.25)$$

Note that weak deflection angle for prograde and retrograde motion of light rays for far distance is given for leading order in weak field approximation. Higher order terms  $\mathcal{O}\left(\frac{M^2}{b^3}\right)$  have been truncated. Now setting spin parameter  $a = 0$ , the deflection angle in WDL is brought to the form

$$\hat{\alpha} = \frac{4M}{b}, \quad (2.26)$$

which is a known deflection angle in WDL for Schwarzschild spacetime [29]. There is no concept of prograde or retrograde motion of light ray here since SBH is not a rotating black hole. Thus our analysis of deflection angle in WDL for axi-symmetric KBH is reliable with SBH.

## 2.2 Gravitational lensing in SDL

This section contains a comprehensive review of computation of strong deflection angle of light by a KBH following the article [6]. Here, the geodesic equations are examined for a KBH. The radius of photon sphere and the respective critical impact parameter is also discussed as they serve a primary role in computation of deflection angle. The general deflection angle expression in SDL for impact parameter  $b$  can be described as [6]

$$\hat{\alpha}(b) = -\bar{a} \log\left(\frac{b}{b_c} - 1\right) + \bar{b} + \mathcal{O}((b - b_c) \log(b - b_c)), \quad (2.27)$$

here  $b_c$  is the critical impact parameter,  $\bar{a}$  and  $\bar{b}$  are the coefficients of deflection angle. The line element of KBH is given by the equations (1.6), according to which the metric components are stated as follows

$$\begin{aligned} g_{tt} &= -\frac{\Delta - a^2 \sin^2 \theta}{\Sigma(r, \theta)}, & g_{rr} &= \frac{\Sigma(r, \theta)}{\Delta}, & g_{\theta\theta} &= \Sigma(r, \theta), \\ g_{t\phi} &= -\left(\frac{a \sin^2 \theta (2Mr)}{\Sigma(r, \theta)}\right), & g_{\phi\phi} &= \left((a^2 + r^2)^2 - \Delta a^2 \sin^2 \theta\right) \frac{\sin^2(\theta)}{\Sigma(r, \theta)}. \end{aligned} \quad (2.28)$$

The Lagrangian of a free particle with 4-velocity  $u^\mu$  is defined as

$$\mathcal{L} = \frac{1}{2} g_{\mu\nu} u^\mu u^\nu. \quad (2.29)$$

The Kerr metric admits two Killing vectors, one for time translation symmetry and another for axi-symmetry. The conserved energy and angular momentum are given by 4-velocity of photon together with Killing vectors as

$$\varepsilon = u^\mu \xi_{(t)}^\mu \quad \ell = u^\mu \xi_{(\phi)}^\mu \quad (2.30)$$

The time-like Killing vector  $\xi_{(t)}^\mu = (1, 0, 0, 0)$  is related to conservation of energy  $\varepsilon$ . Conservation of angular momentum  $\ell$  around the axis of symmetry can be explained by space-like Killing vector  $\xi_{(\phi)}^\mu = (0, 0, 0, 1)$ . Since KBH is rotating, the impact parameter  $b_s$  is defined as

$$b_s = s \left| \frac{\ell}{\varepsilon} \right| = sb, \quad (2.31)$$

here  $s$  tells about direction of light ray relative to the rotation of black hole.  $s = +1$  specifies prograde orbiting of light whereas  $s = -1$  refers to retrograde motion of light.

### 2.2.1 Equations for null geodesics

To find the deflection angle in equatorial plane, set  $\theta = \pi/2$  thereafter  $\dot{\theta} = 0$  in expression (2.28). With the use of Euler-Lagrange equation for null

geodesics ( $ds^2 = 0$ ),  $\dot{\phi}$  and  $\dot{r}$ , provided below

$$\dot{\phi} = -\frac{\varepsilon g_{t\phi} + \ell g_{tt}}{g_{t\phi}^2 - g_{\phi\phi} g_{tt}}, \quad (2.32)$$

$$\dot{r} = \sqrt{\frac{1}{g_{rr}} \left( \frac{\varepsilon^2 g_{\phi\phi} + \ell^2 g_{tt} + 2\varepsilon\ell g_{t\phi}}{g_{t\phi}^2 - g_{\phi\phi} g_{tt}} \right)}. \quad (2.33)$$

For Kerr spacetime being cognizant of  $\theta = \pi/2$ , (2.28) and (2.32) gives

$$\dot{\phi} = \frac{1}{r^2} \left[ (l - a\varepsilon) + \frac{a(\varepsilon(r^2 + a^2) - a\ell)}{r^2 + a^2 - 2Mr} \right]. \quad (2.34)$$

(2.33) for Kerr spacetime is as follows

$$\begin{aligned} \dot{r}^2 &= \ell^2 \left[ \left( \frac{\varepsilon}{\ell} \right)^2 + \frac{a^2}{r^2} \left( \frac{\varepsilon}{\ell} \right)^2 + \frac{2Ma^2}{r^3} \left( \frac{\varepsilon}{\ell} \right)^2 - \frac{4Ma}{r^3} \left( \frac{\varepsilon}{\ell} \right) - \frac{1}{r^2} + \frac{2M}{r^3} \right], \\ &= \ell^2 \left[ \frac{1}{b^2} + \frac{a^2}{r^2 b^2} + \frac{2Ma^2}{r^3 b^2} - \frac{4Ma}{r^3 b_s} - \frac{1}{r^2} + \frac{2M}{r^3} \right]. \end{aligned} \quad (2.35)$$

Simple algebraic manipulation brings the equation of motion for radial direction in the form

$$\frac{1}{b^2} = \frac{\dot{r}^2}{\ell^2} + V_{\text{eff}}(r), \quad (2.36)$$

where  $V_{\text{eff}}(r)$  is the effective potential

$$V_{\text{eff}}(r) = \frac{1}{r^2} \left[ 1 - \frac{a^2}{b^2} - \frac{2M}{r} \left( 1 - \frac{a}{b_s} \right)^2 \right]. \quad (2.37)$$

## 2.2.2 Impact parameter

Assume that a light ray from region at spatial infinity advances towards the black hole and returns to an observer in asymptotic region at some ‘‘turning point’’  $r_{tp}$ . The impact parameter  $b$  at  $r_{tp}$  can be found [6]

$$\frac{\dot{r}^2}{\ell^2} \Big|_{r=r_{tp}} = 0. \quad (2.38)$$

Solving for  $b$ , the desired expression of impact parameter for KBH becomes

$$b(r_{tp}) = \frac{1}{2M - r_{tp}} \left[ 2sMa - r_{tp} \sqrt{a^2 + r^2 - 2Mr} \right]. \quad (2.39)$$



### 2.2.3 Radius of photon sphere

The radius of photon sphere  $r_{sc}$  is the minimum distance of a light particle where the curvature of black hole makes the photon to orbit around it. Mathematically it can be found by the maximum of effective potential as

$$\left. \frac{dV_{\text{eff}}}{dr} \right|_{r_{tp}=r_{sc}} = 0, \quad (2.40)$$

Using (2.37) and (2.40), we get

$$r_{sc} = 3M \frac{\left(1 - \frac{a}{b_{sc}}\right)}{\left(1 + \frac{a}{b_{sc}}\right)}. \quad (2.41)$$

The expression of critical impact parameter  $b_{sc}$  is required, for which (2.38) reads

$$r_{tp}^3 - r_{tp}(b(r_{tp})^2 - a^2) + 2M(b_s - a)^2 = 0, \quad (2.42)$$

now that  $r_{tp} \rightarrow r_{sc}$ , hence  $b_s \rightarrow b_{sc}$  implies

$$r_{sc}^3 - r_{sc}(b(r_{sc})^2 - a^2) + 2M(b_{sc} - a)^2 = 0. \quad (2.43)$$

Substitution of (2.41) in (2.43) gives

$$(b_{sc} + a)^3 - 27M^2(b_{sc} - a) = 0. \quad (2.44)$$

Separately rewriting (2.44) for prograde motion  $s = +1$  and retrograde orbiting  $s = -1$ :

$$\begin{aligned} (b_{+c} + a)^3 - 27(b_{+c} + a)M^2 + 54M^2a &= 0, \\ (b_{-c} - a)^3 - 27(b_{-c} - a)M^2 - 54M^2a &= 0, \end{aligned} \quad (2.45)$$

these are cubic equations and the roots can be found using Vieta method,

$$\begin{aligned} b_{+c} &= -a + 6M \cos \left[ \frac{1}{3} \arccos \left( -\frac{a}{M} \right) \right], \\ b_{-c} &= -a - 6M \cos \left[ \frac{1}{3} \arccos \left( \frac{a}{M} \right) \right], \end{aligned} \quad (2.46)$$

writing together both cases in (2.46) as

$$b_{sc} = -a + s6M \cos \left[ \frac{1}{3} \arccos \left( -\frac{sa}{M} \right) \right]. \quad (2.47)$$

This is the critical impact parameter  $b_{sc}$  for Kerr spacetime, the plot is given as in Fig.(2.1). Substitution of (2.47) into (2.44) and then resulting equation into (2.41) gives the radius of photon sphere

$$r_{sc} = 2M \left[ 1 + \cos \left\{ \frac{2}{3} \arccos \left( -\frac{sa}{M} \right) \right\} \right]. \quad (2.48)$$

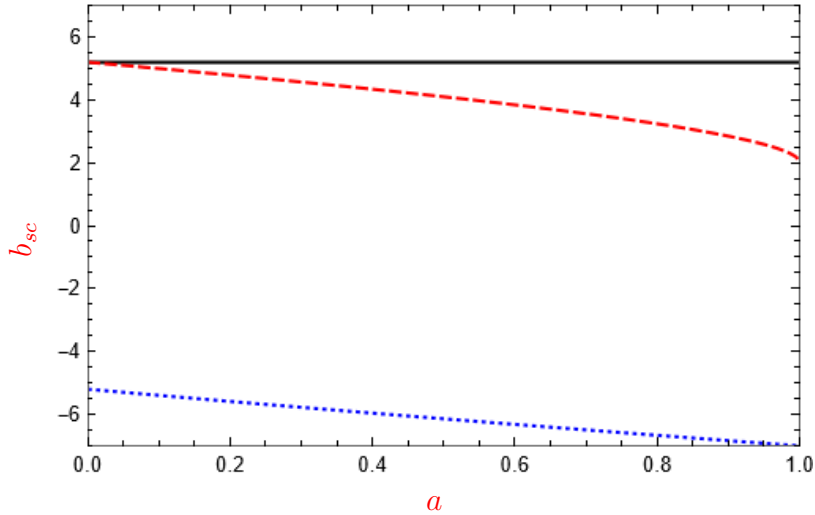


Figure 2.1: The critical impact parameter  $b_{sc}$  is plotted against spin parameter  $a$ . The plot convention reads: Schwarzschild black hole (black), Kerr prograde (dashed red) and Kerr retrograde (dotted blue).

## 2.2.4 Deflection angle in SDL

The calculations for the coefficients  $\bar{a}$  and  $\bar{b}$  of strong lensing are proceeded by defining the variable [6]

$$z = 1 - \frac{r_{tp}}{r}. \quad (2.49)$$

By chain rule, differentiation of  $z$  with respect to  $\phi$

$$\frac{dz}{d\phi} = \frac{dz}{dr} \frac{dr}{d\phi} \equiv \frac{r_{tp} \dot{r}}{r^2 \dot{\phi}}. \quad (2.50)$$

Using geodesic equations  $\dot{r}$  and  $\dot{\phi}$  from (2.34) and (2.35) into (2.50) yields

$$\frac{dz}{d\phi} = \frac{r_{tp} \left(1 - \frac{2M}{r} + \frac{a^2}{r^2}\right)}{\left(1 - \frac{2M}{r} \left(1 - \frac{a}{b_s}\right)\right)} \sqrt{\frac{1}{b^2} - \frac{1}{r^2} \left(1 - \frac{a^2}{b^2}\right) + \frac{2M}{r^3} \left(1 - \frac{a}{b_s}\right)^2}. \quad (2.51)$$

Elimination of  $r$  from (2.49) and (2.51) leads to the form

$$\frac{dz}{d\phi} = \frac{1 - \frac{2M}{r_{tp}}(1-z) + \frac{a^2}{r_{tp}^2}(1-z)^2}{r_{tp} \left[1 - \frac{2M}{r_{tp}}(1-z) \left(1 - \frac{a}{b_s}\right)\right]} \sqrt{B(z, r_{tp})}, \quad (2.52)$$

here  $B(z, r_{tp}) = c_1(r_{tp})z + c_2(r_{tp})z^2 + c_3(r_{tp})z^3$  is a trinomial in  $z$  with coefficients  $c_1$ ,  $c_2$  and  $c_3$  as follows

$$\begin{aligned} c_1(r_{tp}) &= -6Mr_{tp} \left(1 - \frac{a}{b_s}\right)^2 + 2r_{tp}^2 \left(1 - \frac{a^2}{b^2}\right), \\ c_2(r_{tp}) &= 6Mr_{tp} \left(1 - \frac{a}{b_s}\right)^2 - r_{tp}^2 \left(1 - \frac{a^2}{b^2}\right), \\ c_3(r_{tp}) &= -2Mr_{tp} \left(1 - \frac{a}{b_s}\right)^2. \end{aligned} \quad (2.53)$$

Reciprocating (2.52), one gets

$$\frac{d\phi}{dz} = r_{tp} \frac{1 - \frac{2M}{r_{tp}} \left(1 - \frac{a}{b_s}\right) + \frac{2M}{r_{tp}} \left(1 - \frac{a}{b_s}\right) z}{\left[1 - \frac{2M}{r_{tp}} + \frac{a^2}{r_{tp}^2} + \left(\frac{2M}{r_{tp}} - 2\frac{a^2}{r_{tp}^2}\right) z + \frac{a^2}{r_{tp}^2} z^2\right] \sqrt{B(z, r_{tp})}}, \quad (2.54)$$

solving by partial fraction leads to the form

$$\frac{d\phi}{dz} = \frac{r_{tp}^2}{a^2} \left[ \frac{C_-}{z - z_-} + \frac{C_+}{z - z_+} \right] \frac{r_{tp}}{\sqrt{B(z, r_{tp})}}, \quad (2.55)$$

where the coefficients  $C_+$  and  $C_-$  and the roots  $z_+$  and  $z_-$  are found respectively as

$$\begin{aligned} C_+ &= \frac{-a^2 + 2Mr_+ \left(1 - \frac{a}{b_s}\right)}{2r_{tp}\sqrt{M^2 - a^2}}, \\ C_- &= \frac{a^2 - 2Mr_- \left(1 - \frac{a}{b_s}\right)}{2r_{tp}\sqrt{M^2 - a^2}}, \\ z_+ &= 1 - \frac{r_{tp}r_+}{a^2}, \\ z_- &= 1 - \frac{r_{tp}r_-}{a^2}. \end{aligned} \quad (2.56)$$

The deflection angle is defined as under

$$\hat{\alpha}(r_{tp}) = I(r_{tp}) - \pi, \quad (2.57)$$

where

$$I(r_{tp}) = \int_0^1 f(z, r_{tp}) dz. \quad (2.58)$$

With the use of (2.55), the integrand becomes

$$f(z, r_{tp}) = \frac{r_{tp}^2}{a^2} \left[ \frac{C_-}{z - z_-} + \frac{C_+}{z - z_+} \right] \frac{2r_{tp}}{\sqrt{B(z, r_{tp})}}, \quad (2.59)$$

for strong deflection limit  $r_{tp} \rightarrow r_{sc}$  implies  $c_1(r_{tp}) \rightarrow 0$ . Also then  $f(z, r_{tp})$  has the term  $\frac{1}{z}$  which gives rise to the logarithmic divergence for very small value of  $z$ , hence we break the function  $f$  into two parts, namely divergent  $f_D$  and regular  $f_R$  by defining

$$f_D(z, r_{tp}) = \frac{r_{tp}^2}{a^2} \left[ \frac{C_-}{z - z_-} + \frac{C_+}{z - z_+} \right] \frac{2r_{tp}}{\sqrt{c_1(r_{tp})z + c_2(r_{tp})z^2}}. \quad (2.60)$$

The regular part which gives finite value of integral develops as

$$f_R(z, r_{tp}) = f(z, r_{tp}) - f_D(z, r_{tp}). \quad (2.61)$$

The integral of divergent part is first evaluated

$$\begin{aligned}
I_D(r_{tp}) &= \int_0^1 f_D(z, r_{tp}) dz, \\
&= \frac{2r_{tp}^3}{a^2} \int_0^1 \left[ \frac{C_-}{z - z_-} + \frac{C_+}{z - z_+} \right] \frac{1}{\sqrt{c_1(r_{tp})z + c_2(r_{tp})z^2}} dz.
\end{aligned} \tag{2.62}$$

Using *WolframAlpha*, the above integral is computed as

$$\begin{aligned}
I_D(r_{tp}) &= \frac{2r_{tp}^3}{a^2} \left\{ \frac{C_-}{\sqrt{c_1(r_{tp})z_- + c_2(r_{tp})z_-^2}} \right. \\
&\quad \times \log \left[ \frac{\sqrt{c_1(r_{tp})z_- + c_2(r_{tp})z_-} + \sqrt{c_1(r_{tp}) + c_2(r_{tp})z_-}}{\sqrt{c_1(r_{tp})z_- + c_2(r_{tp})z_-} - \sqrt{c_1(r_{tp}) + c_2(r_{tp})z_-}} \right] \\
&\quad + \frac{C_+}{\sqrt{c_1(r_{tp})z_+ + c_2(r_{tp})z_+^2}} \\
&\quad \left. \times \log \left[ \frac{\sqrt{c_1(r_{tp})z_+ + c_2(r_{tp})z_+} + \sqrt{c_1(r_{tp}) + c_2(r_{tp})z_+}}{\sqrt{c_1(r_{tp})z_+ + c_2(r_{tp})z_+} - \sqrt{c_1(r_{tp}) + c_2(r_{tp})z_+}} \right] \right\}.
\end{aligned} \tag{2.63}$$

In SDL, we know that  $r_{tp} \rightarrow r_{sc}$  implies  $c_1(r_{tp}) \rightarrow 0$ . Thus  $c_1(r_{sc}) \equiv c_{1sc} = 0$  relates  $c_{2sc}$  with  $c_{3sc}$  as  $c_{3sc} = -\frac{2}{3}c_{2sc}$ . Also the series expansion of  $c_1(r_{tp})$  and  $b(r_{tp})$  gives (truncating higher order terms)

$$c_1(r_{tp}) = c_{1sc} + c'_{1sc}(r_{tp} - r_{sc}) + \mathcal{O}(r_{tp} - r_{sc})^2, \tag{2.64}$$

$$b(r_{tp}) = b_{sc} + \frac{b''_{sc}}{2}(r_{tp} - r_{sc})^2 + \mathcal{O}(r_{tp} - r_{sc})^3, \tag{2.65}$$

rewriting  $c_1(r_{tp})$  in desired form

$$\lim_{r_{tp} \rightarrow r_{sc}} c_1(r_{tp}) = \lim_{b \rightarrow b_{sc}} c'_{1sc} \left( \frac{b}{b_{sc}} - 1 \right)^{1/2} \sqrt{\frac{2b_{sc}}{b''_{sc}}}. \tag{2.66}$$

Thereby, applying SDL on (2.63), we get

$$\begin{aligned}
I_D(b) &= - \left( \frac{r_{sc}^3 C_{-sc}}{a^2 \sqrt{c_{2sc} z_{-sc}^2}} + \frac{r_{sc}^3 C_{+sc}}{a^2 \sqrt{c_{2sc} z_{+sc}^2}} \right) \log \left( \frac{b}{b_{sc}} - 1 \right) + \frac{r_{sc}^3}{a^2} \frac{C_{-sc}}{\sqrt{c_{2sc} z_{-sc}^2}} \\
&\quad \times \log \left( \frac{16c_{2sc}^2 z_{-sc}^2 b''_{sc}}{c_{1sc}^2 2b_{sc} (z_{-sc} - 1)^2} \right) + \frac{r_{sc}^3}{a^2} \frac{C_{-sc}}{\sqrt{c_{2sc} z_{-sc}^2}} \log \left( \frac{16c_{2sc}^2 z_{-sc}^2 b''_{sc}}{c_{1sc}^2 2b_{sc} (z_{-sc} - 1)^2} \right).
\end{aligned} \tag{2.67}$$

Now that divergent part has been determined, comparison of (2.67) and right hand side of (2.27) describes the coefficient  $\bar{a}$  (plotted in Fig. 2.2) and the contribution of  $I_D(b)$  in  $\bar{b}$  respectively as

$$\bar{a} = \frac{r_{sc}^3 C_{-sc}}{a^2 \sqrt{c_{2sc} z_{-sc}^2}} + \frac{r_{sc}^3 C_{+sc}}{a^2 \sqrt{c_{2sc} z_{+sc}^2}}, \quad (2.68)$$

and

$$b_D = \bar{a} \log \left( \frac{8c_{2sc}^2 b''_{sc}}{c_{1sc}^2 b_{sc}} \right) + \frac{2r_{sc}^3}{\sqrt{c_{2sc}}} \left\{ \frac{C_{-sc}}{r_{sc} r_- - a^2} \log \left( 1 - \frac{a^2}{r_{sc} r_-} \right) + \frac{C_{+sc}}{r_{sc} r_+ - a^2} \log \left( 1 - \frac{a^2}{r_{sc} r_+} \right) \right\} \quad (2.69)$$

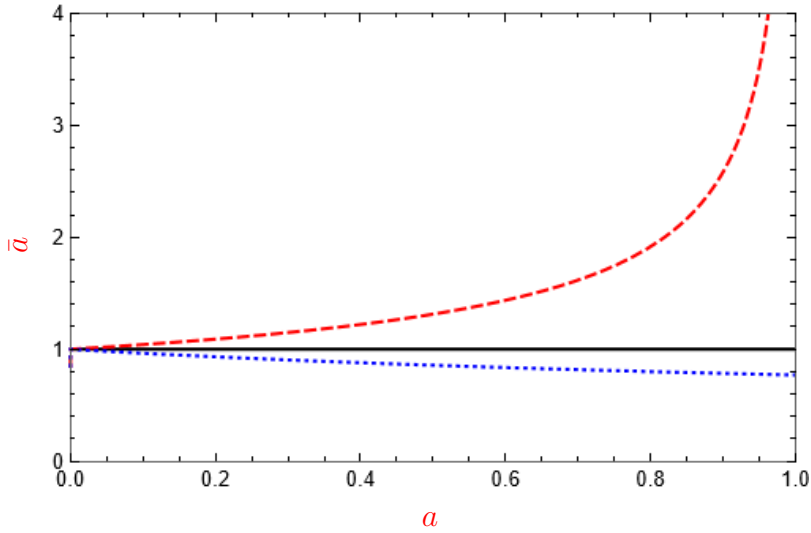


Figure 2.2: The spin parameter  $a$  is plotted against coefficient  $\bar{a}$  of deflection angle. The plot convention reads: Schwarzschild black hole (black) for  $a = 0$ , Kerr prograde (dashed red) and Kerr retrograde (dotted blue).

Now for regular part in SDL, the contribution in  $\bar{b}$  denoted by  $b_R$  after

applying strong deflection limit becomes

$$\begin{aligned}
b_R &= \int_0^1 f_R(z, r_{sc}) dz \\
&= \frac{2r_{sc}^3}{a^2} \frac{C_{-sc}}{\sqrt{c_{2sc}z_{-sc}}} \log \left( \frac{z_{-sc}c_{3sc}}{4(z_{-sc}-1)c_{2sc}} \frac{\sqrt{c_{2sc}+c_{3sc}}+\sqrt{c_{2sc}}}{\sqrt{c_{2sc}+c_{3sc}}-\sqrt{c_{2sc}}} \right) + \frac{C_{-sc}}{\sqrt{c_{2sc}+c_{3sc}z_{-sc}z_{-sc}}} \\
&\times \frac{2r_{sc}^3}{a^2} \log \left( \frac{\sqrt{c_{2sc}+c_{3sc}z_{-sc}}+\sqrt{c_{2sc}}}{\sqrt{c_{2sc}+c_{3sc}z_{-sc}}-\sqrt{c_{2sc}}} \frac{\sqrt{c_{2sc}+c_{3sc}z_{-sc}}-\sqrt{c_{2sc}+c_{3sc}}}{\sqrt{c_{2sc}+c_{3sc}z_{-sc}}+\sqrt{c_{2sc}+c_{3sc}}} \right) \\
&+ \frac{2r_{sc}^3}{a^2} \frac{C_{+sc}}{\sqrt{c_{2sc}z_{+sc}}} \log \left( \frac{z_{+sc}c_{3sc}}{4(z_{+sc}-1)c_{2sc}} \frac{\sqrt{c_{2sc}+c_{3sc}}+\sqrt{c_{2sc}}}{\sqrt{c_{2sc}+c_{3sc}}-\sqrt{c_{2sc}}} \right) + \frac{C_{+sc}}{\sqrt{c_{2sc}+c_{3sc}z_{+sc}z_{+sc}}} \\
&\times \frac{2r_{sc}^3}{a^2} \log \left( \frac{\sqrt{c_{2sc}+c_{3sc}z_{+sc}}+\sqrt{c_{2sc}}}{\sqrt{c_{2sc}+c_{3sc}z_{+sc}}-\sqrt{c_{2sc}}} \frac{\sqrt{c_{2sc}+c_{3sc}z_{+sc}}-\sqrt{c_{2sc}+c_{3sc}}}{\sqrt{c_{2sc}+c_{3sc}z_{+sc}}+\sqrt{c_{2sc}+c_{3sc}}} \right).
\end{aligned} \tag{2.70}$$

The coefficient  $\bar{b}$  is defined combining the contribution of regular and divergent part as follows

$$\bar{b} = -\pi + b_R + b_D. \tag{2.71}$$

In SDL,  $c_{1sc} = 0$ . Thus using  $c_1$  from (2.53), we get

$$3Mr_{sc} \left(1 - \frac{a}{b_{sc}}\right)^2 = r_{sc}^2 \left(1 - \frac{a^2}{b^2}\right). \tag{2.72}$$

Substitute this in the coefficient  $c_2$  of (2.53), we get

$$c_{2sc} = 3Mr_{sc} \left(1 - \frac{a}{b_{sc}}\right)^2. \tag{2.73}$$

Comparison of (2.73) with the coefficient  $c_3$  in (2.53) for  $r_{tp} \rightarrow r_{sc}$  yields the relation as follows

$$c_{3sc} = -\frac{2}{3}c_{2sc}. \tag{2.74}$$

Using this relation (2.74) and expression of  $z_+$  and  $z_-$  in  $b_R$  and then making

required substitutions in (2.71), we get

$$\begin{aligned}
\bar{b} = & \frac{2a\sqrt{3}r_{sc}^3 C_{-sc}}{(a^2 - 2r_{sc}r_-)\sqrt{c_{2sc}(a^2 + 2r_{sc}r_-)}} \\
& \times \log \left[ \frac{\sqrt{a^2 + 2r_{sc}r_-} - a}{\sqrt{a^2 + 2r_{sc}r_-} + a} \times \frac{\sqrt{a^2 + 2r_{sc}r_-} + \sqrt{3}a}{\sqrt{a^2 + 2r_{sc}r_-} - \sqrt{3}a} \right] \\
& + \frac{2a\sqrt{3}r_{sc}^3 C_{+sc}}{(a^2 - 2r_{sc}r_+)\sqrt{c_{2sc}(a^2 + 2r_{sc}r_+)}} \\
& \times \log \left[ \frac{\sqrt{a^2 + 2r_{sc}r_+} - a}{\sqrt{a^2 + 2r_{sc}r_+} + a} \times \frac{\sqrt{a^2 + 2r_{sc}r_+} + \sqrt{3}a}{\sqrt{a^2 + 2r_{sc}r_+} - \sqrt{3}a} \right] \\
& + \bar{a} \log \left( \frac{36}{7 + 4\sqrt{3}} \frac{8b_{sc}'' c_{2sc}^2}{c_{1sc}^2 b_{sc}} \right) - \pi.
\end{aligned} \tag{2.75}$$

For spin  $a = 0$ , the expressions of  $\bar{a}$  and  $\bar{b}$  for Kerr spacetime reduces to that for Schwarzschild black hole as follows:

$$\begin{aligned}
\bar{a} &= 1, \\
\bar{b} &= -\pi + \log \left[ 216(7 - 4\sqrt{3}) \right] \equiv -0.40023.
\end{aligned} \tag{2.76}$$

## Summary

This chapter contained a comprehensive review of gravitational lensing by a KBH. In section 2.1, we analyzed the weak gravitational lensing. In weak field limits, deflection angle of axi-symmetric Kerr spacetime was determined using Gauss Bonnet theorem. For spin  $a \rightarrow 0$ , the expression of bending angle can be seen to reduce to that of Schwarzschild spacetime. In section 2.2 assessment of strong gravitational lensing has been done. Equations of null geodesics are computed and the analytical expressions of strong lensing coefficients  $\bar{a}$  and  $\bar{b}$  are also evaluated. Results of deflection angle for Kerr spacetime successfully match to that of Schwarzschild black hole in strong deflection limit. The strong deflection angle coefficients are also visually depicted in figure 2.2 and 2.3 for strong lensing.



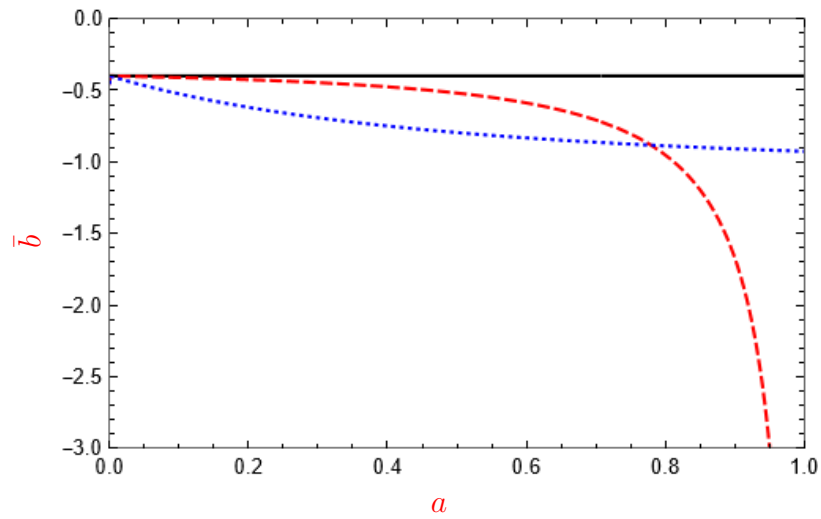


Figure 2.3: The spin parameter  $a$  is plotted against coefficient  $\bar{b}$  of deflection angle, the plot convention reads: Schwarzschild black hole (black) for  $a = 0$ , Kerr prograde (dashed red) and Kerr retrograde (dotted blue).

## Chapter 3

# Gravitational Lensing by *Special* Buchdahl-Inspired Metric

The marvellous work of Einstein, namely General Relativity theory, has been most successful physical theory to study the wide-ranging astronomical phenomena in over a century now. He predicted about deflection of light due to spacetime curvature leading to the phenomenon of gravitational lensing. Recently, the achievement of Event Horizon Telescope to produce the images of massive M87\* black hole at the center of galaxy M87 followed by imaging of Sgr A\* black hole at the heart of Milky Way corroborated Einstein's postulate of light deflection phenomenon [10, 48].

The gravitational lensing in the weak deflection limits (WDL) has been actively explored in the past 25 years by researchers [25, 29, 49]. Gauss Bonnet theorem (GBT), which relates spacetime geometry to its topology, is one of the methods to compute deflection angle in WDL. To do so, GBT was first employed by Gibbons and Werner [29] and was later investigated extensively

by other researchers in late 2010's [46, 50]. Gravitational lensing in strong deflection limits was first investigated in [26] and later in [28]. They gave the general expressions of the deflection angle defining two strong gravitational lensing coefficients  $\bar{a}$  and  $\bar{b}$ . Moreover M. Bettinelli, M. Simioni and others reported a discovery of an optical Einstein ring which led to substantiation of the luminous source[3]. This instigated the interest of researchers in Einstein ring observation.

The exclusive pure  $\mathcal{R}^2$  gravity theory, was discovered by Hans A. Buchdahl in early 1960's. Soon after, he launched a program to seek static spherically symmetric class of metrics for pure  $\mathcal{R}^2$  action. Unfortunately, he did not finish his goal despite being very close to it. His work terminated after formulation of a second-order Buchdahl ODE [51], which was left unnoticed until recently. The original second order *non-linear* ordinary differential equation as given in [51] is as follows:

$$2t \frac{d^2q}{dt^2} + \left( \frac{1+t}{1-t} - \frac{3k^2}{4q^2} \right) \frac{dq}{dt} = 0, \quad (3.1)$$

where  $k$  is the Buchdahl parameter.

Nguyen resumed the work and solved the Buchdahl's second-order ordinary differential equation questing the metric coefficients [52]. The action in pure  $\mathcal{R}^2$  gravity is given by:

$$\mathcal{S} = \int d^4x \sqrt{-g} \mathcal{R}^2. \quad (3.2)$$

The vacuo field equations resulting from this action is as follows

$$\mathcal{R} \left( \mathcal{R}_{\mu\nu} - \frac{1}{4} g_{\mu\nu} \mathcal{R} \right) + g_{\mu\nu} \square \mathcal{R} - \nabla_\mu \nabla_\nu \mathcal{R} = 0. \quad (3.3)$$

The analytic vacuum solutions of this 4th order equation which are a novel class of metrics, named Buchdahl-inspired metrics [52]. Extending his work in the following year, he found an asymptotically flat solution in the exhaustive

class of those metrics. Since the metric is Ricci scalar flat and non-Ricci flat, thus is asymptotically flat and was titled *special* Buchdahl-inspired (SBI) metric. This static, asymptotically flat metric is very interesting as it involves a free Buchdahl parameter  $\tilde{k}$ . For  $\tilde{k} = 0$ , the SBI metric reduces to Schwarzschild spacetime. Moreover, it is mentioned in [53] that for different real values of Buchdahl parameter, SBI metric corresponding geometries. For  $\tilde{k} \in (-\infty, -1) \cup (0, +\infty)$ , the metric allows the behaviour of naked singularity. For  $\tilde{k} \in (-1, 0)$ , the metric behaves like a traversable Morris–Thorne wormhole, which is a two way wormhole. For very specific choice  $\tilde{k} = -1$ , the metrics becomes some non- Schwarzschild structure.

This explicit chapter is structured as : Section 3.1 is devoted to the brief overview of the *special* Buchdahl-inspired metric. Section 3.2 investigates weak gravitational lensing of the aforementioned spacetime, deflection angle is computed making use of Gauss Bonnet theorem. Observables (magnification and image distortion) of corresponding images in WDL considering black hole M87\* as a lens will also be discussed. Section 3.3 produces analytical expression of deflection angle in SDL. Moreover, lensing observables such as image positions and Einstein rings are also estimated.

### 3.1 Metric overview

SBI metric characterising a static, spherically symmetric vacuum configuration, is described by [54]

$$ds^2 = \left|1 - \frac{r_s}{r}\right|^{\tilde{k}} \left\{ -\left(1 - \frac{r_s}{r}\right) dt^2 + \left(\frac{\rho(r)}{r}\right)^4 \frac{dr^2}{1 - \frac{r_s}{r}} + \left(\frac{\rho(r)}{r}\right)^2 r^2 d\Omega^2 \right\}, \quad (3.4)$$

where the function  $\rho(r)$  is related to radial co-ordinate following

$$\left(\frac{\rho(r)}{r}\right)^2 = \frac{\zeta^2 \left|1 - \frac{r_s}{r}\right|^{\zeta-1}}{(1-s) \left|1 - \frac{r_s}{r}\right|^\zeta} \left(\frac{r_s}{r}\right)^2. \quad (3.5)$$

The script  $s$  is set for  $\pm 1$  which signifies the sign of  $(1 - \frac{r_s}{r})$ . The parameter  $\tilde{k}$  is the re-scaled Buchdahl parameter and  $r_s$  plays the role of Schwarzschild radius

$$\tilde{k} := \frac{k}{r_s}, \quad \zeta := \sqrt{1 + 3\tilde{k}^2}, \quad . \quad (3.6)$$

where both  $\tilde{k}$  and the parameter  $\zeta$  are dimensionless.

Since focus of this research is the computation of deflection angle and studying lensing observables for SBI metric, the region  $r > r_s$  is considered. This means that in the line element (3.4)  $s = +1$  shall be studied onwards. Henceforth, the metric is represented as

$$ds^2 = \left(1 - \frac{r_s}{r}\right)^{\tilde{k}} \left\{ -\left(1 - \frac{r_s}{r}\right) dt^2 + \left(\frac{\rho(r)}{r}\right)^4 \frac{dr^2}{1 - \frac{r_s}{r}} + \left(\frac{\rho(r)}{r}\right)^2 r^2 d\Omega^2 \right\}, \quad (3.7)$$

and  $\rho(r)$  is restated as per

$$\left(\frac{\rho(r)}{r}\right)^2 = \frac{\zeta^2 \left(1 - \frac{r_s}{r}\right)^{\zeta-1}}{\left(1 - \left(1 - \frac{r_s}{r}\right)^\zeta\right)^2} \left(\frac{r_s}{r}\right)^2. \quad (3.8)$$

### 3.1.1 Asymptotic flatness of SBI metric

In general; a static and spherically symmetric spacetime has the line element described by [28]

$$ds^2 = -\mathcal{A}(r)dt^2 + \mathcal{B}(r)dr^2 + \mathcal{C}(r)d\Omega^2 \quad (3.9)$$

where  $d\Omega^2 = d\theta^2 + \sin^2\theta d\phi^2$ . To check for asymptotic flatness, the behaviour of spacetime metric is examined at spatial infinity in the following manner

$$\begin{aligned} \lim_{r \rightarrow \infty} \mathcal{A}(r) &= 1, \\ \lim_{r \rightarrow \infty} \mathcal{B}(r) &= 1, \\ \lim_{r \rightarrow \infty} \mathcal{C}(r) &= r^2. \end{aligned} \quad (3.10)$$

Note that the conditions given in (3.10) ensure asymptotic flatness since these lead (3.9) to the Minkowski spacetime. In comparison with the SBI spacetime (3.7) the components of the metric acquire the form

$$\begin{aligned}\mathcal{A}(r) &= \left(1 - \frac{r_s}{r}\right)^{\tilde{k}} \left(1 - \frac{r_s}{r}\right), \\ \mathcal{B}(r) &= \left(1 - \frac{r_s}{r}\right)^{\tilde{k}} \left(\frac{\rho(r)}{r}\right)^4 \frac{1}{1 - \frac{r_s}{r}}, \\ \mathcal{C}(r) &= \left(1 - \frac{r_s}{r}\right)^{\tilde{k}} \left(\frac{\rho(r)}{r}\right)^2 r^2.\end{aligned}\tag{3.11}$$

At spatial infinity, (3.11) becomes Minkowski spacetime (3.10) for all the values of  $\tilde{k}$ . Therefore SBI metric is categorized now as a asymptotically flat spacetime.

## 3.2 Weak gravitational lensing in SBI spacetime

It is discussed in the section (3.1) that the SBI spacetime is static, asymptotically flat and spherically symmetric. In order to find deflection angle in WDL, the GBT is applied on the optical metric of the SBI metric.

### 3.2.1 The optical metric

Consider SBI metric described by line element in (3.7). Since it is spherically symmetric, set  $\theta = \frac{\pi}{2}$  to restrict light rays to orbit in the equatorial plane. This reduces  $d\Omega^2 = d\theta^2 + \sin^2\theta d\phi^2$  to  $d\phi^2$ , thereby attaining the new line element

$$ds^2 = \left(1 - \frac{r_s}{r}\right)^{\tilde{k}} \left\{ - \left(1 - \frac{r_s}{r}\right) dt^2 + \left(\frac{\rho(r)}{r}\right)^4 \frac{dr^2}{1 - \frac{r_s}{r}} + \left(\frac{\rho(r)}{r}\right)^2 r^2 d\phi^2 \right\},\tag{3.12}$$

To derive the optical metric  $dt^2 = \bar{g}_{ij} dx^i dx^j$  where  $i, j$  can be  $\{r, \phi\}$ , making the use of null geodesic condition  $ds^2 = 0$  leads to

$$\left(1 - \frac{r_s}{r}\right)^{\bar{k}} \left\{ - \left(1 - \frac{r_s}{r}\right) dt^2 + \left(\frac{\rho(r)}{r}\right)^4 \frac{dr^2}{1 - \frac{r_s}{r}} + \left(\frac{\rho(r)}{r}\right)^2 r^2 d\phi^2 \right\} = 0.$$

Algebraic rearranging for  $dt^2$  results in

$$dt^2 = \left(\frac{\rho(r)}{r}\right)^4 \frac{dr^2}{\left(1 - \frac{r_s}{r}\right)^2} + \left(\frac{\rho(r)}{r}\right)^2 \frac{r^2}{1 - \frac{r_s}{r}} d\phi^2. \quad (3.13)$$

Therefore, rewriting the optical metric (3.13) for SBI spacetime in the form

$$dt^2 = \bar{g}_{rr} dr^2 + \bar{g}_{\phi\phi} d\phi^2, \quad (3.14)$$

where

$$\bar{g}_{rr} = \left(\frac{\rho(r)}{r}\right)^4 \frac{1}{\left(1 - \frac{r_s}{r}\right)^2} \quad \text{and} \quad \bar{g}_{\phi\phi} = \left(\frac{\rho(r)}{r}\right)^2 \frac{r^2}{1 - \frac{r_s}{r}}. \quad (3.15)$$

### 3.2.2 Deflection angle computation

Gibbon and Werner demonstrated that weak deflection angle for asymptotically flat spacetime can be calculated for the observer and the source, at spatial infinity, in the weak field approximation as [29]

$$\hat{\alpha} = - \int \int_{D_\infty} \mathcal{K} dS, \quad (3.16)$$

where  $\mathcal{K}$  represents the Gaussian curvature and  $dS$  is a surface element. The Gaussian curvature provides information about curvature of the spacetime and its mathematical form can be found in [55] (see page 147) as

$$\mathcal{K} = - \frac{1}{\sqrt{\bar{g}_{rr}\bar{g}_{\phi\phi}}} \left[ \frac{\partial}{\partial r} \left( \frac{1}{\sqrt{\bar{g}_{rr}}} \frac{\partial}{\partial r} (\sqrt{\bar{g}_{\phi\phi}}) \right) + \frac{\partial}{\partial \phi} \left( \frac{1}{\sqrt{\bar{g}_{\phi\phi}}} \frac{\partial}{\partial \phi} (\sqrt{\bar{g}_{rr}}) \right) \right]. \quad (3.17)$$

Since SBI metric is independent of  $\phi$ , thereby Gaussian curvature reads

$$\mathcal{K} = - \frac{1}{\sqrt{\bar{g}_{rr}\bar{g}_{\phi\phi}}} \left[ \frac{\partial}{\partial r} \left( \frac{1}{\sqrt{\bar{g}_{rr}}} \frac{\partial}{\partial r} (\sqrt{\bar{g}_{\phi\phi}}) \right) \right]. \quad (3.18)$$

Now using the components of optical metric (3.15),  $\mathcal{K}$  becomes

$$\mathcal{K} = -\frac{\left(1 - \frac{r_s}{r}\right)^2 \left[1 - \left(1 - \frac{r_s}{r}\right)\zeta\right]^3}{r_s^2 \zeta^3 \left(1 - \frac{r_s}{r}\right)^{\zeta/2}}. \quad (3.19)$$

The surface element of the optical metric is defined by the relation

$$dS = \sqrt{\det \bar{g}_{ij}} dx^i dx^j \equiv \sqrt{\bar{g}_{rr} \bar{g}_{\phi\phi}} dr d\phi. \quad (3.20)$$

Substitution of  $\bar{g}_{rr}$  and  $\bar{g}_{\phi\phi}$  for SBI metric in (3.20) yields

$$dS = \frac{r_s^3 \zeta^3 \left(1 - \frac{r_s}{r}\right)^{3\zeta/2}}{r^2 \left(1 - \frac{r_s}{r}\right)^3 \left[1 - \left(1 - \frac{r_s}{r}\right)\zeta\right]^3} dr d\phi. \quad (3.21)$$

Now for weak deflection angle make use of the straight line approximation which is given by  $r = \frac{b}{\sin \phi}$  (see [56] and equation (35) in [57]) and  $0 \leq \phi \leq \pi$ . Also substitution of the optical Gaussian curvature from (3.19) and the surface element (3.21) into (3.16) yields

$$\hat{\alpha} = \int_0^\pi \int_{\frac{b}{\sin \phi}}^\infty \frac{r_s \left(1 - \frac{r_s}{r}\right)^\zeta}{r^2 \left(1 - \frac{r_s}{r}\right)} dr d\phi, \quad (3.22)$$

which is evaluated in *Mathematica* to give

$$\hat{\alpha} = \frac{\pi}{\zeta} - \frac{\pi}{\zeta} {}_2F_1 \left[ \frac{1-\zeta}{2}, -\frac{\zeta}{2}, 1, \frac{r_s^2}{b^2} \right] + \frac{2r_s}{b} {}_P F_Q \left[ \left\{ 1, \frac{1-\zeta}{2}, 1 - \frac{\zeta}{2} \right\}, \left\{ \frac{3}{2}, \frac{3}{2} \right\}, \frac{r_s^2}{b^2} \right]. \quad (3.23)$$

Here,  ${}_2F_1$  is the hypergeometric function and  ${}_P F_Q$  denotes the generalized hypergeometric function. The deflection angle (3.23) is plotted versus the impact parameter  $b$  in Fig. (3.1). With the decrease in impact parameter, the deflection angle increases for the considered values of  $\tilde{k}$ . For Buchdahl parameter  $\tilde{k} = 0$ , the deflection angle in WDL (3.23) transforms into

$$\hat{\alpha} = \frac{2r_s}{b} \equiv \frac{4M}{b}. \quad (3.24)$$

This is the weak deflection angle for Schwarzschild spacetime. Thus, the new finding (3.23) is consistent with Schwarzschild black hole.



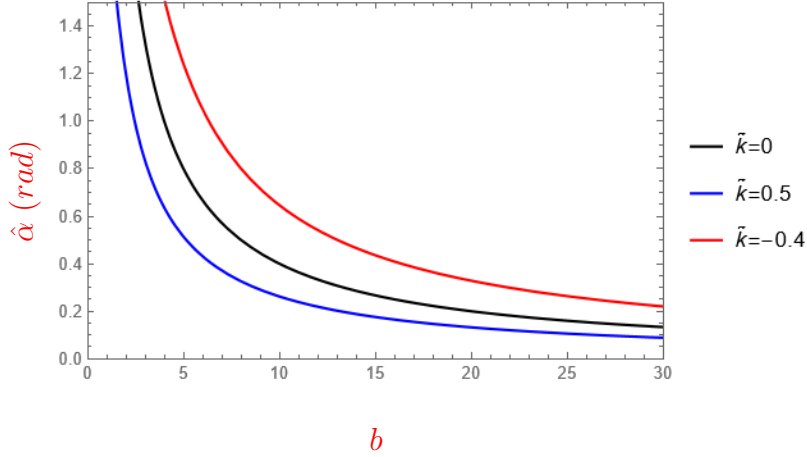


Figure 3.1: The weak deflection angle  $\hat{\alpha}$  of SBI metric is plotted vs impact parameter  $b$  for different values of Buchdahl parameter  $\tilde{k}$ , corresponding to three different cases. The black curve shows the angle in WDL for Schwarzschild black hole.

### 3.2.3 Image magnification and distortion

To observe gravitational lensing phenomenon due to deflection of light in weak deflection limit, the lens equation as expressed in [25] is given by

$$\tan \beta = \tan \theta - \alpha, \quad (3.25)$$

where  $\alpha$  is defined as

$$\alpha = \frac{D_{LS}}{D_{OS}} \tan(\hat{\alpha} - \theta). \quad (3.26)$$

Here,  $\hat{\alpha}$  is the deflection/bending angle. The symbols  $\beta$  and  $\theta$  represents the angular position of the luminous source and position of the image, respectively. Also  $D_{LS}$  represents the lens-source distance and  $D_{OS}$  signifies observer-source distance. The impact parameter can be rewritten in relation with the position of image as

$$b = D_{OL} \sin \theta, \quad (3.27)$$

where  $D_{OL}$  denotes the observer-lens distance. For weak field approximation, the lens equation (3.25) becomes

$$\beta = \theta - \hat{\alpha}\mathcal{D}, \quad (3.28)$$

$\hat{\alpha}$  is the weak deflection angle and parameter  $\mathcal{D}$  is defined by  $\frac{D_{LS}}{D_{OS}}$ . The magnification of an image is defined as the ratio of flux of image to that of unlensed source. Liouville's theorem tells that brightness of surface is conserved in the deflection of light. Hence, the aforementioned ratio transforms into the ratio of angle of image to that of unlensed source. Thus, the total magnification  $\mu$ , radial magnification and tangential magnification are respectively described as [49]

$$\begin{aligned} \mu &= \mu_t \mu_r, \\ \mu_r &= \left( \frac{d\beta}{d\theta} \right)^{-1}, \\ \mu_t &= \left( \frac{\sin \beta}{\sin \theta} \right)^{-1}. \end{aligned} \quad (3.29)$$

To verify if there is no image from the particular source missed in observations, Virbhadra came up with a hypothesis that there exists a distortion parameter such that the distortions of all images must be summed to obtain *zero*. The distortion parameter of images is defined using tangential and radial magnification as follows [49]

$$\Delta = \frac{\mu_t}{\mu_r}, \quad (3.30)$$

thus the logarithmic distortion parameter can be expressed as [49]

$$\delta = \log_{10} |\Delta|. \quad (3.31)$$

Statement of Virbhadra hypothesis can mathematically be delineated as

$$\sum_{i=1}^n \Delta_i = 0, \quad (3.32)$$

here  $n$  quantifies the total number of images formed by a single lens and source.

In this thesis, the massive black hole M87\* is modeled as a SBI lens. The mass of M87\* is  $6.5 \times 10^9 M_\odot$  and the distance  $D_{OL}$  is  $16.8 Mpc$ . Therefore, mass-distance ratio becomes  $1.84951 \times 10^{-11}$ . For gravitational lensing by SBI spacetime in weak deflection limit, magnification of both primary and secondary images are investigated here.

Solving the lens equation (3.28) for  $\theta$  yields the primary and secondary image positions as  $\theta_p$  and  $\theta_s$ , respectively. Using these image positions the radial, tangential and total magnifications are obtained for both primary images and secondary images. The magnifications of primary and secondary images are hence plotted in the Figure 3.2 and Figure 3.3. Figure 3.2-(a) and (b) demonstrates that the primary tangential and absolute secondary tangential magnification for three different values of Buchdahl parameter  $\tilde{k}$  increases with the increase in value of  $\mathcal{D}$ , all the curves are concave down at all points in graph. Graph labeled (c) is the plot for primary radial magnification versus the parameter  $\mathcal{D}$ . It can be seen that magnification drops rapidly and then decrease at a slower rate. The graph (d) is depicting the absolute secondary radial magnification versus the parameter  $\mathcal{D}$ . It is expressed that magnification is increasing. These plots show that the magnification approaches infinity and for small values of distance parameter, very bright image can be observed. This represents the region of caustics, due to weak lensing the magnification is not sharp but is defused. The plots labeled as (e) and (f) respectively are primary total magnification and absolute secondary total magnification versus  $\mathcal{D}$ . Curves are close together and magnification is increasing for all the considered values of  $\tilde{k}$ .

In Figure 3.3: Respectively in graph (a) and (b), it is shown that primary

tangential and absolute secondary tangential magnification increases when plotted against  $M/D_{OL}$  for three different values of Buchdahl parameter. The graph with label (c) shows that the primary radial magnification at first drops rapidly and then at a slower rate when plotted against dimensionless parameter ratio  $M/D_{OL}$ . Also (d) depicts that the absolute secondary radial magnification rises promptly and then its increase rate slows down as the parameter on the x-axis increases. These plots show that the magnification approaches infinity and for small values of the ratio  $M/D_{OL}$ , very bright image can be observed. This represents the region of caustics, due to weak lensing the magnification is not sharp but is defused. The total primary magnification  $\mu_p$  and the absolute total secondary magnification  $|\mu_s|$  is plotted against  $M/D_{OL}$  in (e) and (f), respectively. In graphs it can be seen that both primary and secondary total magnification increases.

Here if we compare the radial, tangential and total magnification curves for  $\tilde{k} = 0$  in all the twelve plots with the respective plots in Schwarzschild lensing in [49], we can clearly see the similar behaviours of all the three magnifications. Henceforth, our plots are consistent with SBH magnification.

In order to investigate the image distortion, again model the M87\* black hole of massive galaxy M87 as a SBI lens. The distortion parameter for SBI metric can be obtained in *Mathematica* using the general expression (3.31). Next the logarithmic distortion parameter  $\delta$  is plotted against some parameters in Figure 3.4. In plot (a), (b) and (c) respectively, logarithmic distortion is graphed against the source position  $\beta$ , the dimensionless parameter  $\mathcal{D}$  and the ratio  $M/D_{OL}$ . The logarithmic distortion parameter for both primary and secondary images can be observed to increase for the increase in both  $\mathcal{D}$  and  $M/D_{OL}$ . However, the parameter  $\delta$  decreases for the increase in  $\beta$  for primary images and secondary images. The curves in all the graphs are iden-

tical for primary and secondary images for corresponding individual values of Buchdahl parameter. Thus, the values of primary distortion parameter and secondary distortion parameter (not absolute) are incredibly close but with opposite sign. Therefore, making the sum of both primary and secondary distortions nearly zero.

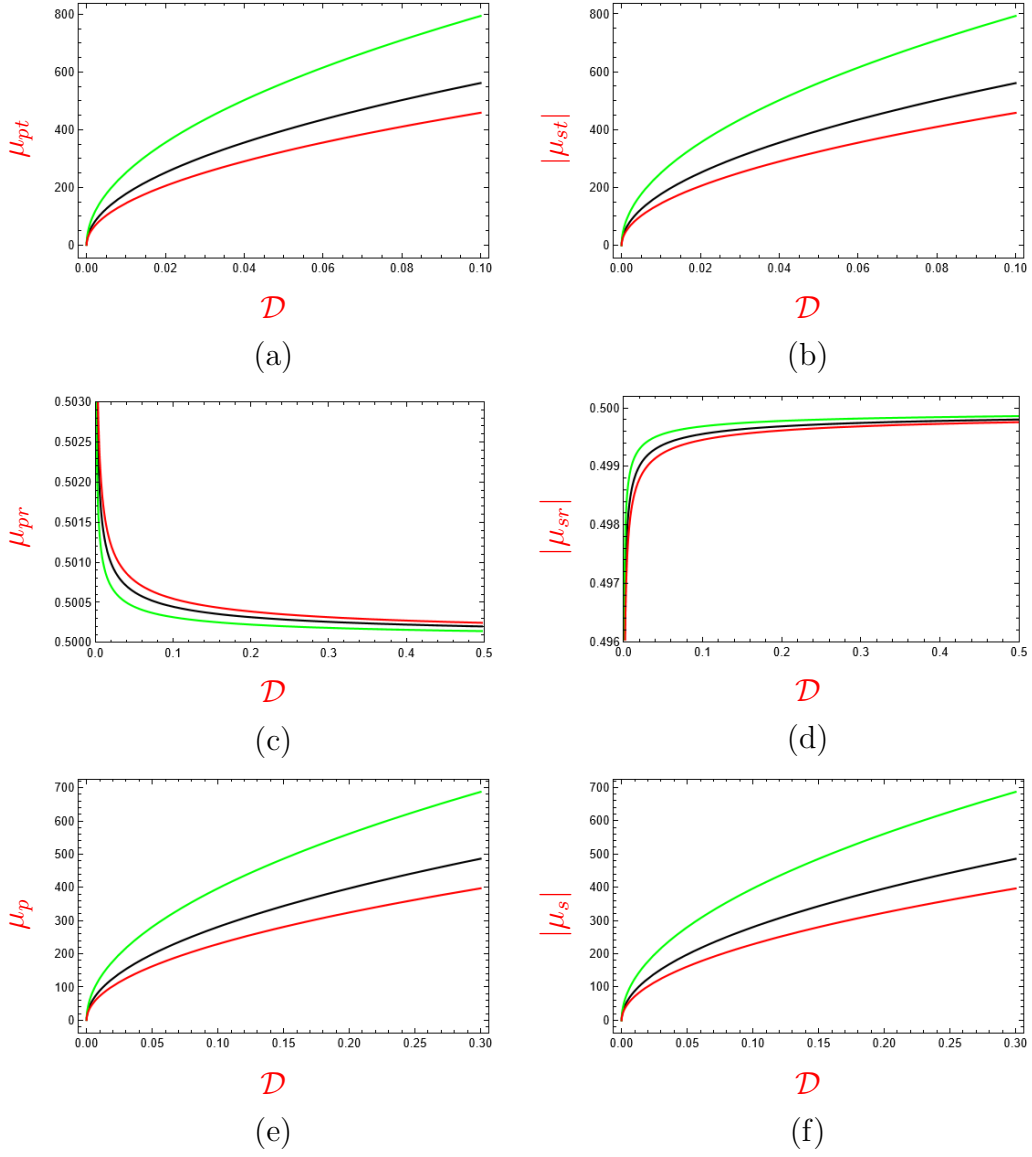


Figure 3.2: Magnification of images for SBI spacetime is plotted against parameter  $\mathcal{D}$  in WDL. For primary images, the tangential magnification  $\mu_{pt}$ , radial magnification  $\mu_{pr}$  and total magnification  $\mu_p$  are graphed respectively in (a), (c) and (e) - against the dimensionless parameter  $\mathcal{D}$ . For secondary images; the absolute tangential magnification  $|\mu_{st}|$ , the absolute radial magnification  $|\mu_{sr}|$  and the absolute total magnification  $|\mu_s|$  is plotted against the parameter  $\mathcal{D}$  in (b), (d) and (f), each in order. Plot convention: The black, green and red curves are respectively representing the plots for parameter values  $\tilde{k} = 0, -0.5$  and  $0.5$ .

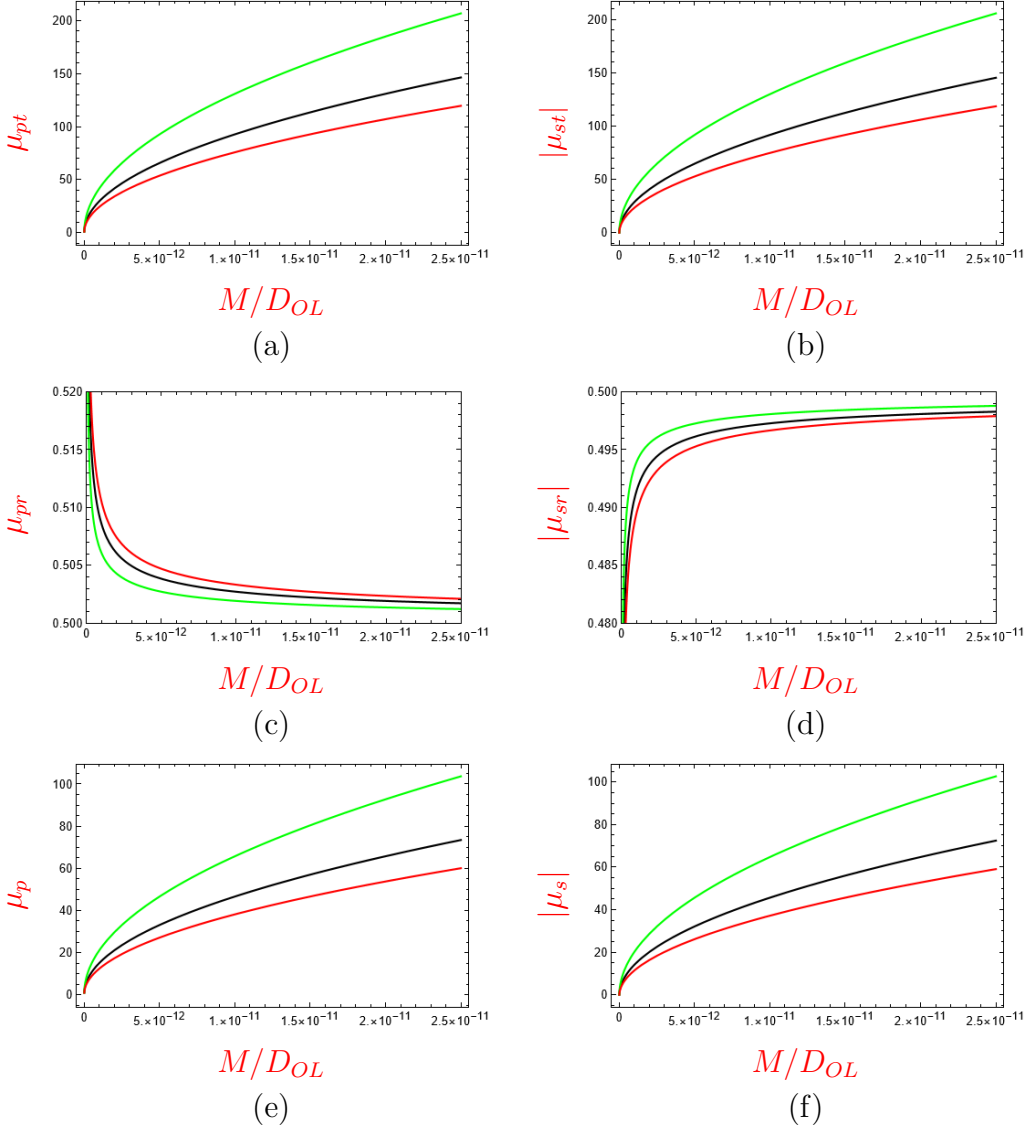
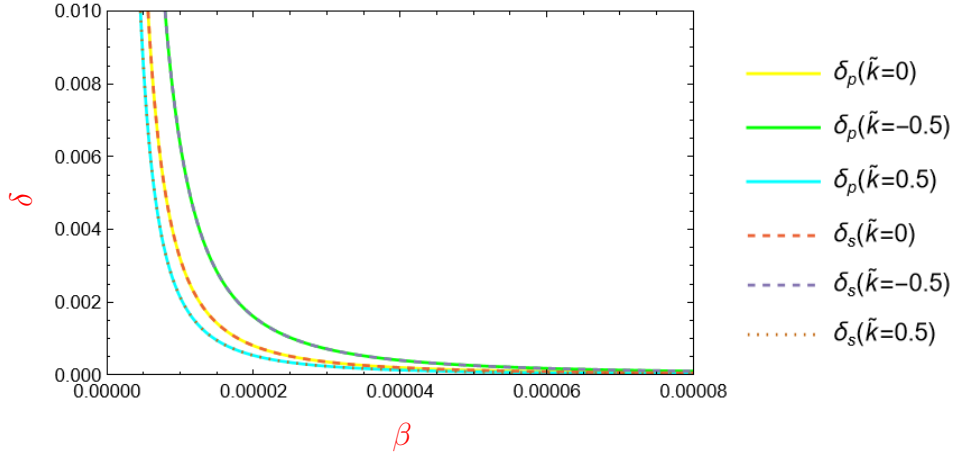
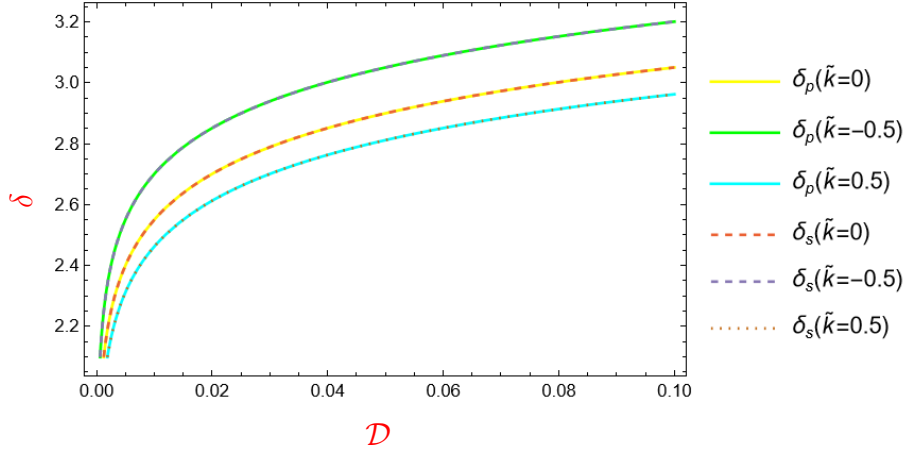


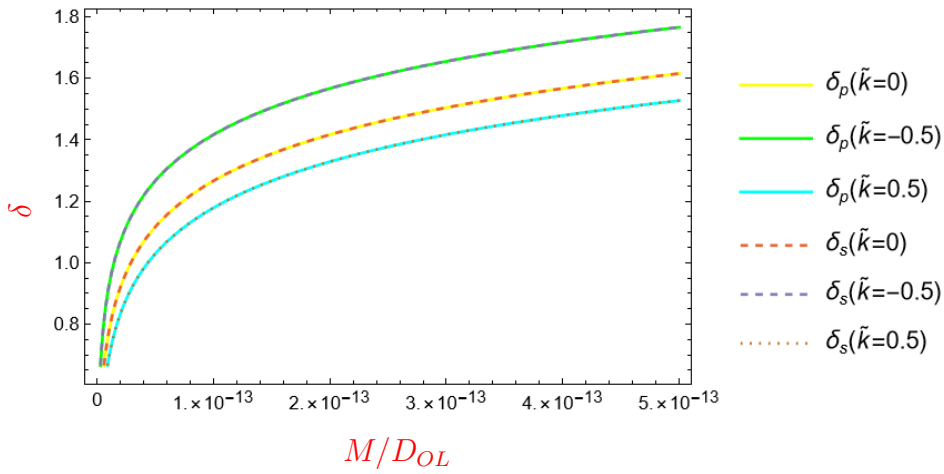
Figure 3.3: Magnification of images for SBI spacetime is plotted against ratio  $M/D_{OL}$  in WDL. For primary images, the tangential magnification  $\mu_{pt}$ , radial magnification  $\mu_{pr}$  and total magnification  $\mu_p$  are graphed respectively in (a), (c) and (e) - against ratio  $M/D_{OL}$ . For secondary images; the absolute tangential magnification  $|\mu_{st}|$ , the absolute radial magnification  $|\mu_{sr}|$  and the absolute total magnification  $|\mu_s|$  is plotted against  $M/D_{OL}$  in (b), (d) and (f), each in order. Plot convention: The black, green and red curves are respectively representing the plots for parameter values  $\tilde{k} = 0, -0.5$  and  $0.5$ .



(a)



(b)



(c)

Figure 3.4: Logarithmic distortion is plotted for SBI spacetime in WDL. The logarithmic distortion of the primary images ( $\delta_p$ ) and the secondary images ( $\delta_s$ ) is plotted against angular position of source  $\beta$ , distance parameter  $\mathcal{D}$  and  $M/D_{OL}$  in (a), (b) and (c), respectively.



### 3.3 Gravitational lensing in SDL

In this focused section, deflection angle by SBI metric is determined in the strong deflection limit. The spacetime described as (3.7) has the components  $\mathcal{A}(r)$ ,  $\mathcal{B}(r)$  and  $\mathcal{C}(r)$  as given in (3.11), rewriting those after substitution of the function  $\rho(r)$  from equation (3.8) leads

$$\begin{aligned}
 f(r) &:= 1 - \frac{r_s}{r}, \\
 \mathcal{A}(r) &= f(r)^{\bar{k}+1}, \\
 \mathcal{B}(r) &= f(r)^{\bar{k}-3} \frac{\zeta^4 f(r)^{2\zeta}}{[1 - f(r)\zeta]^4} \left(\frac{r_s}{r}\right)^4, \\
 \mathcal{C}(r) &= f(r)^{\bar{k}} \left( \frac{\zeta^2 r_s^2 f(r)^{\zeta-1}}{[1 - f(r)\zeta]^2} \right) = \mathcal{A}(r) \left( \frac{\zeta^2 r_s^2 f(r)^{\zeta-2}}{[1 - f(r)\zeta]^2} \right).
 \end{aligned} \tag{3.33}$$

#### 3.3.1 Equations for null Geodesic

The spacetime under consideration is spherically symmetric which allows to set  $\theta = \pi/2$ . The Lagrangian of a particle with 4-velocity is defined as

$$\mathcal{L} = \frac{1}{2} g_{\mu\nu} \dot{x}^\mu \dot{x}^\nu \tag{3.34}$$

The Euler-Lagrange equation is described by

$$\frac{\partial \mathcal{L}}{\partial x^\mu} = \frac{d}{d\lambda} \frac{\partial \mathcal{L}}{\partial \dot{x}^\mu} \tag{3.35}$$

These equations for SBI metric in case of  $\mu = 0$  and  $\mu = 3$  yields

$$\varepsilon = \mathcal{A}(r) \dot{t} \quad \text{and} \quad \ell = \mathcal{C}(r) \dot{\phi}, \tag{3.36}$$

where  $\varepsilon$  and  $\ell$  are representing the conserved energy of light rays and conserved angular momentum, respectively. Also,  $\dot{t}$  and  $\dot{\phi}$  represents derivative with respect to affine parameter  $\lambda$ . From (3.36), it follows that

$$\dot{t} = \frac{\varepsilon}{\mathcal{A}(r)} \equiv \frac{\varepsilon}{f(r)^{\bar{k}+1}}, \tag{3.37}$$

$$\dot{\phi} = \frac{\ell}{f(r)^{\bar{k}} \left[ \frac{\zeta^2 r_s^2 f(r)^{\zeta-1}}{[1-f(r)^\zeta]^2} \right]}. \quad (3.38)$$

Now, using the null geodesic condition  $ds^2 = 0$ , for spherically symmetric spacetime and introducing the impact parameter  $b := \ell/\varepsilon$ ,

$$-\mathcal{A}(r)\dot{t}^2 + \mathcal{B}(r)\dot{r}^2 + \mathcal{C}(r)\dot{\phi}^2 = 0, \quad (3.39)$$

alternatively,

$$\begin{aligned} \dot{r}^2 &= V_{\text{eff}}(r) \equiv \frac{1}{\mathcal{B}(r)} \left[ \mathcal{A}(r)\dot{t}^2 - \mathcal{C}(r)\dot{\phi}^2 \right], \\ &= \ell^2 \left\{ \frac{1}{b^2} \frac{1}{\mathcal{A}(r)\mathcal{B}(r)} - \frac{1}{\mathcal{B}(r)\mathcal{C}(r)} \right\}. \end{aligned} \quad (3.40)$$

Use of equations (3.37)-(3.40) for SBI metric (3.33) gives the radial component of geodesic equation as

$$\dot{r}^2 = \frac{\ell^2 r^4 f(r)^{2-2\zeta-2\bar{k}} [1-f(r)^\zeta]^4 \left[ \frac{1}{b^2} - \frac{f(r)^{2-\zeta} [1-f(r)^\zeta]^2}{\zeta^2 r_s^2} \right]}{\zeta^4 r_s^4}. \quad (3.41)$$

### 3.3.2 Impact parameter

Consider an incoming light ray from a source at asymptotic region which reaches at a minimum distance  $r_{tp}$  from the black hole and arriving to observer in another direction in asymptotic region. The impact parameter can be found in terms of this closest distance  $r_{tp}$  by using the vanishing kinetic energy of light particle [6] as follows

$$\left. \frac{\dot{r}^2}{\ell^2} \right|_{r=r_{tp}} = 0, \quad (3.42)$$

For SBI metric, (3.41) gives

$$\frac{r^4 \left(1 - \frac{r_s}{r}\right)^{2-2\zeta-2\bar{k}} \left[1 - \left(1 - \frac{r_s}{r}\right)^\zeta\right]^4}{\zeta^4 r_s^4} \left[ \frac{1}{b^2} - \frac{\left(1 - \frac{r_s}{r}\right)^{2-\zeta} \left[1 - \left(1 - \frac{r_s}{r}\right)^\zeta\right]^2}{\zeta^2 r_s^2} \right]_{r=r_{tp}} = 0. \quad (3.43)$$

Solving for  $b$  brings the expression of impact parameter  $b(r)|_{r=r_{tp}}$  in the form

$$b(r_{tp}) = \frac{\zeta r_s \left(1 - \frac{r_s}{r_{tp}}\right)^{\frac{\zeta}{2}}}{\left(1 - \frac{r_s}{r_{tp}}\right) \left(1 - \left(1 - \frac{r_s}{r_{tp}}\right)^\zeta\right)^2}. \quad (3.44)$$

### 3.3.3 Photon sphere

When the closest approach distance  $r_{tp}$  is located at the maximum of effective potential  $V_{\text{eff}}$ , this distance is called radius of photon sphere  $r_c$ . Theoretically, at  $r_c$  the photons can travel in circular orbits because of strong enough gravity. This radius of photon sphere can be computed using [6]

$$\left. \frac{dV_{\text{eff}}(r)}{dr} \right|_{r=r_c} = 0. \quad (3.45)$$

Using equation (3.40) for the expression of effective potential and evaluate derivative with respect to  $r$  being cognizant of the finding that impact parameter is a function of  $r_{tp}$

$$\left. \frac{dV_{\text{eff}}(r)}{dr} \right|_{r=r_c} = \frac{\ell^2}{\mathcal{BC}} \left[ (\ln \mathcal{C})' - (\ln \mathcal{A})' \right] \Big|_{r=r_c} = 0. \quad (3.46)$$

Using the last line in (3.33),  $(\ln \mathcal{C})' = (\ln \mathcal{A})' + (\zeta - 2) [\ln f(r)]' - 2 \{ \ln [1 - f(r)^\zeta] \}'$ , yields  $(\zeta - 2) [\ln f(r)]' \Big|_{r=r_c} = 2 \{ \ln [1 - f(r)^\zeta] \}' \Big|_{r=r_c}$ , that is,

$$\zeta - 2 + (\zeta + 2) f(r_c)^\zeta = 0. \quad (3.47)$$

Knowing that  $f(r_c) > 0$  (because  $r_c > r_s$ ), this last equation admits a solution only if<sup>1</sup>  $\zeta < 2$ , yielding the radius of the photon sphere for SBI metric as

$$r_c = \frac{r_s}{1 - \left(\frac{2-\zeta}{2+\zeta}\right)^{\frac{1}{\zeta}}} = \frac{r_s}{1-p}, \quad p := \left(\frac{2-\zeta}{2+\zeta}\right)^{\frac{1}{\zeta}}. \quad (3.48)$$

---

<sup>1</sup>Constraints on  $\tilde{k}$  [Eur. Phys. J. C (2024) 84, 330, <https://doi.org/10.1140/epjc/s10052-024-12610-2>] have shown that  $\zeta$  is closer to unity.

The corresponding critical impact parameter  $b_c$  can be determined using (3.44) for  $r_{tp} = r_c$  to get

$$b_c = \frac{r_s(\zeta + 2)}{2} \left( \frac{2 - \zeta}{\zeta + 2} \right)^{\frac{\zeta - 2}{2\zeta}}. \quad (3.49)$$

For  $\tilde{k} = 0$ , radius of photon sphere (3.48) and critical impact parameter (3.49) are respectively as follows

$$r_c = 3M, \quad (3.50)$$

$$b_c = 3\sqrt{3}M. \quad (3.51)$$

These (3.50) and (3.51) are respectively the radius of photon sphere with the corresponding critical impact parameter for Schwarzschild spacetime. Thus our general expressions (3.48) and (3.49) are consistent with SBH.

### 3.3.4 Deflection angle in the strong field limits

From the geodesic equations (3.38) and (3.41), following can easily be extracted

$$\frac{d\phi}{dr} = \frac{\zeta r_s}{r^2 \sqrt{f(r_{tp})^{2-\zeta} [1 - f(r_{tp})^\zeta]^2 - f(r)^{2-\zeta} [1 - f(r)^\zeta]^2}}. \quad (3.52)$$

As a function of closest approach distance  $r_{tp}$ , the deflection angle is defined in [6] as follows

$$\hat{\alpha}(r_{tp}) = I(r_{tp}) - \pi, \quad (3.53)$$

with

$$I(r_{tp}) = 2 \int_{r_{tp}}^{\infty} \frac{\zeta r_s dr}{r^2 \sqrt{f(r_{tp})^{2-\zeta} [1 - f(r_{tp})^\zeta]^2 - f(r)^{2-\zeta} [1 - f(r)^\zeta]^2}}. \quad (3.54)$$

The analytic evaluation of this integral is quite challenging. It is discussed in the section 3.1 that SBI metric is asymptotically flat, static and spherically

symmetric spacetime. Therefore, the methodology given by N. Tsukamoto in [28] is adopted here to find the coefficients  $\bar{a}$  and  $\bar{b}$  for the deflection angle of SBI metric in strong limit. Let us introduce a new variable  $z$  and change the integrand and the integration limits appropriately

$$z = 1 - \frac{r_{tp}}{r}. \quad (3.55)$$

Then the integral  $I(r_{tp})$  is expressed [28] generally as

$$I(r_{tp}) = \int_0^1 h(z, r_{tp}) dz, \quad (3.56)$$

where

$$h(z, r_{tp}) = \frac{2\zeta r_s}{r_{tp}} \frac{1}{\sqrt{f(r_{tp})^{2-\zeta} [1 - f(r_{tp})^\zeta]^2 - f(r)^{2-\zeta} [1 - f(r)^\zeta]^2}}. \quad (3.57)$$

We have  $f(r_{tp})^{2-\zeta} [1 - f(r_{tp})^\zeta]^2 - f(r)^{2-\zeta} [1 - f(r)^\zeta]^2$  has series:

$$\begin{aligned} &= \frac{r_s (r_{tp} - r_s)^{1-\zeta} [1 - f(r_{tp})^\zeta] [\zeta - 2 + (\zeta + 2) f(r_{tp})^\zeta]}{r_{tp}^{2-\zeta}} z \\ &- \frac{r_s^2 \left(\frac{r_{tp}}{r_{tp} - r_s}\right)^\zeta \{2[1 - f(r_{tp})^\zeta]^2 - 3[1 - f(r_{tp})^{2\zeta}] \zeta + [1 + f(r_{tp})^{2\zeta}] \zeta^2\}}{2r_{tp}^2} z^2 + \dots, \end{aligned} \quad (3.58)$$

and using (3.48) we see that the coefficient of  $z$  vanishes if we replace  $r_{tp}$  by  $r_c$ . This shows that the integral (3.56) has a divergent term proportional to  $\ln z$  in the limit  $r_{tp} \rightarrow r_c$  of strong deflection ( $b \rightarrow b_c$ ). In this limit, we separate the regular part from the divergent part of the integral as follows [28]

$$I_R(r_c) = \int_0^1 [h(z, r_c) - h_D(z, r_c)] dz, \quad (3.59)$$

where, using (3.33) and (3.58),  $h_D(z, r_c) = 2/z$ . Now, we introduce the new variable  $y$

$$y := \left[1 - \left(\frac{2-\zeta}{2+\zeta}\right)^{\frac{1}{\zeta}}\right] z + \left(\frac{2-\zeta}{2+\zeta}\right)^{\frac{1}{\zeta}} = (1-p)z + p, \quad p := \left(\frac{2-\zeta}{2+\zeta}\right)^{\frac{1}{\zeta}}, \quad (3.60)$$

in terms of which we write (3.59) as

$$I_R(r_c) = 2\zeta \int_p^1 \left\{ \frac{1}{\sqrt{\frac{4\zeta^2 p^2}{4-\zeta^2} - y^{2-\zeta} (1-y^\zeta)^2}} - \frac{1}{\zeta(y-p)} \right\} dy. \quad (3.61)$$

This integral cannot be evaluated in terms of elementary functions for all values of  $\zeta$ . For  $\zeta = 1$  (corresponding to Schwarzschild metric with  $\tilde{k} = 0$ ), we obtain the exact value  $\phi_R(1) = 2 \ln[6(2 - \sqrt{3})]$ .

The coefficient  $\bar{a}$  has the general expression defined in [28] as

$$\bar{a} = \sqrt{\frac{2\mathcal{B}(r_c)\mathcal{A}(r_c)}{\mathcal{C}''(r_c)\mathcal{A}(r_c) - \mathcal{C}(r_c)\mathcal{A}''(r_c)}}. \quad (3.62)$$

Using the coefficients  $\mathcal{A}(r)$ ,  $\mathcal{B}(r)$  and  $\mathcal{C}(r)$  from (3.33), the coefficient  $\bar{a}$  for SBI spacetime becomes

$$\bar{a} = 1. \quad (3.63)$$

The next task is to find the coefficient  $\bar{b}$  which is described in [28] generally by

$$\bar{b} = \bar{a} \log \left[ (r_c)^2 \left( \frac{\mathcal{C}''(r_c)}{\mathcal{C}(r_c)} - \frac{\mathcal{A}''(r_c)}{\mathcal{A}(r_c)} \right) \right] + I_R(r_c) - \pi, \quad (3.64)$$

substitution of  $\mathcal{A}(r)$ ,  $\mathcal{C}(r)$  and their second derivatives with respect to  $r$  along with the value of  $\bar{a}$  followed by the use of radius of photon sphere (3.48) yields

$$\bar{b} = -\pi + \log \left[ \frac{1}{2} (2 + \zeta)(2 - \zeta)^{1-\frac{2}{\zeta}} \left[ (2 - \zeta)^{\frac{1}{\zeta}} - (2 + \zeta)^{\frac{1}{\zeta}} \right]^2 \right] + I_R(r_c), \quad (3.65)$$

where  $I_R(r_c)$  for SBI metric is evaluated in equation (3.61). Therefore the deflection angle for SBI metric in the strong field limit has been brought to the form

$$\hat{\alpha}(b) = -\bar{a} \log \left( \frac{b}{b_c} - 1 \right) + \bar{b} + \mathcal{O}((b - b_c) \log(b - b_c)), \quad (3.66)$$

where the coefficients  $\bar{a}$  and  $\bar{b}$  have the expressions as determined in (3.63) and (3.65), respectively. The plot for deflection angle against the impact

parameter  $b$  is given in Fig. (3.5). The deflection angle decreases when the impact parameter increases. For Buchdahl parameter  $\tilde{k} = 0$ , the expressions of  $\bar{a}$  and  $\bar{b}$  reduces to that for Schwarzschild spacetime

$$\begin{aligned}\bar{a} &= 1. \\ \bar{b} &= -\pi + \log(216(7 - 4\sqrt{3})).\end{aligned}\tag{3.67}$$

Thus our results are consistent with SBH.

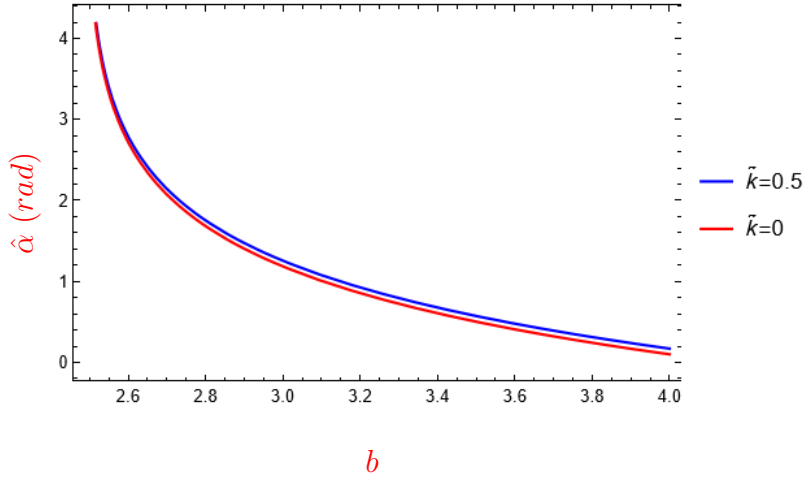


Figure 3.5: The deflection angle  $\hat{\alpha}$  of SBI metric is plotted vs impact parameter  $b$  for two different values of Buchdahl parameter  $\tilde{k}$  in SDL. The black curve represents the case of Schwarzschild black hole in SDL.

### 3.3.5 Observables

Assume that in asymptotically flat SBI spacetime, light source and observer are aligned, and near the lens curvature affects the deflection angle strongly. The strong deflection observables can be studied using the famous lens equation [58]

$$\beta = \theta - \frac{D_{LS}}{D_{OS}} \Delta\alpha_n,\tag{3.68}$$

where  $\beta$  and  $\theta$  represent the position of source and the position of image, respectively.  $D_{LS}$  denotes the distance between the black hole lens to be considered and the light source.  $D_{OS}$  symbolizes the distance between the source and observer. Also,  $\Delta\alpha_n$  is the offset of deflection angle  $\hat{\alpha}$ . When the photon orbits around the lens  $n$ - number of times then the offset of deflection angle is obtained after deflection angle subtracting  $2n\pi$ . Thus,  $\Delta\alpha_n$  can be described as  $\Delta\alpha_n = \hat{\alpha} - 2n\pi$ . Moreover, the impact parameter, in relation with the image position is given by

$$b = D_{OL} \tan \theta \approx D_{OL} \theta, \quad (3.69)$$

where  $D_{OL}$  is the observer-lens distance. In strong deflection limit, small angular position of source  $\beta$  is considered thus expectedly, the angular position of image  $\theta$  is also small. Then using small angle identities, impact parameter is also small. Substitution of (3.69) into (3.66) modifies expression for deflection angle as

$$\hat{\alpha}(b) = -\bar{a} \log \left( \frac{D_{OL} \theta}{b_c} - 1 \right) + \bar{b}. \quad (3.70)$$

Deflection angle together with (3.68) reads the *zeroth* order angular position of the  $n$ th image as

$$\theta_n^0 = \frac{b_c}{D_{OL}} (1 + e_n), \quad (3.71)$$

where

$$e_n = \exp \left( \frac{\bar{b} - 2n\pi}{\bar{a}} \right). \quad (3.72)$$

Since the source, lens and observer are aligned, the Einstein ring for  $n$ th relativistic image is described by

$$\theta_n^E = \frac{b_c}{D_{OL}} (1 + e_n), \quad (3.73)$$

Another important observable is the image magnification described in [26] as

$$\mu_n = \frac{1}{\beta} \left[ \frac{b_c(1 + e_n)}{D_{OL}} \left\{ \frac{D_{OS} b_c e_n}{D_{OL} D_{LS} \bar{a}} \right\} \right], \quad (3.74)$$



we know that  $D_{OS} = 2D_{LS}$ . Thus magnification of n-loop images becomes

$$\mu_n = \frac{1}{\beta} \left[ \frac{b_c(1 + e_n)}{D_{OL}} \left\{ \frac{2b_c e_n}{D_{OL} \bar{a}} \right\} \right]. \quad (3.75)$$

Here in this work we consider the case when the outermost image  $\theta_1$  can be separated and all the other relativistic images are gathered at asymptotic image position  $\theta_\infty$ , two observable characteristics are described as [26]

$$\theta_\infty = \frac{b_c}{D_{OL}}, \quad (3.76)$$

and

$$\bar{s} = \theta_1 - \theta_\infty \approx \theta_\infty \exp\left(\frac{\bar{b} - 2n\pi}{\bar{a}}\right). \quad (3.77)$$

In the limits  $n \rightarrow \infty$ , photon sphere's radius is represented by  $\theta_\infty$ . This tells the asymptotic angular position of set of images. Whereas  $\theta_1$  expresses the outermost angular image position. Further  $\bar{s}$  is the angular separation between the outermost image and the set of images at asymptotic position. Now we will use these general expressions to see observables for SBI metric.

In order to study gravitational lensing in SDL for SBI metric, two massive black holes are taken separately as a lens here.

Firstly, the supermassive black hole Sgr A\* at the galactic center of Milky Way galaxy is modeled here as a SBI lens. The mass of Sgr A\* is approximated in recent studies [58] to be  $4 \times 10^6 M_\odot$  and the observer-lens distance is 0.008 Mpc. We numerically approximate the angular position of the outermost image  $\theta_1$ , the innermost image  $\theta_\infty$  and angular separation between the outermost and the relativistic images packed together with the innermost image. To do so, (3.71), (3.76) and (3.77) are utilized for deflection angle coefficients we computed in (3.63) and (3.65). The results are tabulated in the Table 3.1 for six different values of Buchdahl parameter  $\tilde{k}$ .

Also, we estimate the outermost Einstein ring radius using (3.73) substituting  $n = 1$  for the coefficients  $\bar{a}$  and  $\bar{b}$  for the case of SBI spacetime behaving

$\tilde{k}$	-0.02	-0.01	0	0.01	0.02
$b_c/r_s$	2.5826	2.5942	2.5981	2.5942	2.5826
$\bar{a}$	1	1	1	1	1
$\bar{b}$	-0.40014	-0.40021	-0.40023	-0.40021	-0.40014
$\theta_\infty (\mu as)$	26.1681	25.9049	25.6462	25.3919	25.1419
$\theta_1 (\mu as)$	26.2008	25.9373	25.6783	25.4237	25.1733
$\bar{s} (\mu as)$	0.03275	0.03242	0.03210	0.03178	0.03147

Table 3.1: Some relativistic images observables estimates for SBI spacetime in strong lensing using Sgr A\* as a lens. Also, the lensing coefficients  $\bar{a}$  and  $\bar{b}$  for different values of Buchdahl parameter  $\tilde{k}$  has been approximated.

like a SBH  $\tilde{k} = 0$ , a Morris Thorne wormhole, which is a two-way wormhole, when  $\tilde{k} \in (-1, 0)$  and a naked singularity for  $\tilde{k} \in (-\infty, -1) \cup (0, \infty)$ . Arbitrarily choosing one value of  $\tilde{k}$  for each case, we approximate the value of Einstein ring radius. For  $\tilde{k} = 0$  (SBH), the Einstein ring radius value is estimated as  $25.6783 \mu as$ . The Einstein ring radius value for  $\tilde{k} = 0.03$  is  $24.9271 \mu as$  corresponding to naked singularity case. Also for  $\tilde{k} = -0.04$  the Einstein ring radius for relativistic outer most image formation is  $26.7419 \mu as$ . Rings are depicted in Figure 3.6. The Einstein ring for  $\tilde{k} = 0$  is similar to the ER in the work [58]. Thus our results are consistent with Schwarzschild black hole. Also the magnification of the outermost image assuming  $n = 1$  has been observed for three values of Buchdahl parameter. The graph plotted in Figure 3.7 shows that magnification is maximum as the angular source position  $\beta \rightarrow 0$ . Thereby, the source must be perfectly aligned in order to maximize the magnification of image.

Next we model the M87\* black hole of the Messier 87 galaxy as a lens for SBI spacetime to investigate the lensing observables. The mass of M87\*

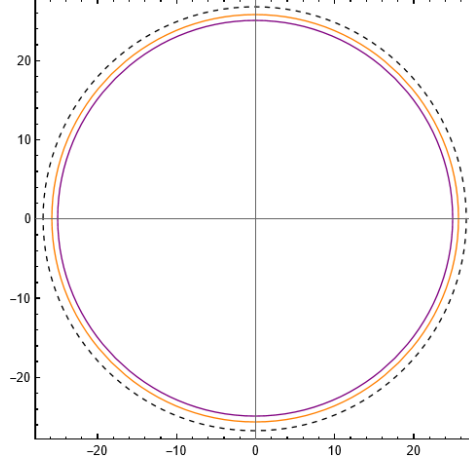


Figure 3.6: Einstein Rings of outermost relativistic images of SBI spacetime for  $\tilde{k} = 0$  (orange),  $\tilde{k} = 0.03$  (purple) and  $\tilde{k} = -0.04$  (dashed) is depicted modelling supermassive black hole Sgr A\* as a SBI lens.

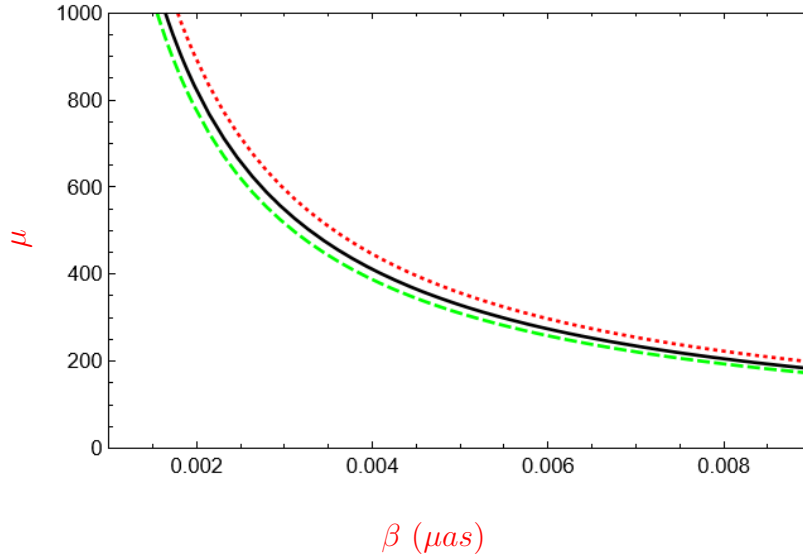


Figure 3.7: Magnification of the outermost image for SBI spacetime for  $\tilde{k} = 0$  (black),  $\tilde{k} = 0.03$  (green) and  $\tilde{k} = -0.04$  (red) has been plotted versus angular source position modelling Sgr A\* as a SBI lens.

$\tilde{k}$	-0.02	-0.01	0	0.01	0.02
$b_c/r_s$	2.5826	2.5942	2.5981	2.5942	2.5826
$\bar{a}$	1	1	1	1	1
$\bar{b}$	-0.40014	-0.40021	-0.40023	-0.40021	-0.40014
$\theta_\infty$ ( $\mu as$ )	20.2491	20.0455	19.8453	19.6485	19.4550
$\theta_1$ ( $\mu as$ )	20.2745	20.0706	19.8701	19.6731	219.4794
$\bar{s}$ ( $\mu as$ )	0.02534	0.02509	0.02484	0.02459	0.02435

Table 3.2: Approximates for observables and strong lensing coefficients of SBIM in SDL, considering M87\* black hole as a lens, for different values of Buchdahl parameter  $\tilde{k}$ .

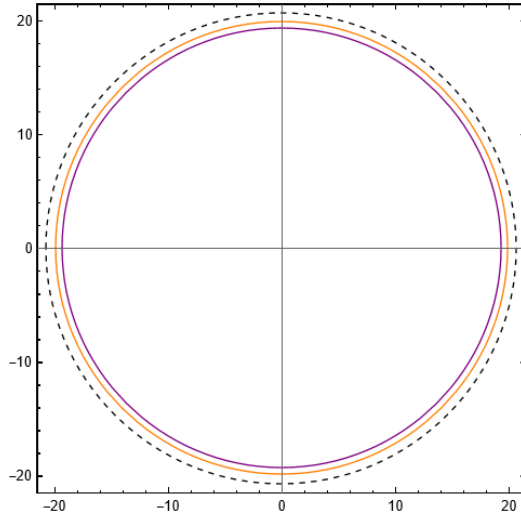


Figure 3.8: Formation of Einstein Rings of outermost relativistic images of SBI spacetime for  $\tilde{k} = 0$  (orange),  $\tilde{k} = 0.03$  (purple) and  $\tilde{k} = -0.04$  (dashed) is demonstrated modelling massive black hole M87\* as a SBI lens.

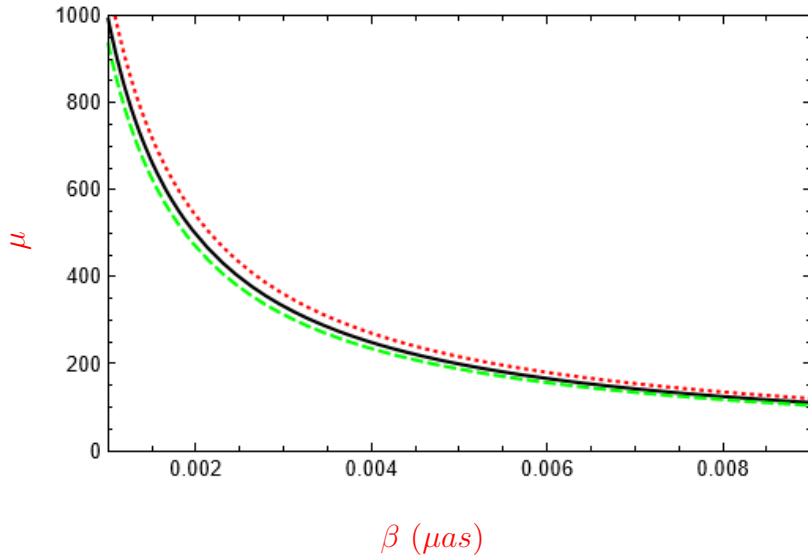


Figure 3.9: Magnification of the outermost image for SBI spacetime for  $\tilde{k} = 0$  (black),  $\tilde{k} = 0.03$  (green) and  $\tilde{k} = -0.04$  (red) has been plotted versus angular source position modelling M87\* as SBI spacetime lens.

is  $6.5 \times 10^9 M_\odot$  and the observer to lens distance is 16.8 Mpc [58]. The angular position of the outermost image represented by  $\theta_1$ , the innermost image  $\theta_\infty$  and the angular separation between both of them  $\bar{s}$ ; are investigated here for SBI spacetime using the aforementioned black hole as a lens. The numerical computations are tabulated in the Table 3.2 for six different values of Buchdahl parameter  $\tilde{k}$ . Moreover, we estimate the radius of the outermost Einstein ring for three different values of Buchdahl parameter. For  $\tilde{k} = 0$ , Buchdahl spacetime reduces to SBH and we have Einstein ring radius  $19.8701 \mu as$ . For  $\tilde{k} = 0.03$  (naked singularity case), the Einstein ring radius becomes  $19.2888 \mu as$ . The case when SBIM behaves like Morris-Thorne wormhole, we arbitrarily choose  $\tilde{k} = -0.04$  and have the corresponding numerical value for acquired radius  $20.6932 \mu as$ . Thus, the Einstein rings for angular position of the outermost relativistic images for all these values are illustrated in the Figure 3.8. The Einstein ring for  $\tilde{k} = 0$  is similar to the ER in the work [58].

Thus our results are consistent with Schwarzschild black hole. The graph plotted in Figure 3.9 shows that magnification is maximum as the angular source position  $\beta \rightarrow 0$ . Thereby, the source must be perfectly aligned in order to obtain the most magnified image.

## Summary

In this chapter, the expressions for deflection angle of Weak and Strong deflection for asymptotically flat *special* Buchdahl-inspired (SBI) metric are determined. In section 3.2, weak gravitational lensing is discussed, and bending angle  $\hat{\alpha}$  is obtained according to GBT using Gibbons and Werner's approach. Also the black hole M87\* in the center of galaxy M87 is modeled as a SBI lens. The mass of considered lens is  $6.5 \times 10^9 M_{\odot}$  and the source-lens distance is 16.8 Mpc. Using this, the radial, tangential and total magnifications are plotted. It is observed that the tangential and total magnification for both primary and secondary images and radial magnification for secondary images are increasing for parameter  $\mathcal{D}$  and  $M/D_{OL}$ . Whereas, the radial magnification for primary images is seen to be decreasing. Moreover the distortion parameter's behaviour for source position, the parameter  $\mathcal{D}$ , and the ratio  $M/D_{OL}$  is investigated. The sum of distortion parameter of primary and secondary images vanishes and thus our result aligns with the hypothesis of Virbhadra [49]. The deflection angle in strong deflection limits is analytically found in the section 3.3. The graphs of the coefficients  $\bar{a}$  and  $\bar{b}$  of the deflection angle is plotted and the results are seen to be consistent with Schwarzschild black hole for Buchdahl parameter  $\tilde{k} = 0$ . Also, the lensing observables are tabulated that estimates image position for the innermost, the outermost and the separation between them modeling Sgr A\* and M87\* black holes as SBIM lens. Moreover the Einstein rings are also plotted arbi-

trarily choosing three values for different cases of SBI metric. Magnification of the outermost relativistic image has been investigated. It can be observed that for angular source position  $\beta \rightarrow 0$ , the magnification is maximum.

## Chapter 4

# Gravitational Lensing by axi-symmetric SBI Metric in Pure $\mathcal{R}^2$ Gravity

Buchdahl extended Einstein's General Relativity theory by introducing pure  $\mathcal{R}^2$  gravity theory [59].  $\mathcal{R}^2$  gravity stands out being scale-invariant in ghost-free class of theories. The implication was immediately followed by Buchdahl when he pioneered a program to quest for static spherically symmetric novel class of spacetimes using pure  $\mathcal{R}^2$  action [51]. This action has one single term  $\frac{1}{2\kappa} \int d^4x \sqrt{-g} \mathcal{R}^2$  with a dimensionless parameter  $\kappa$ . Buchdahl revealed that due to the higher derivative configuration of theory, the vacua has non constant scalar curvature in general. He culminated his work producing a second-order ordinary differential equation which was non-linear. That equation was unfortunately abandoned to be solved by him.

Later, as mentioned initially in Chapter 3, Nguyen completed unfinished work of Buchdahl obtaining compact form of exhaustive class of Buchdahl-inspired metrics in pure  $\mathcal{R}^2$  gravity [52]. The closed form of the metrics



representing  $\mathcal{R}^2$  vacuum solutions leads to generalized axi-symmetric setup. Therein, an exact stationary vacuum solution involving rotation was established [60]. The axi-symmetric SBI solution contains a conformal factor  $\mathcal{A}(q, \theta; a)$  that was determined numerically but its analytical expression is not known yet. Also the metric is attributed by new (Buchdahl) parameter, represented by  $\tilde{k}$ , and Schwarzschild radius  $r_s$ .

Study of weak gravitational lensing has been an active area of research in the domain of astrophysics. One of the approaches to compute weak deflection angle was given by Gibbons and Werner [29]. They used Gauss Bonnet theorem on the asymptotically flat spacetimes particularly finding deflection angle of Schwarzschild black hole in weak deflection limit (WDL). Then, Werner extended the work on Kerr black hole by applying GBT using Kerr-Renders optical geometry [30]. Following this, approach of finite distance of lens to the observer and source was applied by Ishihara, Asada, Ono, and Suzuki [61]. They computed the deflection angle in WDL for a static, spherically symmetric and asymptotically flat spacetime. Ono, Ishihara and Asada (OIA) extended their work by using GBT to analytically find deflection angle in weak field limits for stationary, axi-symmetric spacetimes [46].

The motivation behind this chapter is the progress in GBT approach for weak deflection angle computation together with the recent development in axi-symmetric solution of Buchdahl's ordinary differential equation. Either weak or strong gravitational lensing is being investigated by spacetime perspective, the use of null geodesic condition is always required. Hence, we can ignore the conformal factor term  $\mathcal{A}(q, \theta; a)$  and determine the deflection angle expression of the subject axi-symmetric SBI metric in weak deflection limit by OIA approach analytically.

The organization of this chapter is as follows: Section 4.1 contains a

brief overview of stationary axi-symmetric SBI spacetime solution in pure  $\mathcal{R}^2$  gravity. Plots for ergosphere and event horizon are given in section 4.2. Section 4.3 produces analytical expression of deflection angle of the considered axi-symmetric SBI metric in weak field limits by employing the GBT. Also, magnification and distortion of images are investigated in WDL.

## 4.1 Metric overview

An exact stationary, rotating and axi-symmetric SBI solution in pure  $\mathcal{R}^2$  gravity is described in [62]

$$dt^2 = \mathcal{A}(q, \theta; a) \left[ -\frac{\Delta(q) - a^2 \sin^2 \theta}{\rho^2} dt^2 + \frac{2a \sin^2 \theta}{\rho^2} (\Delta(q) - r^2(q) - a^2) dt d\phi \right. \\ \left. + \frac{\rho^2}{\Delta(q)} dq^2 + \rho^2 d\theta^2 + \frac{\Sigma}{\rho^2} \sin^2 \theta d\phi^2 \right], \quad (4.1)$$

where the functions and parameters involved are given below

$$\begin{aligned} \rho^2(q, \theta) &= r^2(q) + a^2 \cos^2 \theta, \\ \Sigma(q, \theta) &= (a^2 + r^2(q))^2 - a^2 \Delta(q) \sin^2 \theta, \\ \Delta(q) &= (q - q_-)(q - q_+) + a^2, \\ r^2(q) &= (q - q_-)^{-\frac{2q_-}{q_+ - q_-}} (q - q_+)^{\frac{2q_+}{q_+ - q_-}}, \\ q_{\pm} &= \pm \frac{r_s}{2} \left( \sqrt{1 + 3\tilde{k}^2} \mp 1 \right). \end{aligned} \quad (4.2)$$

Here  $a$  represents the spin (rotation),  $r_s = \frac{2M}{1+\tilde{k}}$  is the Schwarzschild radius and  $\tilde{k}$  is the Buchdahl parameter defined by  $\frac{k}{r_s}$ . The line element of stationary, axi-symmetric spacetime in polar co-ordinates  $(q, \theta)$  is generally given by

$$ds^2 = -A(q, \theta) dt^2 - 2H(q, \theta) dt d\phi + B(q, \theta) dq^2 + C(q, \theta) d\theta^2 + D(q, \theta) d\phi^2, \quad (4.3)$$

where the metric components are functions of  $q$  and  $\theta$  only. Now the axisymmetric spacetime (4.1), in comparison with the general form (4.3) gives the components as follows

$$\begin{aligned}
A(q, \theta) &= \frac{\Delta(q) - a^2 \sin^2 \theta}{\rho^2}, \\
B(q, \theta) &= \frac{\rho^2}{\Delta(q)}, \\
C(q, \theta) &= \rho^2, \\
D(q, \theta) &= \frac{\Sigma}{\rho^2} \sin^2 \theta, \\
H(q, \theta) &= \frac{a \sin^2 \theta}{\rho^2} \times (r^2(q) + a^2 - \Delta(q)),
\end{aligned} \tag{4.4}$$

here we have ignored the conformal factor  $\mathcal{A}(q, \theta; a)$  throughout our computations since the null geodesic condition is always required to be satisfied while determining deflection angle.

## 4.2 Event horizon and ergosphere

The conformal factor  $\mathcal{A}(q, \theta; a)$  has no zeros, the plots of which can be found in the work [54]. Thus the boundary beyond which not even light can escape, called as the event horizon, can be found by solving  $\Delta(q) = 0$  for  $q$ . Using  $\Delta(q)$  from (4.2) for the axisymmetric spacetime, we have the roots as follows

$$q_{\pm} = \frac{(q_- + q_+)}{2} \pm \frac{\sqrt{(q_- - q_+)^2 - 4a^2}}{2}, \tag{4.5}$$

where  $q_+$  represents outer event horizon and  $q_-$  represents inner event horizon (also called as Cauchy horizon) for the considered axisymmetric spacetime.

Located outside the event horizon, ergosphere is the region which drags matter (any object) along with the direction of spin of the axisymmetric spacetime. Dissimilar from event horizon, ergosphere allows the particles

to escape from its boundary called ergosurface. Mathematically, it can be determined by setting time component  $g_{tt}$  of considered spacetime zero. For the axi-symmetric SBI metric in  $\mathcal{R}^2$  gravity (4.1) we have

$$g_{tt} = \frac{\Delta(q) - a^2 \sin^2 \theta}{\rho^2} = 0. \quad (4.6)$$

The solution of this equation for  $q$  reads the radius of ergosphere as

$$q_{ergo\pm}(\theta) = \frac{1}{2} \left( -r_s \pm \sqrt{-2a^2 + r_s^2 + 3\tilde{k}^2 r_s^2 - 2a^2 \cos 2\theta} \right), \quad (4.7)$$

where  $q_{ergo+}$  and  $q_{ergo-}$  are the outer and inner ergosphere's radius, respectively.

The parametric plots for outer ergosphere with radius  $q_{ergo+}$  along with the outer event horizon with radius  $q_+$  are present in the graph (4.1), (4.2) and (4.3) respectively corresponds to the Buchdahl parameter  $\tilde{k} = 0$ ,  $\tilde{k} = 0.7$  and  $\tilde{k} = -0.4$ . For the increase in value of parameter  $\tilde{k}$ , the radius of event horizon decreases and the ergoregion increases.

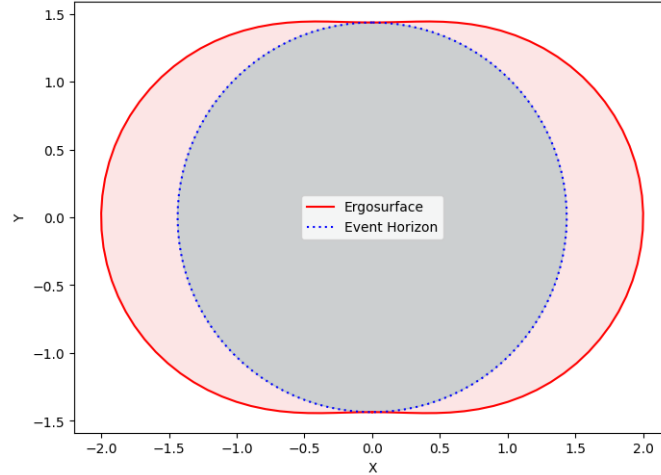


Figure 4.1: Ergosphere is plotted for axi-symmetric spacetime in  $\mathcal{R}^2$  gravity in WDL for  $\tilde{k} = 0$ . Shaded pink region depicts ergoregion.

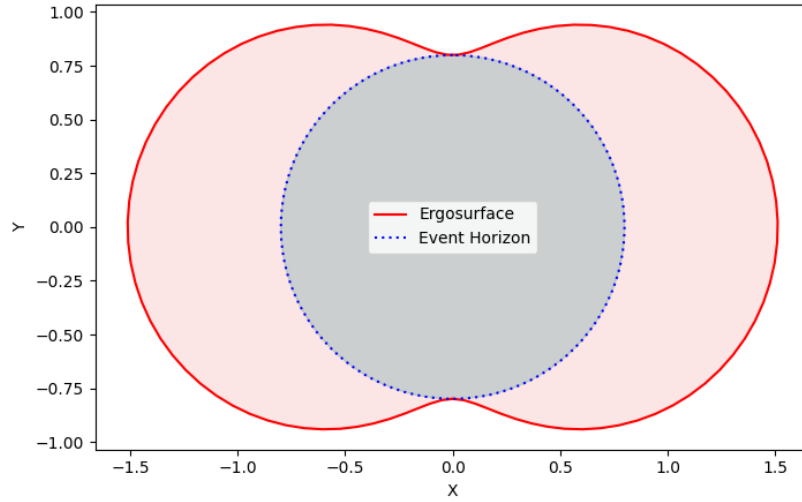


Figure 4.2: Ergosphere is plotted for axis-symmetric spacetime in  $\mathcal{R}^2$  gravity in WDL for  $\tilde{k} = 0.7$ . Shaded pink region depicts ergoregion.

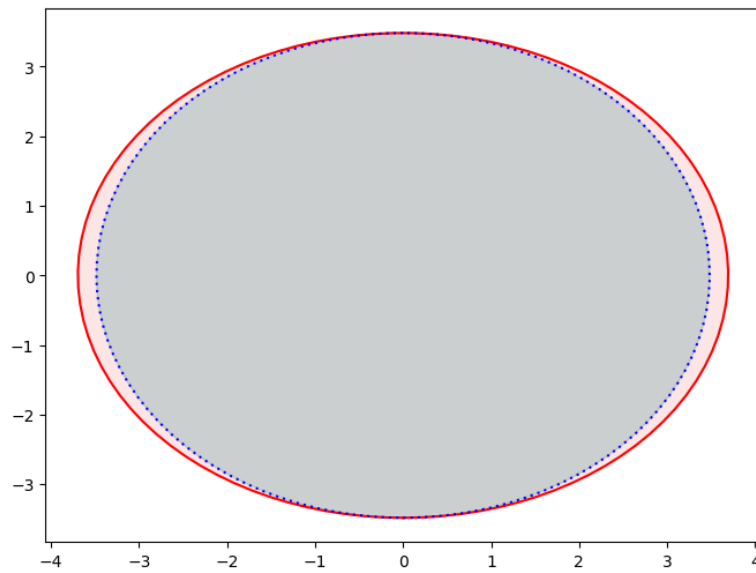


Figure 4.3: Ergosphere is plotted for axis-symmetric spacetime in  $\mathcal{R}^2$  gravity in WDL for  $\tilde{k} = -0.4$ . Shaded pink region depicts ergoregion.

### 4.3 Deflection angle in the weak field limit

In this section, main focus is to find the deflection angle in the weak field approximations of axi-symmetric spacetime (4.1) using finite distance approach by OIA, methodology as given in the literature review of this thesis (see section 2.1)

#### 4.3.1 The optical metric

The null geodesic condition  $ds^2 = 0$  for finding deflection angle leads to the optical metric which has the general form

$$dt = \sqrt{\gamma_{ij}dx^i dx^j} + \beta_i dx^i, \quad (4.8)$$

where the general expression of  $\gamma_{ij}$  is described as

$$\gamma_{ij}dx^i dx^j = \frac{B(q, \theta)}{A(q, \theta)} dq^2 + \frac{C(q, \theta)}{A(q, \theta)} d\theta^2 + \frac{A(q, \theta)D(q, \theta) + H^2(q, \theta)}{A^2(q, \theta)} d\phi^2, \quad (4.9)$$

and the component  $\beta_i$  is given as

$$\beta_i dx^i = -\frac{H(q, \theta)}{A(q, \theta)} d\phi. \quad (4.10)$$

Now that we have metric components of axi-symmetric SBI solution in  $\mathcal{R}^2$  defined in (4.4), thereby the metric (4.9) produces

$$\begin{aligned} \gamma_{ij}dx^i dx^j &= \frac{\rho^4}{\Delta(\Delta - a^2 \sin^2 \theta)} dq^2 + \frac{\rho^4}{(\Delta - a^2 \sin^2 \theta)} d\theta^2 \\ &+ \frac{\Sigma(\Delta - a^2 \sin^2 \theta) \sin^2 \theta + [a \sin^2 \theta(r^2(q) + a^2 - \Delta)]^2}{(\Delta - a^2 \sin^2 \theta)^2} d\phi^2. \end{aligned} \quad (4.11)$$

Also, using the expressions of  $A(q, \theta)$  and  $H(q, \theta)$  into (4.10) yields

$$\beta_i dx^i = -\frac{a \sin^2 \theta(r^2(q) + a^2 - \Delta)}{\Delta - a^2 \sin^2 \theta} d\phi. \quad (4.12)$$

### 4.3.2 OIA approach of Gauss Bonnet theorem

For axi-symmetric spacetimes in equatorial plane, the weak deflection angle for the source  $S$  and observer  $R$  is defined employing the GBT by OIA [46] as follows

$$\hat{\alpha} = - \int \int_{R^\infty \square S^\infty} \mathcal{K} dS + \int_S^R \kappa_g dl, \quad (4.13)$$

here  $\mathcal{K}$  represents Gaussian curvature and the geodesic curvature of light rays is denoted by  $\kappa_g$ . Further  $dl$  and  $dS$  represents the arc length element and surface element, respectively. Note that the sign of arc length  $\ell$  is taken in accordance with the direction of motion of light, positive meaning prograde motion and negative depicts retrograde orbiting of light ray.

#### Surface Integral

The Gaussian curvature gives information about how the surface is curved, and is mathematically defined by Riemann curvature as follows

$$\mathcal{K} = \frac{R_{q\phi q\phi}}{\gamma} \equiv \frac{1}{\sqrt{\gamma}} \left[ \frac{\partial}{\partial \phi} \left( \frac{\sqrt{\gamma}}{\gamma_{qq}} \Gamma_{q\phi}^{\phi} \right) - \frac{\partial}{\partial q} \left( \frac{\sqrt{\gamma}}{\gamma_{q\phi}} \Gamma_{q\phi}^{\phi} \right) \right]. \quad (4.14)$$

Since the components of the metric  $\gamma_{ij} dx^i dx^j$  are not a function of  $\phi$ , therefore

$$\begin{aligned} \mathcal{K} &= \frac{1}{\sqrt{\gamma}} \left[ -\frac{\partial}{\partial q} \left( \frac{\sqrt{\gamma}}{\gamma_{qq}} \Gamma_{q\phi}^{\phi} \right) \right], \\ &= -\frac{1}{\sqrt{\gamma}} \left[ \frac{\partial}{\partial q} \left( \frac{\sqrt{\gamma}}{2\gamma_{qq}} \gamma^{\phi\phi} \frac{\partial}{\partial q} (\gamma_{\phi\phi}) \right) \right]. \end{aligned} \quad (4.15)$$

To restrict the light ray in equatorial plane set  $\theta = \frac{\pi}{2}$  implying  $\dot{\theta} = 0$ . Using the metric components of (4.11), the Gaussian curvature has the form

$$\begin{aligned} \mathcal{K} &= \frac{4r_s \left( q - \frac{r_s}{2} \left( -1 + \sqrt{1 + 3\tilde{k}^2} \right) \right)^{\frac{2}{\sqrt{1+3\tilde{k}^2}}} \left( q + \frac{r_s}{2} \left( 1 + \sqrt{1 + 3\tilde{k}^2} \right) \right)^{-\frac{2}{\sqrt{1+3\tilde{k}^2}}}}{(-4q^2 - 4qr_s + 3\tilde{k}^2 r_s^2)^3} \\ &\times \left[ 24a^2(2q + r_s) + (4q + r_s - 3\tilde{k}^2 r_s)(4q^2 + 4qr_s - 3\tilde{k}^2 r_s^2) \right]. \end{aligned} \quad (4.16)$$

We apply the weak field and slow rotation on (4.16). Therefore expanding the series brings the simplified form

$$\mathcal{K} = -\frac{2M}{(1 + \tilde{k})q^3} + \mathcal{O}\left(\frac{a^2 M^2}{q^5}\right). \quad (4.17)$$

Now seeking the surface element  $dS$ , the formula is  $dS = \sqrt{\det \gamma_{ij}} dx^i dx^j$ , for axi-symmetric SBI spacetime

$$\begin{aligned} dS &= \sqrt{\det \gamma_{ij}} dq d\phi, \\ &= \left( q + \frac{5M}{1 + \tilde{k}} \right) dq d\phi + \mathcal{O}(M^2). \end{aligned} \quad (4.18)$$

In the last line: expressions of  $q_+$ ,  $q_-$  and  $r_s$  have been substituted. Since the Gaussian curvature  $\mathcal{K}$  begins with  $\mathcal{O}(M)$ , therefore linear order of surface element is enough in our computation of deflection angle.

In weak field limit, surface integral of the Gaussian curvature (4.17) using the surface element (4.18) thus proceeds as

$$\begin{aligned} - \int \int_{R^\infty S^\infty} \mathcal{K} dS &= - \int_{q_{OE}}^{\infty} dq \int_{\phi_S}^{\phi_R} d\phi \left( -\frac{2M}{(1 + \tilde{k})q^3} \right) \left( q + \frac{5M}{1 + \tilde{k}} \right), \\ &= - \int_{q_{OE}}^{\infty} dq \int_{\phi_S}^{\phi_R} d\phi \left( -\frac{2M}{(1 + \tilde{k})q^2} \right) + \mathcal{O}\left(\frac{M^2}{q^3}\right), \\ &= \frac{2M}{(1 + \tilde{k})} \int_{\infty}^{q_{OE}} dq \int_{\phi_S}^{\phi_R} d\phi \left( -\frac{1}{q^2} \right) + \mathcal{O}\left(\frac{M^2}{q^3}\right). \end{aligned} \quad (4.19)$$

Now that the straight line approximation in *zeroth* order gives  $q = \frac{b}{\sin \phi}$ , making the substitution  $u = q^{-1}$  implies that  $u = \frac{\sin \phi}{b}$ . Surface integral (4.19) attains the form

$$\begin{aligned} - \int \int_{R^\infty S^\infty} \mathcal{K} dS &= \frac{2M}{(1 + \tilde{k})} \int_0^{\frac{\sin \phi}{b}} du \int_{\phi_S}^{\phi_R} d\phi + \mathcal{O}(M^2 u^3), \\ &= \frac{2M}{(1 + \tilde{k})b} \int_{\phi_S}^{\phi_R} \sin \phi d\phi + \mathcal{O}(M^2 u^3), \\ &= \frac{2M}{(1 + \tilde{k})b} [\cos \phi_S - \cos \phi_R] + \mathcal{O}(M^2 u^3), \end{aligned}$$



$$= \frac{2M}{(1 + \tilde{k})b} \left[ \sqrt{1 - b^2 u_S^2} + \sqrt{1 - b^2 u_R^2} \right] + \mathcal{O}(M^2 u^3). \quad (4.20)$$

## Path integral

The geodesic curvature measures how far the boundary curve deviates from the geodesic. For axi-symmetric spacetimes, it has the general expression [46]

$$\kappa_g = -\frac{1}{\sqrt{\gamma\gamma^{\theta\theta}}} \beta_{\phi,q}. \quad (4.21)$$

In matrix form, the spacetime (optical)  $\gamma$  is a diagonal  $3 \times 3$  matrix with entries  $\gamma_{qq}$ ,  $\gamma_{\theta\theta}$  and  $\gamma_{\phi\phi}$ . The inverse components are determined by reciprocating each diagonal entry. Thus

$$\gamma^{\theta\theta} = \frac{1}{\gamma_{\theta\theta}}. \quad (4.22)$$

For axi-symmetric SBI metric, (4.22) becomes

$$\begin{aligned} \gamma^{\theta\theta} &= \frac{(\Delta - a^2 \sin^2 \theta)}{\rho^4}, \\ &= (q - q_+)^{1 - \frac{4q_+}{q_+ - q_-}} (q - q_-)^{1 + \frac{4q_-}{q_+ - q_-}}. \end{aligned} \quad (4.23)$$

This is obtained setting  $\theta = \pi/2$  and using expressions of certain parameters. The term  $\gamma$  in the denominator of (4.21) for optical metric of axi-symmetric spacetime (4.1) is as follows

$$\gamma = \det \gamma_{ij} = \det \begin{vmatrix} \frac{\rho^4}{\Delta(\Delta - a^2 \sin^2 \theta)} & 0 & 0 \\ 0 & \frac{\rho^4}{(\Delta - a^2 \sin^2 \theta)} & 0 \\ 0 & 0 & \frac{(\Delta - a^2 \sin^2 \theta) \Sigma \sin^2 \theta + [a \sin^2 \theta (a^2 + r^2 (q) - \Delta)]^2}{(\Delta - a^2 \sin^2 \theta)^2} \end{vmatrix}.$$

Using parameters from (4.2), setting  $\theta = \frac{\pi}{2}$  followed by simplification gives us

$$\gamma = (q - q_+)^{4 \frac{2q_+ + q_-}{q_+ - q_-}} (q - q_-)^{-4 \frac{q_+ + 2q_-}{q_+ - q_-}}. \quad (4.24)$$

Now that the component  $\beta_\phi$  from (4.12) is written as

$$\beta_\phi = \frac{a \sin^2 \theta (r^2(q) + a^2 - \Delta)}{\Delta - a^2 \sin^2 \theta}, \quad (4.25)$$

substitute the expressions of  $r^2(q)$ ,  $\Delta$  from (4.2) followed by the use of  $\theta = \frac{\pi}{2}$  to get

$$\beta_\phi = a \left[ 1 - (q - q_+)^{\frac{q_+ + q_-}{q_+ - q_-}} (q - q_-)^{-\frac{q_+ + q_-}{q_+ - q_-}} \right]. \quad (4.26)$$

Differentiation of (4.26) with respect to  $q$  using *Mathematica* yields

$$\beta_{\phi,q} = -a(q - q_+)^{\frac{2q_-}{q_+ - q_-}} (q - q_-)^{-\frac{2q_+}{q_+ - q_-}} (q_+ - q_-). \quad (4.27)$$

Substitution of (4.23), (4.24) and (4.27) into (4.21) and simple algebraic simplification bring geodesic curvature into the form

$$\kappa_g = a(q_+ + q_-)(q - q_-)^{-\frac{1}{2} + \frac{2q_-}{-q_- + q_+}} (q - q_+)^{-\frac{5}{2} + \frac{2q_-}{q_- - q_+}}. \quad (4.28)$$

After using the parameter  $q_+$ ,  $q_-$  and  $r_s$ , (4.28) reads

$$\kappa_g = -\frac{2aM}{(1 + \tilde{k})q^3}. \quad (4.29)$$

Linear approximation for the photon orbit  $q = \frac{b}{\cos \phi}$  and  $\ell = b \tan \phi$  gives

$$d\ell = \frac{b}{\cos^2 \phi} d\phi. \quad (4.30)$$

Path integral of geodesic curvature can now be determined as follows

$$\begin{aligned} \int_S^R \kappa_g dl &= \int_S^R -\frac{2aM}{(1 + \tilde{k})q^3} dl + \mathcal{O}\left(\frac{aM^2}{q^4}\right), \\ &= -\frac{2aM}{(1 + \tilde{k})b^2} \int_{\phi_S}^{\phi_R} \cos \phi d\phi + \mathcal{O}\left(\frac{aM^2}{b^3}\right), \\ &= \frac{2aM}{(1 + \tilde{k})b^2} [\sin \phi_S - \sin \phi_R] + \mathcal{O}\left(\frac{aM^2}{b^3}\right), \end{aligned}$$

with the use of  $\sin \phi_S = \sqrt{1 - b^2 u_S^2}$  and  $\sin \phi_R = -\sqrt{1 - b^2 u_R^2}$  the ultimate form of path integral of geodesic curvature becomes

$$\int_S^R \kappa_g dl = \pm \frac{2aM}{(1 + \tilde{k})b^2} \left[ \sqrt{1 - b^2 u_S^2} + \sqrt{1 - b^2 u_R^2} \right] + \mathcal{O}\left(\frac{aM^2}{b^3}\right). \quad (4.31)$$

In this integral, the sign + indicates prograde case  $dl > 0$  and the sign - indicates retrograde case of light rays  $dl < 0$ .

### Weak deflection angle

Now that the path integral of geodesic curvature and the surface integral of Gaussian curvature have been obtained, it is straightforward to work out the deflection angle analytically in weak deflection limit. Through the use of (4.20), (4.31) in (4.13), the deflection angle in finite distance is determined as follows

$$\hat{\alpha} = - \int \int_{R^\infty S^\infty} \mathcal{K} dS - \int_R^S \kappa_g dl, \quad (4.32)$$

For prograde and retrograde orbits, the deflection angles respectively are:

$$\hat{\alpha}_{prog} = \frac{2M}{(1 + \tilde{k})b} \left[ \sqrt{1 - b^2 u_S^2} + \sqrt{1 - b^2 u_R^2} \right] - \frac{2aM}{(1 + \tilde{k})b^2} \left[ \sqrt{1 - b^2 u_S^2} + \sqrt{1 - b^2 u_R^2} \right], \quad (4.33)$$

$$\hat{\alpha}_{retro} = \frac{2M}{(1 + \tilde{k})b} \left[ \sqrt{1 - b^2 u_S^2} + \sqrt{1 - b^2 u_R^2} \right] + \frac{2aM}{(1 + \tilde{k})b^2} \left[ \sqrt{1 - b^2 u_S^2} + \sqrt{1 - b^2 u_R^2} \right]. \quad (4.34)$$

Recall that this is for the source  $S$  and observer  $R$  at finite distance. Higher order terms have been truncated. For far limits of both, there is  $u_R \rightarrow 0$  and  $u_S \rightarrow 0$ . Therefore, for infinite distance limit the deflection angle (4.33) and (4.34) attains the form respectively as

$$\hat{\alpha}_{prog} = \frac{4M}{(1 + \tilde{k})b} - \frac{4aM}{(1 + \tilde{k})b^2}, \quad (4.35)$$

$$\hat{\alpha}_{retro} = \frac{4M}{(1 + \tilde{k})b} + \frac{4aM}{(1 + \tilde{k})b^2}. \quad (4.36)$$

Note that weak deflection angle for prograde and retrograde motion of light rays for far distance is given for leading order of weak field approximation. The weak deflection angle is plotted against the impact parameter  $b$  for prograde motion in Fig. (4.4). As the impact parameter increases, the gravitational pull of axisymmetric spacetime weakens and thus the deflection angle

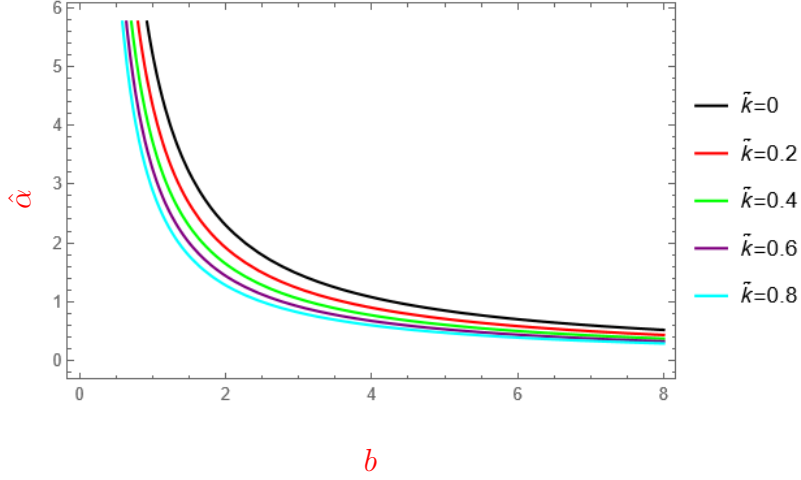


Figure 4.4: The weak deflection angle  $\hat{\alpha}_{prog}$  for prograde light ray is plotted for different values of Buchdahl parameter  $\tilde{k}$  against impact parameter  $b$  for axisymmetric spacetime. The spin is taken as  $a = 0.3$ .

of light decreases. For the Buchdahl parameter  $\tilde{k} = 0$  and the spin  $a = 0$ , the weak deflection angle becomes

$$\hat{\alpha} = \frac{4M}{b}, \quad (4.37)$$

which is a known deflection angle in WDL for SBH [29]. Thus our analysis of deflection angle in WDL for axisymmetric SBI metric is reliable with SBH.

### 4.3.3 Image magnification and distortion

Gravitational lens equation to investigate the lensing phenomenon for small as well as large deflection angles is defined in [25] as

$$\tan \beta = \tan \theta - \alpha, \quad (4.38)$$

where  $\alpha$  is given by

$$\alpha = \frac{D_{LS}}{D_{OS}} \tan(\hat{\alpha} - \theta), \quad (4.39)$$

here  $\hat{\alpha}$  is representation for deflection angle. The Greek letters  $\beta$  and  $\theta$  express angular source position and angular image position, respectively.  $D_{LS}$  symbolizes the distance between lens and the luminous source. Also, the distance between observer and light source is characterized by  $D_{OS}$ . The distance parameter is  $\mathcal{D} = \frac{D_{LS}}{D_{OS}}$ . Rewriting the impact parameter  $b$  in relation with angular image position

$$b = D_{OL} \sin \theta, \quad (4.40)$$

where  $D_{OL}$  represents observer-lens distance. Also the general expression of circularly symmetric lensing magnification (total)  $\mu$  is described in [49] as

$$\mu = \mu_t \mu_r, \quad (4.41)$$

here the tangential magnification  $\mu_t$  and radial magnification  $\mu_r$  can be defined as

$$\mu_t = \left( \frac{\sin \beta}{\sin \theta} \right)^{-1}, \quad \mu_r = \left( \frac{d\beta}{d\theta} \right)^{-1}. \quad (4.42)$$

The distortion parameter  $\Delta$  and logarithmic distortion parameter  $\delta$  as explained in subsection (3.2.3) has the general expressions

$$\Delta = \frac{\mu_t}{\mu_r}, \quad \delta = \log_{10} |\Delta|. \quad (4.43)$$

For the axi-symmetric SBI metric in pure  $\mathcal{R}^2$  gravity (4.1), consider the black hole M87\* as a lens. The mass of which is  $6.5 \times 10^9 M_\odot$  and the distance  $D_{OL}$  is 16.8 Mpc [58]. Therefore, the ratio of mass to distance becomes  $1.84951 \times 10^{-11}$ . Gravitational lensing in weak deflection limit of axi-symmetric SBI metric in pure  $\mathcal{R}^2$ , magnification of both primary images and secondary images are investigated here.

The primary image (represented by  $\theta_p$ ) and the secondary image (represented by  $\theta_s$ ), are the roots of lens equation. Thus can be obtained by

solving the equation (4.38) for  $\theta$ . The prograde deflection angle  $\hat{\alpha}$  (4.35) for axi-symmetric spacetime in  $\mathcal{R}^2$  gravity in WDL is considered here. The total  $\mu_p$ , tangential  $\mu_{pt}$  and radial  $\mu_{pr}$  magnifications for primary image are computed in *Mathematica* using expressions of angular primary image position. Also, with use the of angular secondary image position- the absolute total  $\mu_s$ , absolute tangential  $\mu_{st}$  and absolute radial  $\mu_{sr}$  magnifications are found. These all magnifications are illustrated in the Figure 4.5. Their behaviour is checked for three different values of Buchdahl parameter  $\tilde{k} = 0$ ,  $\tilde{k} = -0.5$  and  $\tilde{k} = 0.5$ . The graph labeled as (a) is the plot for primary tangential magnification  $\mu_{pt}$  and absolute secondary tangential magnification  $|\mu_{st}|$  against the dimensionless distance parameter  $\mathcal{D}$ . All the curves; three for primary images and three for secondary images are increasing with increase in  $\mathcal{D}$ . Also, the graph in label (d) shows that primary tangential magnification  $\mu_{pt}$  and absolute secondary tangential magnification  $|\mu_{st}|$  when plotted against  $M/D_{OL}$ , has increasing behaviour for considered values of Buchdahl parameter  $\tilde{k}$ . The graphs in the labels (b) and (e) demonstrate the primary radial magnifications  $\mu_{pr}$  and absolute secondary radial magnifications  $|\mu_{sr}|$  for three values of  $\tilde{k}$ . They are graphed against dimensionless parameter  $\mathcal{D}$  and the ratio  $M/D_{OL}$ . Both plots have similar behaviour, the primary radial magnifications  $\mu_{pr}$  for  $\tilde{k} = -0.5$  (dashed blue),  $\tilde{k} = 0$  (dashed orange) and  $\tilde{k} = 0.5$  (dashed green) promptly drops first and then decrease slowly. The absolute secondary radial magnifications  $|\mu_{sr}|$  for  $\tilde{k} = -0.5$  (black),  $\tilde{k} = 0$  (red) and  $\tilde{k} = 0.5$  (green) can be seen to rise rapidly and later increase with slower rate. The total primary magnification  $\mu_p$  and the absolute total secondary magnification  $|\mu_s|$  is plotted against dimensionless parameter  $\mathcal{D}$  and the mass to distance ratio  $M/D_{OL}$  in graph labeled (c) and (e), respectively. Graphs depict that total magnification increases with the increase in param-

eters on x-axis for  $\tilde{k} = -0.5$ ,  $\tilde{k} = 0$  and  $\tilde{k} = 0.5$ . Here if we compare the radial, tangential and total magnification curves for  $\tilde{k} = 0$  in all the six plots with the respective plots in Schwarzschild lensing in [49], we can clearly see the similar behaviours of all the three magnifications. Henceforth, our plots are consistent with SBH magnification.

In order to investigate the image distortion, again model M87\* black hole as a lens for the axi-symmetric spacetime in pure  $\mathcal{R}^2$  gravity. The logarithmic distortion parameter for secondary  $\delta_s$  and primary  $\delta_p$  images can be obtained using *Mathematica* and are plotted in the Figure 4.6. In plots (a) and (b) respectively, the primary logarithmic distortion parameter  $\delta_p$  and secondary logarithmic distortion parameter  $\delta_s$  against the angular position of source is plotted for three different values of Buchdahl parameter. The graphs labeled (c) and (d) is for the plot of  $\delta_p$  and  $\delta_s$ , respectively, versus the dimensionless parameter  $\mathcal{D}$ . The graphs (e) and (f) shows the plot for  $\delta_p$  and  $\delta_s$  against the ratio  $M/D_{OL}$ . The logarithmic distortion parameter for both primary and secondary images can be observed to increase for the increase in parameter  $\mathcal{D}$  and the ratio  $M/D_{OL}$ . However, the logarithmic distortion parameter  $\delta_p$  and  $\delta_s$  when graphed against the angular position of luminous source  $\beta$  can be seen to decrease for considered values of Buchdahl parameter. Also the curves in graphs for the primary and secondary distortion for corresponding values of  $\tilde{k}$  are very close (or same). Keep in mind that the primary and secondary distortion parameters have opposite signs. Thus, when the distortion parameters (not absolute) for primary and secondary images are summed up, gives answer approximately *zero*.

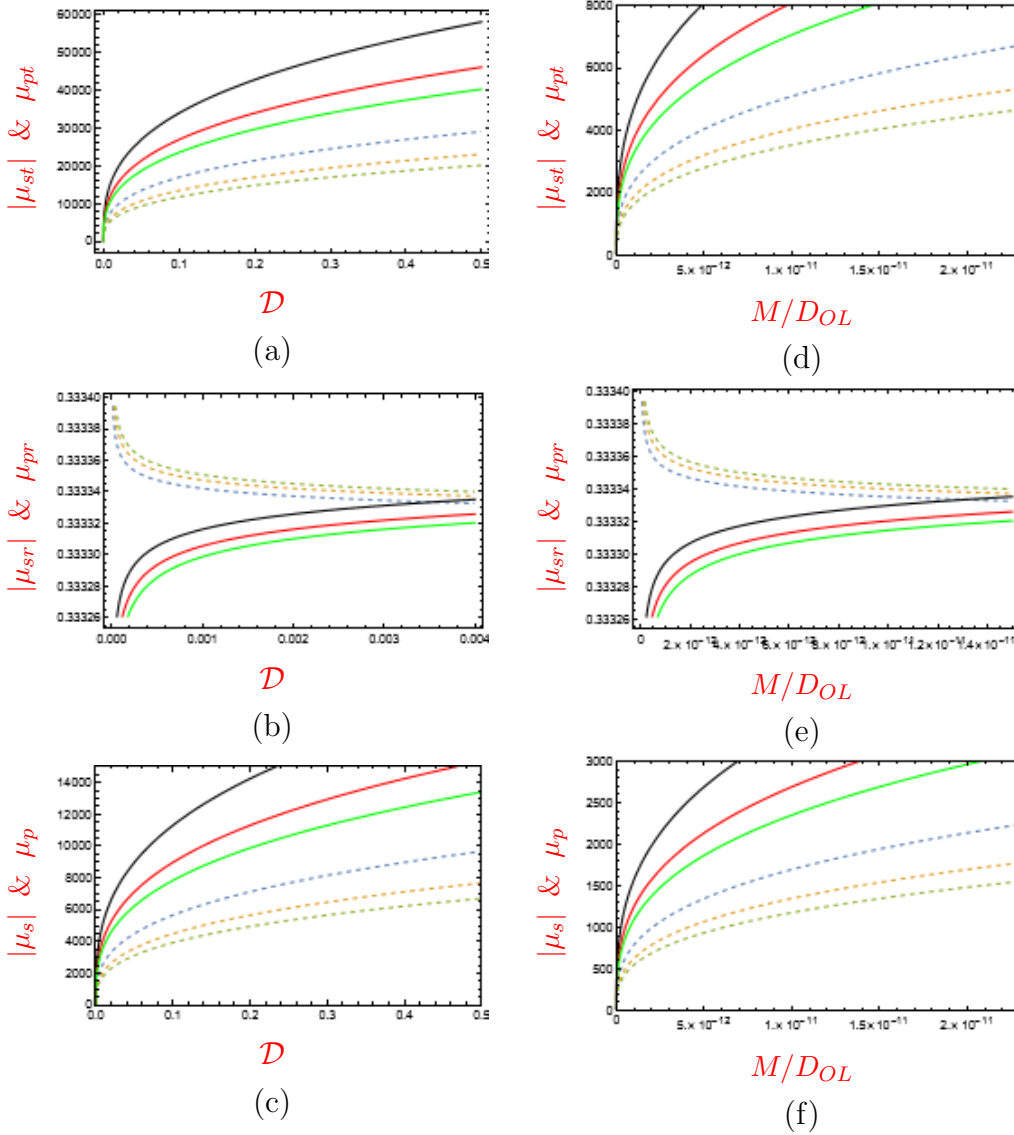


Figure 4.5: Magnification is plotted for axi-symmetric spacetime in  $\mathcal{R}^2$  gravity in WDL. Plots for tangential, radial and total magnifications versus the dimensionless parameter  $\mathcal{D}$  is given in (a), (b) and (c); each in order. In graphs (c), (d) and (f) respectively; tangential, radial and total magnifications are plotted against the ratio  $M/D_{OL}$ . Plot convention: Primary magnifications for  $\tilde{k} = -0.5, \tilde{k} = 0$  and  $\tilde{k} = 0.5$  are respectively represented by dashed blue, orange and green curves. Secondary magnifications for  $\tilde{k} = -0.5, \tilde{k} = 0$  and  $\tilde{k} = 0.5$  are respectively represented by solid black, red and green curves.



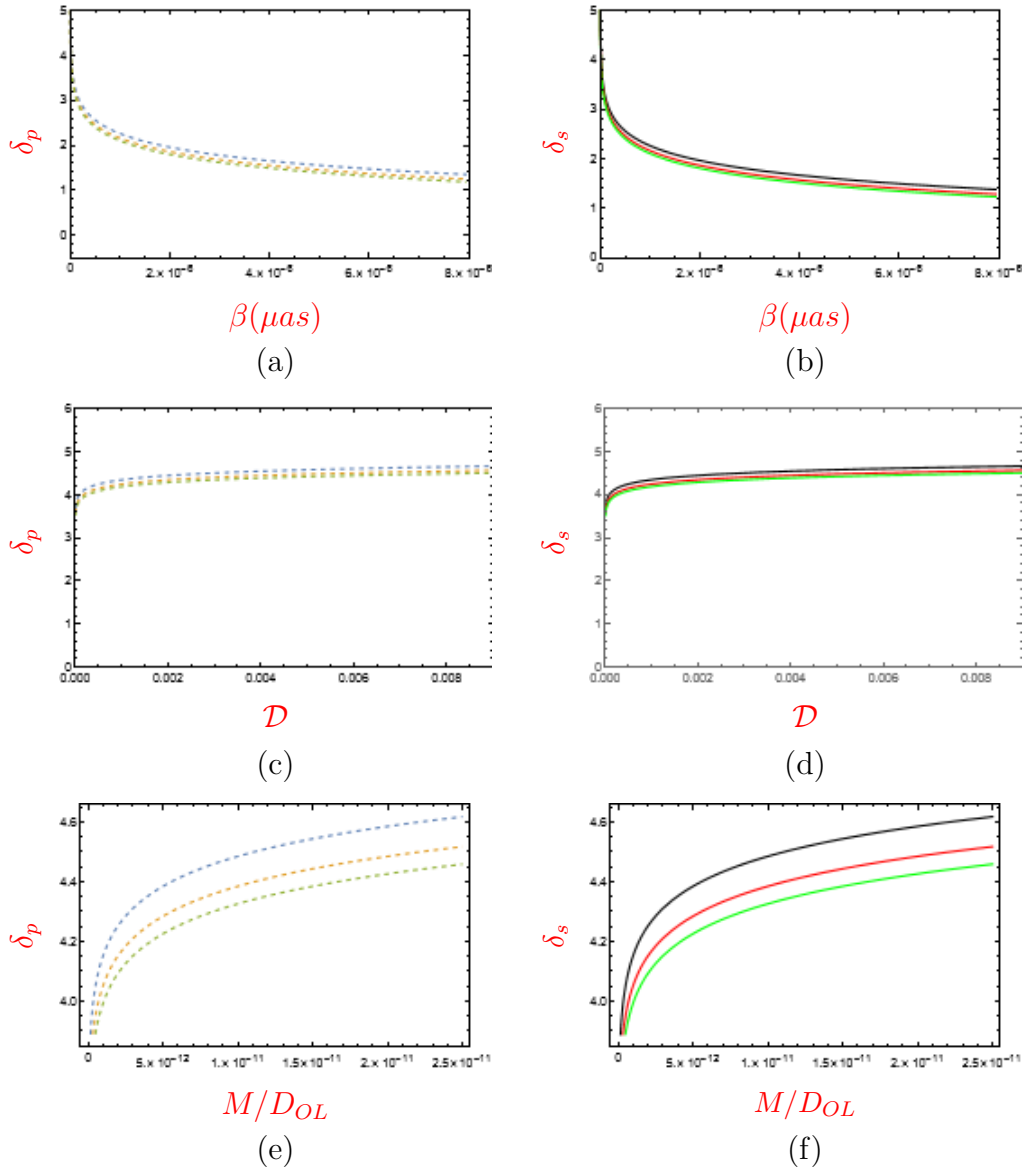


Figure 4.6: Logarithmic distortion is plotted for axi-symmetric metric in  $\mathcal{R}^2$  gravity. The primary logarithmic distortion ( $\delta_p$ ) and the secondary logarithmic distortion ( $\delta_s$ ) is plotted against angular position of source  $\beta$  in (a) and (b). The primary logarithmic distortion ( $\delta_p$ ) and secondary logarithmic distortion ( $\delta_s$ ) is plotted against the dimensionless parameter  $\mathcal{D}$  in (c) and (d). The primary( $\delta_p$ ) and secondary( $\delta_s$ ) logarithmic distortion is plotted against  $M/D_{OL}$  in (e) and (f). Plot convention: Primary logarithmic distortion for  $\tilde{k} = -0.5, \tilde{k} = 0$  and  $\tilde{k} = 0.5$  are respectively represented by dashed blue, orange and green curves. Secondary logarithmic distortion for  $\tilde{k} = -0.5, \tilde{k} = 0$  and  $\tilde{k} = 0.5$  are respectively represented by solid black, red and green curves.

## Summary

In weak deflection limit, the analytical expressions of prograde  $\hat{\alpha}_{prog}$  and retrograde  $\hat{\alpha}_{retro}$  deflection angle for the stationary, axi-symmetric SBI spacetime in pure  $\mathcal{R}^2$  gravity is determined in this chapter. To do so, OIA approach applying Gauss Bonnet theorem has been used here. To investigate the images formed by weak gravitational lensing, we have modeled M87\* located in the center of Messier 87 as a lens of considered axi-symmetric spacetime. The black hole has a mass  $6.5 \times 10^9 M_{\odot}$ . The radial, tangential and total magnification for both primary and absolute secondary images has been plotted. Radial magnification for secondary images, tangential and total magnification for both primary and secondary images can be observed increasing for the dimensionless parameter  $\mathcal{D}$  and  $M/D_{OL}$ . On the other hand radial magnification for primary images decreases with increase in the parameters on x-axis. Moreover, the behaviour of logarithmic distortion parameter has also been explored using black hole M87\* as a lens. It is seen that sum of distortion parameter (not absolute) is approximately *zero* satisfying Virbhadra's hypothesis [49].

# Chapter 5

## Results and Discussions

This dissertation involves the comprehensive exploration of gravitational lensing for diverse spacetime geometries using the foundational understanding of general relativity. After analyzing gravitational lensing of Kerr metric in WDL and SDL, we successfully extended the research of gravitational lensing on *special* Buchdahl-inspired (SBI) metric and axi-symmetric metric in  $\mathcal{R}^2$  gravity. First two chapters are based on literature review and the rest of chapters contain new research.

Chapter 1 established a theoretical framework based on dynamics of general relativity with a particular focus on spacetimes, black hole, geodesics, gravitational lensing and lens equations.

Chapter 2 involves the comprehensive review of gravitational lensing by axi-symmetric Kerr spacetime. By employing Gauss-Bonnet theorem, deflection angle of weak lensing was reduced to that of Schwarzschild spacetime for spin  $a = 0$ . Similarly for very small spin  $a \approx 0$ , coefficients  $\bar{a}$  and  $\bar{b}$  of strong lensing were evaluated leading to the relevance of deflection angle with Schwarzschild black hole.

Chapter 3 determined the expression for deflection angle of weak and

strong deflection for asymptotically flat *special* Buchdahl-inspired (SBI) metric. Bending angle according to Gauss Bonnet theorem was calculated employing Gibbons and Werner's approach in WDL. Tangential and total magnifications for primary and secondary images by model black hole M87\* with mass  $6.5 \times 10^9 M_\odot$  are observed increasing when plotted against dimensionless parameter  $\mathcal{D}$  and ratio  $M/D_{OL}$ . While the radial magnification varies for primary images (increase) and secondary images (decrease). Moreover, the sum of distortion parameter of primary and secondary image vanishes as aligning with hypothesis of Virbhadra[49]. The graphs of the deflection angle in strong field are depicted for three cases supported by SBIM i.e, Morris Thorne wormhole for  $\tilde{k} \in (-1, 0)$ , SBH for  $\tilde{k} = 0$ , and a naked singularity for  $\tilde{k} \in (-\infty, -1) \cup (0, \infty)$ . Additionally, learning observables were used to estimate the positions of images and distance between innermost and outermost image by modelling Sgr A\* and M87\*, black holes of Milky Way and Messier 87, as SBIM lens. Einstein rings are also plotted choosing three values for three different cases of SBIM. Magnification of outermost relativistic image setting  $n = 1$  has been investigated. It can be observed that for angular source position  $\beta \rightarrow 0$ , the magnification of images is maximum.

Chapter 4 employs OIA approach to determine analytic expressions of deflection angle in weak deflection limit for the stationary, axi-symmetric spacetime in pure  $\mathcal{R}^2$  gravity. To investigate the images formed by weak lensing, M87\* was modeled as a lens of axi-symmetric spacetime. Radial magnification for secondary images, tangential and total magnification for both primary and secondary images can be observed increasing for the dimensionless parameter  $\mathcal{D}$  and ratio  $M/D_{OL}$ . On the other hand radial magnification for primary images decreases with increase in the parameters on x-axis. Moreover, sum of distortion parameter (zero) showed consistency

with Virbhadra's hypothesis. This study explores the effect of curvature of spacetime influenced by massive black hole spin on trajectories of light rays and characteristics of lensed images.

# Bibliography

- [1] E. H. T. Collaboration, “Astronomers capture first image of a black hole.”
- [2] E. H. T. Colaboration, “First image of black hole at the centre of Milky Way.”
- [3] M. Bettinelli, M. Simioni, A. Aparicio, S. L. Hidalgo, S. Cassisi, A. R. Walker, G. Piotto, and F. Valdes, “The Canarias Einstein ring: a newly discovered optical Einstein ring,” *Monthly Notices of the Royal Astronomical Society: Letters*, vol. 461, pp. L67–L71, 2016.
- [4] H. Arakida, “Light deflection and Gauss–Bonnet theorem: definition of total deflection angle and its applications,” *General Relativity and Gravitation*, vol. 50, p. 48, 2018.
- [5] S. Paul, “Strong gravitational lensing by a strongly naked null singularity,” *Physical Review D*, vol. 102, no. 6, p. 064045, 2020.
- [6] T. Hsieh, D.-S. Lee, and C.-Y. Lin, “Strong gravitational lensing by Kerr and Kerr–Newman black holes,” *Physical Review D*, vol. 103, no. 10, p. 104063, 2021.
- [7] N. Straumann, *General Relativity*. Springer Science & Business Media, 2012.

- [8] H. Falcke, “Imaging black holes: past, present and future,” in *Journal of Physics: Conference Series*, vol. 942, no. 1, 2017, p. 012001.
- [9] D. Psaltis, “Testing General Relativity with the EHT,” *General Relativity and Gravitation*, vol. 51, no. 10, p. 137, 2019.
- [10] Event Horizon Telescope Collaboration and others, “First M87 Event Horizon Telescope results. I. The shadow of the supermassive black hole,” *Astrophysical Journal Letters*, vol. 875, p. L1, 2019.
- [11] Event Horizon Telescope (EHT) Collaboration and others, “First M87 Event Horizon Telescope results. IV. Imaging the central supermassive black hole,” *Astrophysical Journal Letters*, vol. 875, p. L4, 2019.
- [12] K. Akiyama, A. Alberdi, W. Alef, J. C. Algaba, R. Anantua, K. Asada, R. Azulay, U. Bach, A.-K. Baczko, and D. Ball, “First Sagittarius A\* Event Horizon Telescope results. I. The shadow of the supermassive black hole in the center of the Milky Way,” *The Astrophysical Journal Letters*, vol. 930, no. 2, p. L12, 2022.
- [13] E. H. T. Collaboration *et al.*, “First Sagittarius A\* Event Horizon Telescope Results. II. EHT and Multi-wavelength Observations, Data Processing, and Calibration,” *The Astrophysical Journal Letters*, vol. 930, p. L13, 2023.
- [14] K. Akiyama, A. Alberdi, W. Alef, J. C. Algaba, R. Anantua, K. Asada, R. Azulay, U. Bach, A.-K. Baczko, D. Ball *et al.*, “First Sagittarius A\* Event Horizon Telescope results. III. Imaging of the galactic center supermassive black hole,” *The Astrophysical Journal Letters*, vol. 930, no. 2, p. L14, 2022.

- [15] K. Akiyama, W. Alberdi, A. Algaba, J. C. Alef, R. Anantua, K. Asada, R. Azulay, U. Bach, A.-K. Baczko, D. Ball *et al.*, “First Sagittarius A\* Event Horizon Telescope results. IV. Variability, morphology, and black hole mass,” *The Astrophysical Journal Letters*, vol. 930, no. 2, p. L15, 2022.
- [16] A. Einstein, “Zur allgemeinen Relativitätstheorie,” 1915.
- [17] K. Schwarzschild, “Über das Gravitationsfeld eines Massenpunktes nach der Einsteinschen Theorie,” *Sitzungsberichte der königlich preussischen Akademie der Wissenschaften*, pp. 189–196, 1916.
- [18] H. Reissner, “Über die Eigengravitation des elektrischen Feldes nach der Einsteinschen Theorie,” *Annalen der Physik*, vol. 355, no. 9, pp. 106–120, 1916.
- [19] G. Nordstrom, “On the energy of the gravitation field in Einstein’s theory,” *Koninklijke Nederlandse Akademie van Wetenschappen Proceedings Series B Physical Sciences*, vol. 20, pp. 1238–1245, 1918.
- [20] R. P. Kerr, “Gravitational field of a spinning mass as an example of algebraically special metrics,” *Physical review letters*, vol. 11, no. 5, p. 237, 1963.
- [21] F. W. Dyson, A. S. Eddington, and C. Davidson, “IX. A determination of the deflection of light by the Sun’s gravitational field, from observations made at the total eclipse of May 29, 1919,” *Philosophical Transactions of the Royal Society of London. Series A, Containing Papers of a Mathematical or Physical Character*, vol. 220, no. 571-581, pp. 291–333, 1920.



- [22] S. Liebes Jr, “Gravitational lenses,” *Physical Review*, vol. 133, no. 3B, p. B835, 1964.
- [23] S. Refsdal and J. Surdej, “Gravitational lenses,” *Reports on Progress in Physics*, vol. 57, no. 2, p. 117, 1994.
- [24] A. Einstein, “Lens-like action of a star by the deviation of light in the gravitational field,” *Science*, vol. 84, no. 2188, pp. 506–507, 1936.
- [25] K. S. Virbhadra and G. F. Ellis, “Schwarzschild black hole lensing,” *Physical Review D*, vol. 62, no. 8, p. 084003, 2000.
- [26] V. Bozza, “Gravitational lensing in the strong field limit,” *Physical Review D*, vol. 66, no. 10, p. 103001, 2002.
- [27] Bozza and Valerio, “Quasiequatorial gravitational lensing by spinning black holes in the strong field limit,” *Physical Review D*, vol. 67, no. 10, p. 103006, 2003.
- [28] N. Tsukamoto, “Deflection angle in the strong deflection limit in a general asymptotically flat, static, spherically symmetric spacetime,” *Physical Review D*, vol. 95, no. 6, p. 064035, 2017.
- [29] G. Gibbons and M. Werner, “Applications of the Gauss–Bonnet theorem to gravitational lensing,” *Classical and Quantum Gravity*, vol. 25, no. 23, p. 235009, 2008.
- [30] M. Werner, “Gravitational lensing in the Kerr-Randers optical geometry,” *General Relativity and Gravitation*, vol. 44, pp. 3047–3057, 2012.
- [31] A. Ishihara, Y. Suzuki, T. Ono, T. Kitamura, and H. Asada, “Gravitational bending angle of light for finite distance and the Gauss-Bonnet theorem,” *Physical Review D*, vol. 94, no. 8, p. 084015, 2016.

- [32] K. S. Thorne, C. W. Misner, and J. A. Wheeler, *Gravitation*. Freeman San Francisco, 2000.
- [33] D. J. Raine and E. G. Thomas, *Black holes: An introduction*. Imperial College Press, 2010.
- [34] P. S. marquis de Laplace, *Exposition du système du monde*. Courcier, 1813, vol. 1.
- [35] C. Bambi, “Astrophysical black holes: A compact pedagogical review,” *Annalen der Physik*, vol. 530, no. 6, p. 1700430, 2018.
- [36] S. W. Hawking, “Particle creation by black holes,” *Communications in mathematical physics*, vol. 43, no. 3, pp. 199–220, 1975.
- [37] R. H. Boyer and R. W. Lindquist, “Maximal analytic extension of the Kerr metric,” *Journal of mathematical physics*, vol. 8, no. 2, pp. 265–281, 1967.
- [38] J. O. Shipley, “Strong-field gravitational lensing by black holes,” *arXiv preprint arXiv:1909.04691*, 2019.
- [39] A. Einstein *et al.*, “Über den einfluß der schwerkraft auf die ausbreitung des lichtetes,” *Annalen der Physik*, vol. 35, no. 10, pp. 898–908, 1911.
- [40] A. Gould, “Deflection of light by the earth,” *Astrophysical Journal, Part 2-Letters (ISSN 0004-637X)*, vol. 414, no. 1, p. L37-L40., vol. 414, pp. L37–L40, 1993.
- [41] V. Perlick, “Gravitational lensing from a spacetime perspective,” *Living reviews in relativity*, vol. 7, pp. 1–117, 2004.

- [42] S. Mollerach and E. Roulet, *Gravitational lensing and microlensing*. World Scientific, 2002.
- [43] F. De Paolis, M. Giordano, G. Ingrosso, L. Manni, A. Nucita, and F. Strafella, “The scales of gravitational lensing,” *Universe*, vol. 2, no. 1, p. 6, 2016.
- [44] M. D. Carmo, *Differential geometry of curves and surfaces*, 1st ed. Prentice-Hall, 1976.
- [45] S. Frittelli, T. P. Kling, and E. T. Newman, “Spacetime perspective of Schwarzschild lensing,” *Physical Review D*, vol. 61, no. 6, p. 064021, 2000.
- [46] T. Ono, A. Ishihara, and H. Asada, “Gravitomagnetic bending angle of light with finite-distance corrections in stationary axisymmetric space-times,” *Physical Review D*, vol. 96, no. 10, p. 104037, 2017.
- [47] T. Ono, A. Ishihara, and Asada, “Deflection angle of light for an observer and source at finite distance from a rotating wormhole,” *Physical Review D*, vol. 98, no. 4, p. 044047, 2018.
- [48] K. Akiyama, A. Alberdi, W. Alef, K. Asada, R. Azulay, A.-K. Baczko, D. Ball, M. Baloković, J. Barrett, D. Bintley *et al.*, “First M87 Event Horizon Telescope results. IV. Imaging the central supermassive black hole,” *The Astrophysical Journal Letters*, vol. 875, no. 1, p. L4, 2019.
- [49] K. Virbhadra, “Distortions of images of Schwarzschild lensing,” *Physical Review D*, vol. 106, no. 6, p. 064038, 2022.

- [50] A. Övgün, “Light deflection by Damour-Solodukhin wormholes and Gauss-Bonnet theorem,” *Physical Review D*, vol. 98, no. 4, p. 044033, 2018.
- [51] H. Buchdahl, “On the gravitational field equations arising from the square of the Gaussian curvature,” *Il Nuovo Cimento (1955-1965)*, vol. 23, pp. 141–157, 1962.
- [52] H. K. Nguyen, “Beyond Schwarzschild–de Sitter spacetimes: A new exhaustive class of metrics inspired by Buchdahl for pure  $\mathcal{R}^2$  gravity in a compact form,” *Physical Review D*, vol. 106, no. 10, p. 104004, 2022.
- [53] H. K. Nguyen and M. Azreg-Ainou, “Traversable Morris–Thorne–Buchdahl wormholes in quadratic gravity,” *The European Physical Journal C*, vol. 83, no. 7, p. 626, 2023.
- [54] H. K. Nguyen, “Beyond Schwarzschild–de Sitter spacetimes. II. An exact non-Schwarzschild metric in pure  $\mathcal{R}^2$  gravity and new anomalous properties of  $\mathcal{R}^2$  spacetimes,” *Physical Review D*, vol. 107, no. 10, p. 104008, 2023.
- [55] E. Kreyszig, *Differential geometry*. Dover Publications, 2013.
- [56] W. Javed, I. Hussain, and A. Övgün, “Weak deflection angle of Kazakov–Solodukhin black hole in plasma medium using Gauss–Bonnet theorem and its greybody bonding,” *The European Physical Journal Plus*, vol. 137, no. 1, pp. 1–14, 2022.
- [57] A. Övgün, G. Gyulchev, and K. Jusufi, “Weak Gravitational lensing by phantom black holes and phantom wormholes using the Gauss–Bonnet theorem,” *Annals of Physics*, vol. 406, pp. 152–172, 2019.

- [58] S. U. Islam, S. G. Ghosh, and S. D. Maharaj, “Strong gravitational lensing by Bardeen black holes in 4D EGB gravity: constraints from supermassive black holes,” *Chinese Journal of Physics*, vol. 89, pp. 1710–1724, 2024.
- [59] H. A. Buchdahl, “Non-linear Lagrangians and cosmological theory,” *Monthly Notices of the Royal Astronomical Society*, vol. 150, no. 1, pp. 1–8, 1970.
- [60] M. Azreg-Aïnou and H. K. Nguyen, “A stationary axisymmetric vacuum solution for pure  $\mathcal{R}^2$  gravity,” *Physica Scripta*, vol. 98, no. 12, p. 125025, 2023.
- [61] A. Ishihara, Y. Suzuki, T. Ono, and H. Asada, “Finite-distance corrections to the gravitational bending angle of light in the strong deflection limit,” *Physical Review D*, vol. 95, no. 4, p. 044017, 2017.
- [62] T. Zhu, H. K. Nguyen, M. Azreg-Aïnou, and M. Jamil, “Observational tests of asymptotically flat  $\mathcal{R}^2$  spacetimes,” *The European Physical Journal C*, vol. 84, no. 3, p. 330, 2024.